UNIVERSITY *of the*
WESTERN CAPE

ANALYSIS OF THE STRUCTURAL GEOLOGY OF THE HIGH GRADE METAMORPHIC ROCKS IN PART OF THE KAKAMAS TERRANE OF AN AREA ADJACENT TO THE NEUSSPRUIT SHEAR ZONE SOUTH OF THE ORANGE RIVER, NORTHERN CAPE, SOUTH AFRICA

By

CYRILLE STEPHANE TSAKOU SONWA

THESIS

Presented in fulfilment of the requirements for the degree of

MAGISTER SCIENTIAE

in

GEOLOGY

in the

FACULTY OF SCIENCE

of the

UNIVERSITY OF THE WESTERN CAPE

Supervisor: Prof. Jan van Bever Donker

Co- supervisor: Dr. Russell Bailie

April 2015

DECLARATION

I hereby declare that *analysis of the structural geology of the high grade metamorphic rocks in part of the Kakamas Terrane of an area adjacent to the Neusspruit Shear Zone South of the Orange River, Northern Cape, South Africa,* apart from the help and supervision of Prof. Jan van Bever Donker and Dr. Russell Bailie, is my own work and has not been previously submitted for a degree in any other university or institution of higher education. All the sources I have used or quoted have been indicated and acknowledged by complete references.

Cyrille Stephane Tsakou Sonwa

Date

Place

DEDICATION

I dedicate this work to my late Mom Rose, who could not witness this achievement, my Dad Jacques, and siblings (Eudoxie, Laetitia, and Ulrich). Many thanks for all the encouragement, love and kindness during this time.

ACKNOWLEDGEMENTS

Thank you God, our Saviour through Jesus Christ our Lord…in whom all the wonders are His before all time, and in the present, and beyond all time.

I would like to thank my experienced, wonderful, and patient supervisors, Prof. Jan van Bever Donker and Dr. Russell Bailie, who inspired me with their interest and fruitful discussions during this work. I could not have realized this research without you.

Ignatius Wessels and Errol Brussel from the Karsten Farm and to the Hanekom family from the Die Mas Farm are gratefully acknowledged for the permission they granted us, and the assistance, guidance and hospitality during the collection of the structural data and various samples.

I am grateful to Dr. Antonio Ravaglia of PetroSA for his precious time and guidance for the Move™ software. Peter Meyer is thanked for his assistance during the cutting and preparation of the thin section slides of selected samples.

This research was funded by Inkaba YeAfrica. I am grateful to Prof. Maarten De Wit of AEON at the Nelson Mandela Metropolitan University for his innovative vision in the geosciences. I thank Elronah Schaap for her constant updates and motivation to the Inkaba YeAfrica bursars.

My gratitude goes to Father Pierre Justin Chimba, as well as all the community of the St John and Paul Catholic Church of Belhar. To my friends both within and outside the country that I have come to know while dealing with this research –LaureI and Corine Tsoamene, Rosine F. Melly, Santiago Ondo Ndong Andeme, Santa Rokia Fofana, Brahim Mahamat Mai, Ruffin Mantadi, Takako Nishikawa, Joseph N. Nimpa, Dr. Jules C. Mba, Dr. Justin B. Munyakazi. I thank you for the fun, support, and advice you have portrayed towards me, without forgetting fellow researchers for the enthusiasm and friendship.

Finally to my lecturers at the Department of Geology–Prof. Charles Okujeni, Dr. Abdi Siad, Dr. Mimonitu Opuwari. I thank you for the helps and advices.

ABSTRACT

The Proterozoic Namaqua-Natal Province comprises highly deformed rocks of medium to high grade metamorphism and is bordering the Archean Kaapvaal Craton to the west, south and east in South Africa. The sector to the west of the Craton, namely the Namaqua Sector, is structurally complex and subdivided from west to east into the Bushmanland Subprovince, the Kakamas and Areachap terranes of the Gordonia Subprovince and the Kheis Subprovince. The prominent Neusberg Mountain Range, with exposures to the north and south of the Orange River in the Kakamas Terrane constitutes evidence of crustal shortening as a result of continental collision of the Namaqua Sector block with the Kaapvaal Craton during the Namaquan Orogeny. The Mesoproterozoic Korannaland Group in the Kakamas Terrane is affected by faulting, folding and shearing. The Neusspruit Shear Zone is considered as a significant structural feature trending northwest along the Neusberg Mountain Range, which is located in the central part of the Kakamas Terrane and comprises of metasedimentary rocks, magmatic rocks in the form of granitic gneisses, and metavolcanic rocks and various rocks affected by contact metamorphism and metasomatism. This study was carried out to investigate the structural geology of the metasedimentary rocks and various granitic gneisses along and adjacent to the Neusspruit Shear Zone in the Kakamas Terrane. The objective was two-fold: (i) to examine the texture and mineralogy of the rocks which underwent deformation and (ii) to determine the structural development along and adjacent to the Neusspruit Shear Zone and its relation with the intrusion of the charnockite.

Microstructures such as, foliation, grain recrystallisation, calcite twins, and fractures in zircon were established in various rock types revealing the deformation of the rocks at a microscale in the Kakamas Terrane. The metasedimentary rocks of the Korannaland Group (composed of the Puntsit and Goede Hoop Formations) revealed cross-bedding in places in the Goede Hoop Formation. The post-tectonic charnockite intruded the country rocks and gave rise to various contact rocks, namely the biotite gneiss characterised as the reaction zone between the Goede Hoop Formation and the charnockite. The rocks adjacent to the Neusspruit Shear Zone in the

Kakamas Terrane were subjected to prograde granulite facies metamorphism but also show evidence of retrograde greenschist facies overprinting.

The rocks along and adjacent to the Neusspruit Shear Zone in the Kakamas Terrane were subjected to various deformational events, prominent and intense deformation resulted during the main D_1 deformational event illustrated by isoclinal and open folds in the Kakamas Terrane with the axial traces trending northwest-southeast, revealing an overall compression. Field observations and the interpretations from this study establish that the Neusberg Mountain Range in the Kakamas Terrane is a plunging structure towards northwest-southeast direction developed in a transpressional environment. The presence of shearing is revealed by augen structures within the augen gneiss along the Neusspruit Shear Zone. It is established that a sinistral movement occurred within the Neusspruit Shear Zone as revealed by the presence of asymmetric s-haped folds. Applied stress during the D_1 deformational event resulted in the closure of the structure with flattening directed towards the northwest-southeast direction. Such deformation is supported by the presence of flattened pebbles in the Goede Hoop Formation, with the long axis trending towards the northwest-southeast direction and parallel to the axial traces of the isoclinal folds in the Neusberg Mountain Range. Subsequently, continued shortening during the second deformation event, D_2, gave rise to the Neusberg Thrust Fault, and the presence of breccias within the Neusberg Mountain Range in the southern portion of the Neusberg Mountain Range. It is established that the Neusspruit Shear Zone, together with the Neusberg Thrust Fault, extends further north of the Orange River and constitutes major deformation of a regional scale in the Kakamas Terrane. Joint analysis in this study revealed that the deformational event, D_3, is illustrated by strike-slip movement defining a compressive environment. Lastly, the fourth deformation event, D_4, is revealed by fractures (joints and veins) in the charnockite which are commonly filled with epidote or piemontite mineralization, which are suggestive of uplift and exhumation in the Kakamas Terrane.

ANALYSIS OF THE STRUCTURAL GEOLOGY OF THE HIGH GRADE METAMORPHIC ROCKS IN PART OF THE KAKAMAS TERRANE OF AN AREA ADJACENT TO THE NEUSSPRUIT SHEAR ZONE SOUTH OF THE ORANGE RIVER, NORTHERN CAPE, SOUTH AFRICA

Cyrille Stephane Tsakou Sonwa

KEY WORDS

Kaapvaal Craton

Namaqua Sector

Kakamas Terrane

Korannaland Group

Neusspruit Shear Zone

Fold interference

ANALYSIS OF THE STRUCTURAL GEOLOGY OF THE HIGH GRADE METAMORPHIC ROCKS IN PART OF THE KAKAMAS TERRANE OF AN AREA ADJACENT TO THE NEUSSPRUIT SHEAR ZONE SOUTH OF THE ORANGE RIVER, NORTHERN CAPE, SOUTH AFRICA

Cyrille Stephane Tsakou Sonwa

ABBREVIATIONS

cm= Centimeter

° = Degree

°C= Degree Celsius

e.g. = for example

kbar= Kilobar

km= Kilometer

km^2= Kilometer squared

m = Meter

mm= Millimeter

Ma= Millions years ago

P= Pressure

T= Temperature

Table of Contents

LIST OF FIGURES

LIST OF TABLES

CHAPTER 1

INTRODUCTION

1.1 Background

The Namaqua-Natal Province (NNP) of southern Africa is a Mesoproterozoic orogenic belt bordering the western, southern and eastern margins of the Archean Kaapvaal Craton (Cornell et al., 2006). The NNP forms an arcuate belt (Figure 1.1) up to 1400 km long × 400 km wide (Thomas et al., 1993; Jacobs et al., 2008). Available geological, geochronological and palaeomagnetic data suggest that the Mesoproterozoic time was dominated by accretionary and collisional orogenic processes (Kokonyangi et al., 2006). The Namaqua-Natal Province is underlain by mid-Proterozoic granitoids and medium to high-grade supracrustal rocks (Cornell et al., 1992). The Namaqua Sector (Figure 1.1) is the western part of the Namaqua-Natal Province in which the timing of collision is poorly constrained (Pettersson et al., 2007) and it is structurally complex (Humphreys and van Bever Donker, 1987; van Bever Donker, 1991).

The Namaqua Sector covers an area of more than 100 000 km² (Johnson et al., 2006) and has been subdivided from west to east into the Bushmanland Subprovince, the Kakamas and Areachap terranes of the Gordonia Subprovince and the Kheis Subprovince (Slabbert et al., 1989; Moen, 2007). The Richtersveld Subprovince is juxtaposed to the west of the Gordonia Subprovince (Reid, 1997). The Kakamas Terrane is considered to comprise chiefly metasedimentary rocks which were structurally and thermally reworked during the 1200 - 1000 Ma Namaquan Orogenesis when the Namaqua Sector collided with the Archean Kaapvaal Craton (Thomas et al., 1993). The shear and thrust-zones that now transect the Namaqua Sector are important tools in terrane analysis (Moen, 2007).

The Neusspruit Shear Zone (NSZ) is considered to be a major structural discontinuity in the Kakamas Terrane trending northwest and separating the granitoids of the Keimoes Suite to the east, from the metasedimentary rocks of the Korannaland Group and associated gneisses to the west (Moen, 2007). The principal lithologies of the Kakamas Terrane comprise highly deformed

supracrustal rocks of feldspathic mica-rich quartzite and calc-silicate-rich quartzite, granitic gneisses, along with extensive intrusions of syn- and late-tectonic Namaqua granitoids, such as charnockite (Hartnady et al., 1985; Thomas et al., 1994a; Eglington, 2006; Moen, 2007). This intrusive rock was first described in the Gordonia Subprovince as charnockitic adamellite porphyry (Podervaart and von Backström, 1949; von Backström, 1964; Podervaart, 1966) and as a charnockitic granulite (Schultz, 1978). This unusual granitoid (Moen, 2007) intrudes the metasediments of the Korannaland Group and occurs as a large and continuous body in the central part of the Neusberg Mountain Range in the Kakamas Terrane, where it is in contact with the Puntsit and Goede Hoop Formations in the eastern and north-eastern parts of the study area.

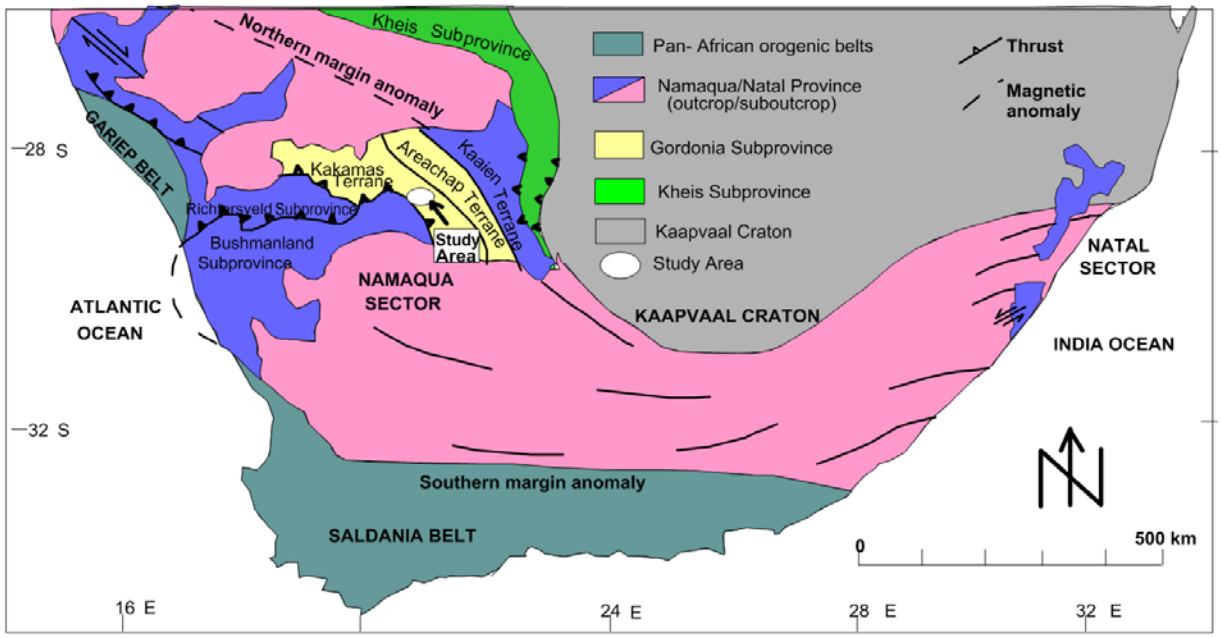

Figure 1.1: General subdivision of the Namaqua Sector (after Cornell et al., 2006).

1.2 Study area

The study area is located along the Orange River in the southern part of the Neusberg Mountain Range, some 19 km east of Kakamas and 80 km west of Upington in the Northern

Cape Province, South Africa. The area is covered by the Upington sheet 2820 at a scale of 1:250 000 (Moen, 1988), and the two 1:50 000 topographic map sheets: 2820 DC Kakamas and 2820 DD Koekoeb. The area under investigation may be accessed by a reasonably well maintained gravel road (R359) from Kakamas in the west or Neilersdrift in the east (Figure 1.2).

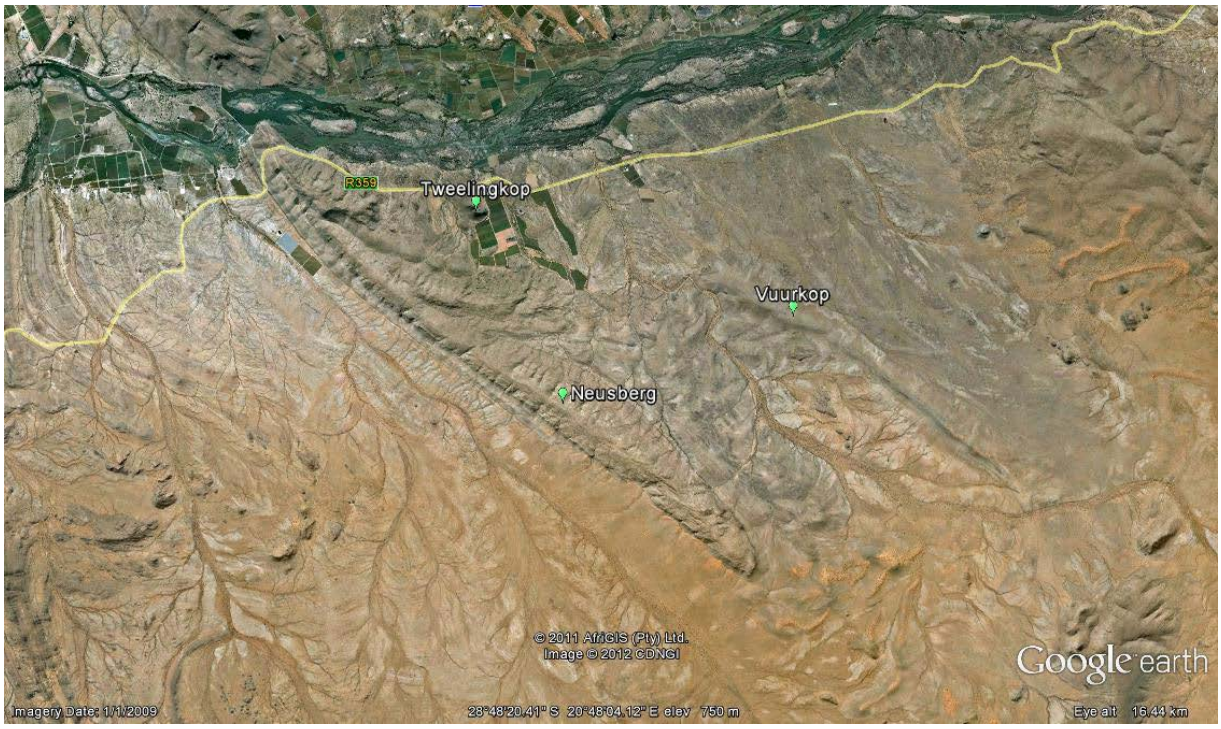

Figure 1.2: Aerial photograph of the study area. The dominant structure in the area is oriented NW, as seen by three areas in the southern part of the Neusberg Mountain Range: Tweelingkop (= Twin Hill) consists of charnockite; Vuurkop (= Fire Hill) is characterized by calc-silicate; the Neusberg is mostly composed of feldspathic quartzite (Google Earth image, 2012/06/02).

Generally, the area is characterised by rugged and dissected topography with remnant hills. The climatic conditions vary from arid to semi-arid, with an average annual rainfall of 130-200 mm and an annual average temperature of 35°C during summer and a mild winter with temperatures plummeting to -7°C (Moen, 2007). The main drainage channel is the Orange River, which is used by the local people for domestic purposes as well as farming. The non-perennial small-scale rivers, such as the Neusspruit and the Kameeldoring River in the study

area, drain into the Orange River. The study area is sparsely vegetated, with xerophytic plants such as the *Rhigozum trichotomum, Parkinsonia africana* (Moen, 2007), and exotic plants, which include the *Prosopis glandulosa* (Mannheimer and Curtis, 2009). The distribution of trees and most shrubs in the study area is well delineated and controlled by the availability of water, soil type and drainage (Moen, 2007).

1.3 Problem statement

The intense folding, faulting, and shearing of rocks during the Namaqua Orogeny produced prominent synformal and antiformal structures which considerably affected the rocks of the Korannaland Group (Slabbert et al., 1999). Due to the structural complexity and high grade of metamorphism of the rocks of the Korannaland Group in the Kakamas Terrane, numerous stratigraphic and structural problems of interpretation have arisen. Firstly, the stratigraphy of the rocks had to be identified in order to understand the stratigraphic, petrographic, and structural evolution of the rocks in the study area. To resolve this problem, clear observations and descriptions of features during the field study were required. Secondly, the Neusspruit Shear Zone**,** which borders the Neusberg Mountain Range to the west in the study area and the surroundings**,** represents an important, yet not well understood discontinuity in the Kakamas Terrane, as the structural characteristics of the metasedimentary, granitic, and contact rocks along and adjacent to the NSZ are poorly defined (Moen, 2007), and need to be investigated.

1.4 Aim and objectives

The aim of this study is to contribute to the understanding of the structural evolution of the rocks along and adjacent to the Neusspruit Shear Zone (NSZ) in the study area. The main objectives are to:

- Establish the lithostratigraphic sequence and to compile a geological map of the area under consideration.

- Petrographically describe the rocks of the Korannaland Group, contact rocks, granitic gneisses and metavolcanic rock in the study area in order to determine their protolith, deformation and metamorphic grade.
- Provide a structural interpretation of the study area with special focus on foliations, lineations, and joints.
- Identify the characteristics of the charnockite in the study area in terms of the metamorphic history and its tectonic development.
- Determine whether the late brittle features in the study area are linked to the intrusion of the charnockite.
- Unravel the structural evolution of the study area including the development of the Neusspruit Shear Zone.
- Investigate a possible development of sheath fold in the study area.

This research will not only present a synthesis of available information in the area under investigation, but will also contribute to an understanding of the tectonic history of the Kakamas Terrane, which constitutes a part of the western portion of the Namaqua Sector.

1.5 Methodology

The approach to any study starts with an idea of the information requirements of the study and how these can be developed into useful tools to apply to the research problem. This part of the study outlines the methods and techniques that are used in this research.

The first of these encompasses a desk study which begins with a comprehensive literature review of the geology of the Kakamas Terrane in the Namaqua Sector, which is a terrane affected by deformational events and medium to high grade metamorphism (Cornell et al., 1992; Moen, 2007). Published structural and geological maps (Humphreys and van Bever Donker, 1987; Moen, 1988; van Bever Donker, 1991) were used for examination and interpretation of geological features.

The second part of the study entails field work based on direct observations and mapping. To obtain a complete geological knowledge of the study area, many tools are used and data are collected manually. A GPS (Geographic Positioning System) is used to obtain the geographic coordinates of each location on the map. Topographic maps combined with aerial photographs are used to find locations taken with a GPS as well as specific outcrops. The hand lens is used for petrographic description of the rocks. A Clar-type compass is used to locate true north and measure dip direction and dip or the general orientation of trends. The mapping aspect of the study is based on topographical and previously published geological maps, aerial-photographs and digital aerial photos to develop a visual understanding and representation of the study area. The 1:250 000, 2820 Upington geological map (Moen, 2007) was used for the regional geology.

The published 1:50 000 topographic maps (2820 CD Kakamas and 2820 DD Koekoeb) from the Department of Mapping and Survey in Mowbray were used as base maps for the study area, where the geology can be interpolated. The orthophoto-map series at a scale of 1:10 000, combined with aerial photographs and digital aerial photos, were used to interpret the geology and structures. Folds and faults were recognized and some differences were identified between the published results concerning the folds and faults of the geological map and what was visible on the orthophoto-map. This proved to be a useful tool to select sites for the field work and to identify features not represented on the maps.

The third part of the study involves analytical aspects, which are subdivided into petrographic and structural analyses:

Petrographic analysis

Detailed petrographic studies were carried out on thin sections of samples collected in the field using transmitted light microscopy. Various samples were selected for petrographic examination with the aim of acquiring information on the deformation and recovery. This was

done at the Department of Earth Sciences, University of the Western Cape. The petrographic analysis in this study is developed at different scales (mesoscopic and microscopic) to understand and interpret the whole process of deformation in the study area. Mineral abbreviations of rocks identified in the study area are adopted from Kretz (1983) and Schmid et al. (2007).

Structural analysis

The Kakamas Terrane in the Namaqua Sector has been subjected to severe deformation (Moen, 2007). The deformation has been described by previous workers (van Bever Donker, 1980, 1983, 1991; Moen, 2007). Various strain features, such as fold axes and axial planes, foliations, and lineations, along with shear sense indicators, such as vorticity indicators, as well as other structural features, such as joints, were observed and recorded. Their orientations are plotted stereographically as well as on rose diagrams using the Geological Software GEOrient version 9.5.0 (Holcombe, 2011), at the Department of Earth Sciences, University of the Western Cape.

Move™ (2013; version 2013.1.0) is a modelling software developed by Midland Valley, Glasgow, United Kingdom. The 2D Move™ is the selected package for this study. The 2D Move™ is used to digitize the area under investigation, and generate the geological map of the study area. This analysis was done at the Department of Earth Sciences, University of the Western Cape.

CHAPTER 2

GEOLOGIC SETTING

2.1 Geodynamic Evolution of the Namaquan Orogen

The Earth's continental crust has developed mainly in episodes of crustal growth, often linked to repeated cyclic events of supercontinents forming and breaking up, the formation and destruction of which is sometimes difficult to establish, due to the repeated heating, deformation and melting of the crust which erases most of the previous recorded history (Pettersson, 2008). An orogeny, as defined by Bates and Jackson (1995), is the creation of mountain belts by tectonic activity, and the affected areas are referred to as orogenic belts or provinces (Pettersson, 2008).

The Namaquan Orogen is therefore seen as an important marker of continent-continent or continent-island arc collision that happened in the past, where it is mostly constituted of areas classified as terranes (Cornell et al., 2006). These terranes have been displaced along major faults in the collision phase (Pettersson, 2008). The orogenic belt can consequently include oceanic island arcs, fragments of older continental crust, oceanic floor and sediments (Pettersson, 2008; Fossen, 2010). These new composite areas are added to the older stable crustal blocks, often described as cratons (Pettersson, 2008). The assemblage of such continental blocks formed the supercontinent Rodinia; its subsequent break-up commenced at approximately 850 Ma and the break-up was completed around 500 Ma (Onstott et al., 1986; Dalziel, 1991; Robb et al., 1999; Powell et al., 2001). The orogenic belts that contributed to the formation of Rodinia are currently scattered all over the globe, and proposed reconstructions of this supercontinent diverge considerably (Li et al., 2008).

The Namaqua-Natal Province (NNP) is the subject of an ongoing debate as to whether the NNP was associated with Rodinia or not (Li et al., 2008). Similarly, in most parts of the world, the precise interpretation of the orogens in plate tectonic terms is still vigorously debated (Powell et al., 2001; Li et al., 2008). Out-board correlations to the NNP can be made with similar

lithologies in Antarctica and the Falkland/Malvinas islands (Armstrong and de Wit, 2007), while further extensions of similar age are found in Namibia, Mozambique, Botswana and Zambia (Grantham et al., 2003; Becker et al., 2006; Armstrong and de Wit, 2007). The NNP is draped around the western, southern and eastern flanks of the Kaapvaal Craton (Cornell et al., 2006; Pettersson, 2008), and externally bounded by an extensive system of Neoproterozoic to lower Palaeozoic fold belts (Thomas et al., 1993), while the NNP is extensively overlain by Phanerozoic cover in its central portion (Eglington and Armstrong, 2003). It has been proposed that the NNP formed a continuous belt (Eglington and Armstrong, 2003). This interpretation was confirmed by geological (Hartnady et al., 1985; Joubert, 1986; Thomas et al., 1993), geophysical (De Beer and Meyer, 1983, 1984) and geochronological (Eglington and Armstrong, 2003) investigations. Various workers have divided the NNP into two major sectors (Cornell et al., 2006), the Natal Sector to the south-east, and the Namaqua Sector to the west of the Archean Kaapvaal Craton (Figure 1.1). In terms of the South African chronostratigraphic terminology, the rocks of the Natal Sector belong to the Mesoproterozoic which is partly underlain by Palaeoproterozoic and Archean basement (SACS, 1980). The rocks of the Namaqua Sector fall within the Mokolian Erathem, which is subdivided into the Kheisian and Namaquan periods (Moen, 2007).

2.2 Geology of the Namaqua Sector

It is four decades since Blignault et al. (1974) first coined the term Namaqua Province to describe an intracrustal domain where the earliest work was carried out by Poldervaart and von Backström (1949). The Namaqua Sector includes a vast (but yet not well known) portion of Palaeoproterozoic rocks that were deformed, subjected to high-grade metamorphism and intruded by voluminous granitoids during the Mesoproterozoic collisional event (Jacobs et al., 2008). The Namaqua Province is also referred to as the Namaqua Sector (Cornell et al., 2006; Bailie et al., 2010, 2011) to be more specific in terms of the subdivision of the NNP (Figure 1.1). The boundaries of the Namaqua Sector are broadly detailed by Cornell et al. (2006), where the eastern boundary is separated from the Kaapvaal Craton by the Kheis Subprovince. The Atlantic Ocean forms the western boundary (Figure 1.1).

The Namaqua Sector is subdivided into four major Subprovinces, namely the Richtersveld, Bushmanland, Gordonia and Kheis Subprovinces (Slabbert et al., 1989; Reid, 1997; Moen, 2007). The Subprovinces are bounded by Mesoproterozoic shear zones, trending mostly northwest (Slabbert et al., 1989; Jacobs et al., 2008). The Gordonia Subprovince is subdivided into the Kakamas and Areachap terranes (Figure 1.1). The Kakamas Terrane is the main terrane of interest for this study, where the area under investigation is located in the southern part of the Neusberg Mountain Range. Some authors (Hartnady et al., 1985; Thomas et al., 1994a, 2006; Moen, 1999; Cornell et al., 2006; Jacobs et al., 2008) have proposed lithostratigraphic components based on chronological order in the Namaqua Sector. Structurally, the Mesoproterozoic history of the Namaqua Sector is composed of E-W and NW-SE to NNW-SSE-oriented crustal stacking (van Bever Donker, 1991; Cornell et al., 2012).

2.3 Geology of the Gordonia Subprovince

The Gordonia Subprovince is one of the tectonic subdivision units of the Namaqua Sector that collided with the western flank of the Archean Kaapvaal Craton (Stowe, 1986; Cornell et al., 2006). The Gordonia Subprovince consists of two portions; the western part is occupied by the Kakamas Terrane which is located east of the Bushmanland Subprovince; the eastern part of the Gordonia Subprovince is occupied by the Areachap Terrane which is located east of the Kakamas Terrane (Figure 1.1). The subdivision of the Gordonia Subprovince is based on structural and lithological grounds (Hartnady et al., 1985). Although the precise geometry remains controversial, it is widely accepted that the rocks of the Gordonia Subprovince are structurally and stratigraphically distinct from those of the Bushmanland Subprovince (Thomas et al., 1993). Similarly, the extent and nature of an older basement in the Gordonia Subprovince is still unclear, due to the lack of precise isotopic age data. The structural geology of the Gordonia Subprovince is complex, and is not fully known (Moen, 2007).

The Gordonia Subprovince extends eastwards to the Kheis Subprovince (Slabbert et al., 1989), along the Trooilapspan Shear Zone east of 21° E (Figure 2.1). Some workers (Slabbert et al., 1989; Moen, 2007) have shown that the westwards extension of the Gordonia Subprovince

goes along the Hartbees River Thrust Zone east of 20° E and along the Swartland Fault west of 20° E. The southern portion of the Gordonia Subprovince extends south to the Kenhardt-Putsonderwater region, where it disappears beneath younger Palaeozoic cover rocks (Johnson et al., 2006). The complete extent and significance of the northwest-trending Neusspruit Shear Zone is not well known (Moen, 2007), a portion of which is located within the study area. As illustrated in Figure 2.2, the stratigraphy of the Gordonia Subprovince (Table 2.1) comprises two different types of rocks: metasedimentary and intrusive rocks (Moen, 2007), which are dissected by faults and shear zones (Slabbert et al., 1989).

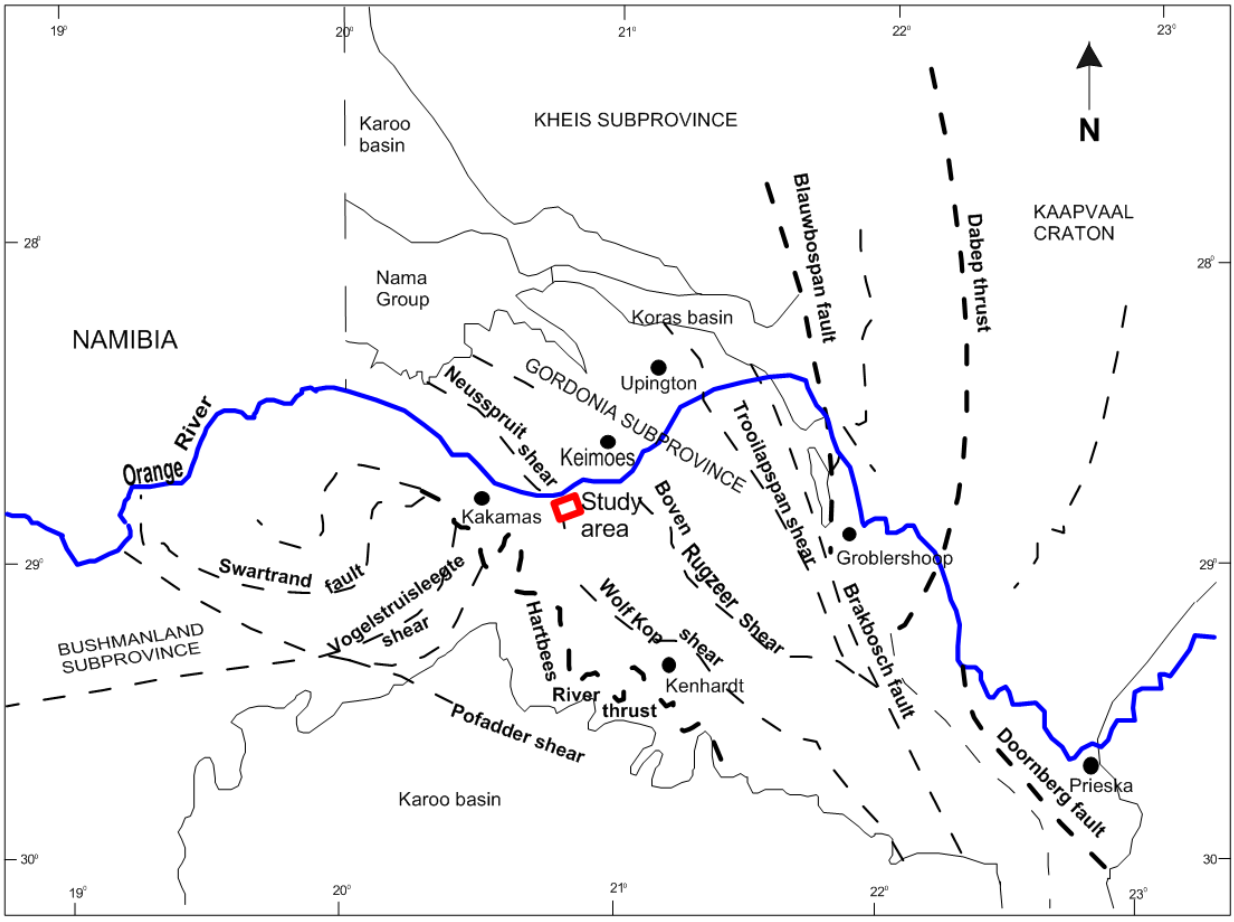

Figure 2.1: General distribution of major tectonic structures in the Namaqua Sector displaying the Gordonia Subprovince and the study area, along with towns indicated by dark circles (after Slabbert et al., 1989).

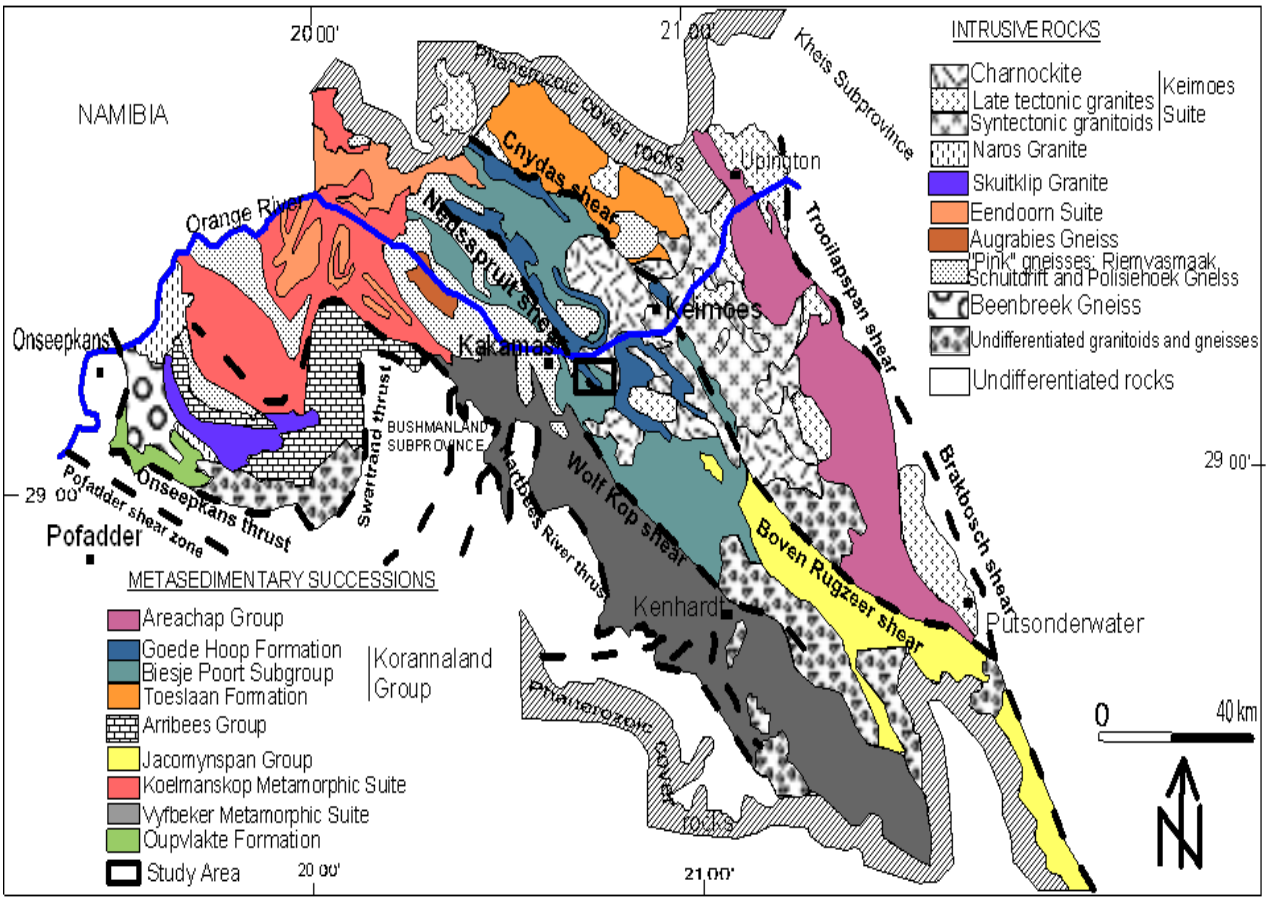

Figure 2.2: Generalized geology of the Gordonia Subprovince, showing the location of the study area in the southern part of the Neusberg Mountain Range (after Moen, 2007).

2.4 Geology of the Kakamas Terrane

The Kakamas Terrane was first investigated by Poldervaart and von Backström (1949), and they published the geology of an area around Kakamas. Their findings were then followed by a report based on the charnockite of an area between the Neusberg Mountain Range (NMR) and Keimoes by von Backström (1964). Subsequently, the structural and metamorphic evolution of the metasedimentary rocks in the study area was investigated by van Bever Donker (1980). The Kakamas Terrane lies to the east of the Bushmanland Subprovince, forming the westernmost portion of the Gordonia Subprovince, with its western boundary taken as being along the Hartbees River Thrust Zone (Harris, 1992; Figure 2.2). To the east, it is assumed that the Kakamas Terrane is bordered by the Boven Rugzeer Shear Zone (BRSZ), which is considered to

separate the Kakamas Terrane from the Areachap Terrane in the Gordonia Subprovince (Moen, 2007; Figure 2.2). Structurally at the base, the lithological units in the Kakamas Terrane are composed of a number of various intrusive rocks represented by undifferentiated granitoids and gneisses, the Beenbreek gneiss, Riemvasmaak, Schuitdrift, Polisiehoek, and Augrabies gneisses, Eendoom Suite, Skuitklip granite, Naros granite, and the Keimoes Suite (Moen, 2007; Figure 2.2). At the top, the lithological unit is composed of various metasedimentary rocks, namely the Oupvlakte Formation, Vyfbeker Metamorphic Suite, Koelmanskop Metamorphic Suite, Jacomynspan Group, Arribees Group, and the Korannaland Group (Moen, 2007; Figure 2.2).

2.4.1 Regional structure and metamorphism

The rocks in the Kakamas Terrane were subjected to various tectonic events: plate convergence, thrusting, shearing, thickening of the crustal sequence, and intense deformation. All this is due to a consistent strain regime with a general movement towards the Kaapvaal Craton (Cornell et al., 2006; Cornell and Pettersson, 2007). The tectonic structures recorded by the metasedimentary rocks of the Korannaland Group in the Kakamas Terrane are related to the compressional and extensional stresses that resulted in the amalgamation of the terranes in the Namaqua Sector. The Korannaland Group has been affected by several deformational events of Namaquan age (1200 - 1000 Ma). Generally, four deformational events (D_1-D_4) have been recognized in the Kakamas Terrane. The first deformational event, D_1, is marked by a pervasive regional foliation and was followed by the more intense and dominant D_2 deformation, which resulted in isoclinal to tight folds. Folds associated with the D_2 deformation event along the Neusspruit Shear Zone (NSZ) have axial traces trending towards the northwest in the Kakamas Terrane (van Bever Donker, 1980). The D_3 deformational event is represented by thrust faults and the development of a number of isolated domes such as the "Central Dome" and ''Warm Zand Dome'' in the Kakamas Terrane, which formed as a result of the superposition of F_3/F_2 folds (van Bever Donker, 1980), imparting a unique aspect to the

macrostructure of the Kakamas Terrane (Johnson et al., 2006). The change in direction of the earlier D_1/D_2 fabrics and linear features orientated E-W in the Bushmanland Subprovince to the NW-SE or NNW-SSE trend in the Gordonia Subprovince (Cornell and Pettersson, 2007) indicates dextral transpressional tectonics (van Bever Donker, 1991; Jacobs et al., 1993). The western boundary of the Kakamas Terrane, the Hartbees River Thrust Zone, is assumed to be an early structure related to the D_1/D_2 structural events (Johnson et al. 2006). The eastern boundary runs along the Boven Rugzeer Shear Zone (Figure 2.2), consisting of younger structures related to the final episode of dextral shearing. The later deformational event, D_4, is identified as a horizontal directed compression, with the shape of the adjacent Kaapvaal Craton acting as an indentor, which propagated the transcurrent shear system (van Bever Donker, 1991; Jacobs et al., 1993).

The metasediments of the Korannaland Group in the Kakamas Terrane are folded and intruded by undeformed granitoids which caused extensive contact metamorphism. However, it is noteworthy to mention that a clear survey of metamorphism of the metasedimentary rocks can be hampered by factors such as the limited exposures and the lack of rocks with suitable compositions (Moen, 2007). The metamorphic conditions that prevailed during D_1 (M_1) were estimated as 540 ± 50 °C at a pressure of around 2 kbar (Moen, 2007). This lower pressure metamorphic event is thought to have extended over much of the Gordonia Subprovince, but it is rarely recognized because of the subsequent amphibolite/granulite event (Moen, 2007). The regional metamorphic event in the Kakamas Terrane varies from amphibolite to granulite facies and is of generally lower grade to the east (Moen, 2007; Pettersson, 2008). The high grade M_2 metamorphic event is related to the granitic intrusions of the Keimoes Suite, presumably resulting in extensive metamorphism of the Korannaland Group in the Kakamas Terrane (Moen, 2007). The M_2 regional contact metamorphic event is linked to the igneous granitoids intrusion, which is assumed to be an overprinting of the earlier M_1 metamorphic event. This is characterised by K-feldspar-cordierite-garnet and garnet-biotite-sillimanite assemblages in metapelitic rocks (Johnson et al., 2006). This is indicative of upper amphibolite to granulite facies P-T conditions of ~700 °C and 4-5 kbar in the vicinity of the Hartbees River Thrust Zone

(Geringer, 1973; van Zyl, 1981; Stowe, 1983b). Similar conditions were determined in the core of the ''Central Dome" west of the Neuspruit Shear Zone in the Kakamas Terrane (van Bever Donker, 1980). The assemblages of garnet-staurolite-andalusite close to the Boven Rugzeer Shear Zone to the east indicate lower amphibolite facies P-T conditions of 550 °C and 1.5-2.5 kbar (Humphreys and van Bever Donker, 1990). There appears to be a regional zonation across the Kakamas Terrane from higher grade in the west to lower grade in the east (Johnson et al., 2006). Evidence of the retrograde M_3 metamorphic event is seen by late growth of biotite and chlorite, often at the expense of garnet (van Bever Donker, 1980; Moen, 2007).

2.4.2 Geochronology

Regional mapping in the Kakamas Terrane of the Namaqua-Natal Province (NNP) has led to the identification of a large number of granitoids and metasedimentary rocks. Mapping along the Orange River led to a classification of metasedimentary rocks and granitoids based on foliation and deformation history (van Bever Donker, 1980, 1991; Moen, 2007). Although the concepts of pre-, syn- and post- tectonic events relative to the Namaqua-Natal orogeny are still applicable, the structural classification has proved to be unreliable in several cases because different rocks had responded differently to the stress fields during intrusion and deformation (Cornell et al., 2012).

The Namaqua Wilson Cycle extended from 1370 to 900 Ma (Cornell et al., 2012). The main orogenic period started about 1220 Ma with the collision of the Areachap, Kakamas and Bushmanland Terranes with the Kaapvaal-Rehoboth Craton, marked by the end of arc-related volcanism and the first metamorphic ages of Lu-Hf analysis of zircon between 1204 and 1190 Ma (Cornell et al., 2012). Tectonically thickened crust in the Kakamas Terrane heated up due to collision, leading to 1165 to 1142 Ma migmatisation and melting in the lower crust, which gave rise to granitoids ranging in age between 1151 ± 14 and 1156 ± 8 Ma (Cornell et al., 2012), which also corresponds to the age found by Pettersson (2008) in the Kakamas Terrane using various approaches such as U-Pb and Sm-Nd dating techniques. Pettersson (2008) and Cornell

et al. (2012) have shown that although some Mesoproterozoic crustal extraction from the mantle did occur, the mantle extraction responsible for crustal growth was mostly Palaeoproterozoic, with additional evidence for the former presence of Archean crust (Kaapvaal Craton). This could be due to the Kakamas Terrane been thrust over the Kaapvaal Craton and Rehoboth Province during the collisional events (Cornell et al., 2012). The Kaapvaal Craton basement is older than 2700 Ma and the Rehoboth Province probably comprises Archean and Palaeoproterozoic components (Cornell et al., 2011). These old crustal blocks became the lower crustal basement to the Kakamas Terrane and contributed material with old crustal residence ages.

The concepts of pre-, syn- and post- tectonic events are viable in the Kakamas Terrane where the granitoids are divided into three clusters relative to the ~1220 Ma collision events according to Cornell et al. (2012): (1) the pre-tectonic cluster has ages of 1371 to 1220 Ma and mainly comprises various granite intrusions (Figure 2.2), (2) the syn-tectonic cluster with ages of 1203 to 1146 Ma comprise mainly granitoids, and (3) the post-tectonic cluster has ages between 1113 and 1078 Ma and include the charnockite and the bimodal volcanic rocks of the upper Koras Group which are about 10 Ma older than the Umkondo intrusions, and certainly reflect melting of already hot mantle (Cornell et al., 2012), in response to late Namaqua dextral transcurrent shear movements (Thomas et al., 1994a). A common feature of felsic-mafic hybrids is observed in the charnockite of the Kakamas Terrane (Cornell et al., 2012).

2.5 Geology of the study area

The study area constitutes the southern portion of the Neusberg Mountain Range (Figure 2.5). It is delineated to the west by the Neusspruit Shear Zone, and to the east it is demarcated by intrusive charnockitic rocks (Figure 2.5). To the north, the study area is bordered by the R359 gravel road linking the towns of Kakamas and Neilersdrift (Figure 2.5). The Neusspruit and the Kameeldoring are the two non-perennial rivers in the study area. These rivers are both tributaries of the Orange River. The geology of the study area is given in the geological map in

Figure 2.5, where the Neusberg Mountain Range and Vuurkop Mountain are characterized by the metasedimentary rocks of the Goede Hoop (feldspathic mica-rich quartzite) and Puntsit (calc-silicate-rich quartzite) Formations (Figure 2.5). The granitic leucogneiss, pink gneiss, augen gneiss, and charnockite outcrop with, or in association with, or close to the metasedimentary rocks. The contact rocks (skarn, wollastonite-bearing calcareous rock and biotite gneiss) are found in various places in the study area (Figure 2.5).

2.5.1 Structure and metamorphic events

The study area is part of the southern extension of the Neusberg Mountain Range, which is located south of the Orange River (Figure 2.5). It is important to mention that the primary bedding (S_0) readings are reported in this study, and sedimentary structures such as cross-beddings are preserved locally. Four deformational events have been identified in the study area, where the first deformational event (D_1) is the most prominent and dominant phase in the study area due to continued deformation during the Namaqua Orogeny, which characterizes the entire shape developed by the Neusberg Mountain Range. It resulted in the formation of folds at various scales and boudins. Lineations are represented by elongated pebbles with NW-directed long axes parallel to the pervasive foliation S_0. The second phase of deformation (D_2) is represented by thrusting in the Neusberg Mountain Range. Such deformation has been identified leading to the formation of breccia, kink bands, and kink folds. The third deformational event (D_3) is illustrated by strike-slip faulting along the Neusberg Mountain Range. The last deformational event (D_4) is easily identified in the charnockite, whereby the uplift and exhumation of the charnockite shows evidence of brittle deformation, as seen by crosscutting fractures and joints. The joints in the charnockite commonly display mineralization of epidote or piemontite.

The study area has been subjected to various metamorphic events, where the first metamorphic event (M_1) is related to the regional metamorphism (Moen, 2007). This event is rarely identified as it is overprinted by the subsequent upper amphibolite/granulite event

(Moen, 2007). The second event (M_2) is linked to high grade of upper amphibolite to granulite facies metamorphism (van Bever Donker, 1980; Moen, 2007). The metamorphic conditions were estimated at 700-800 °C and 4-5 kbar (Moen, 2007). This reflects contact metamorphism, with the emplacement of magmatic rocks and the development of contact rocks in the study area (Figure 2.5). The third metamorphic event (M_3) is a retrograde metamorphic event illustrated by the presence of epidote in the joints crosscutting the charnockite indicating hydrothermal fluid mineralization possibly during the exhumation of the charnockite.

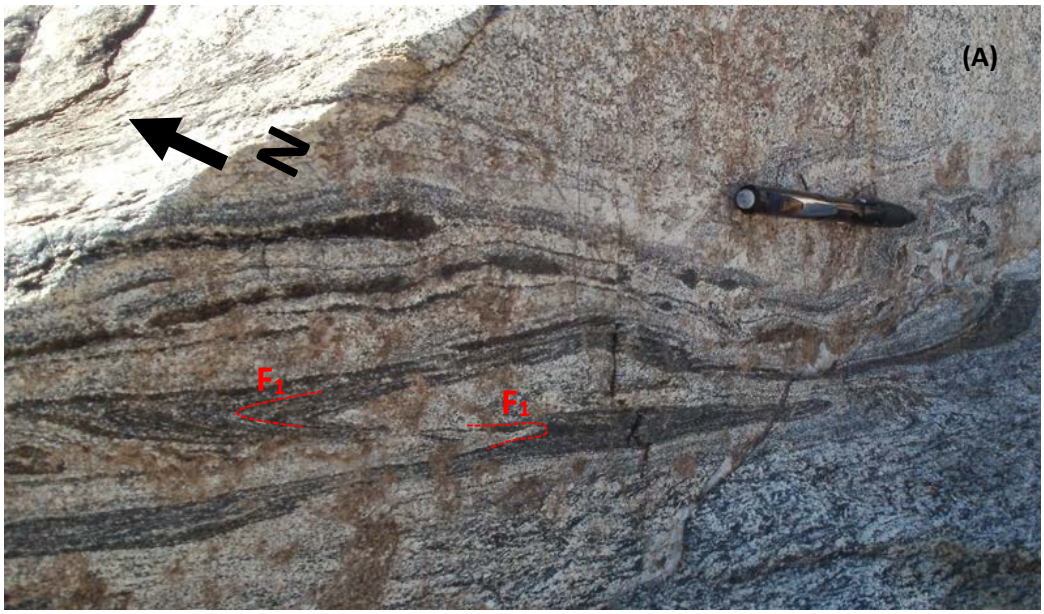

Figure 2.3: Northwest trending shear zone displaying remnant folds (F1) in red dotted lines along the Neusspruit Shear Zone.

2.5.2 Lithostratigraphy of the study area

At least 13 lithological units have been identified as comprising the stratigraphy of the study area near the Neusberg Mountain Range (Figure 2.4), south of the Orange River. The lithostratigraphy is subdivided from the oldest to the youngest, as estimated from field relationships. The units are subdivided from the bottom to the top into:

(1) The base of the lithostratigraphic column is composed of a number of various granitic gneisses associated to an intrusive rock namely the **augen gneiss**, **pink gneiss**, and **leucogneiss** respectively. The thickness of most of the units is unknown due to the fact that the boundaries of the units are not well exposed in the field. The stratigraphic and structural features in the study area are extensively exposed in meso-scale structures, with micro-scale structures inherently apparent using a microscope.

(2) The Mesoproterozoic units of the Korannaland Group are classified as follows (Figure 2.4): The uppermost unit in the succession is the feldspathic mica-rich quartzite of the **Goede Hoop Formation**, wherein the igneous contact with the charnockite is marked by biotite gneiss. This unit is underlain by a calc-silicate rich quartzite intercalated with amphibole schist and is associated with metasomatic units (skarn and wollastonite-bearing calcareous rock) due to the intrusion of the charnockite. The calc-silicate-rich quartzite belongs to the **Puntsit Formation** of the Biesje Poort Subgroup. In addition, there is a rock with an intrusive character, the late- to post-tectonic charnockite of the Keimoes Suite (Moen, 2007). Based on the field-determined age relationships, the charnockite is younger than the Korannaland Group as it intruded the Korannaland Group (Figure 2.5). A number of various contact rocks namely the **wollastonite-bearing calcareous rock**, **skarn**, and **biotite gneiss** were affected by contact metamorphism and metasomatism due to the intrusion of the **charnockite**.

(3) The **Quaternary sand** units, composed of river and aeolian deposits, which are the youngest units in the study area in terms of the relative ages as they are loose, unconsolidated sediments that still need to be lithified and are actively being deposited.

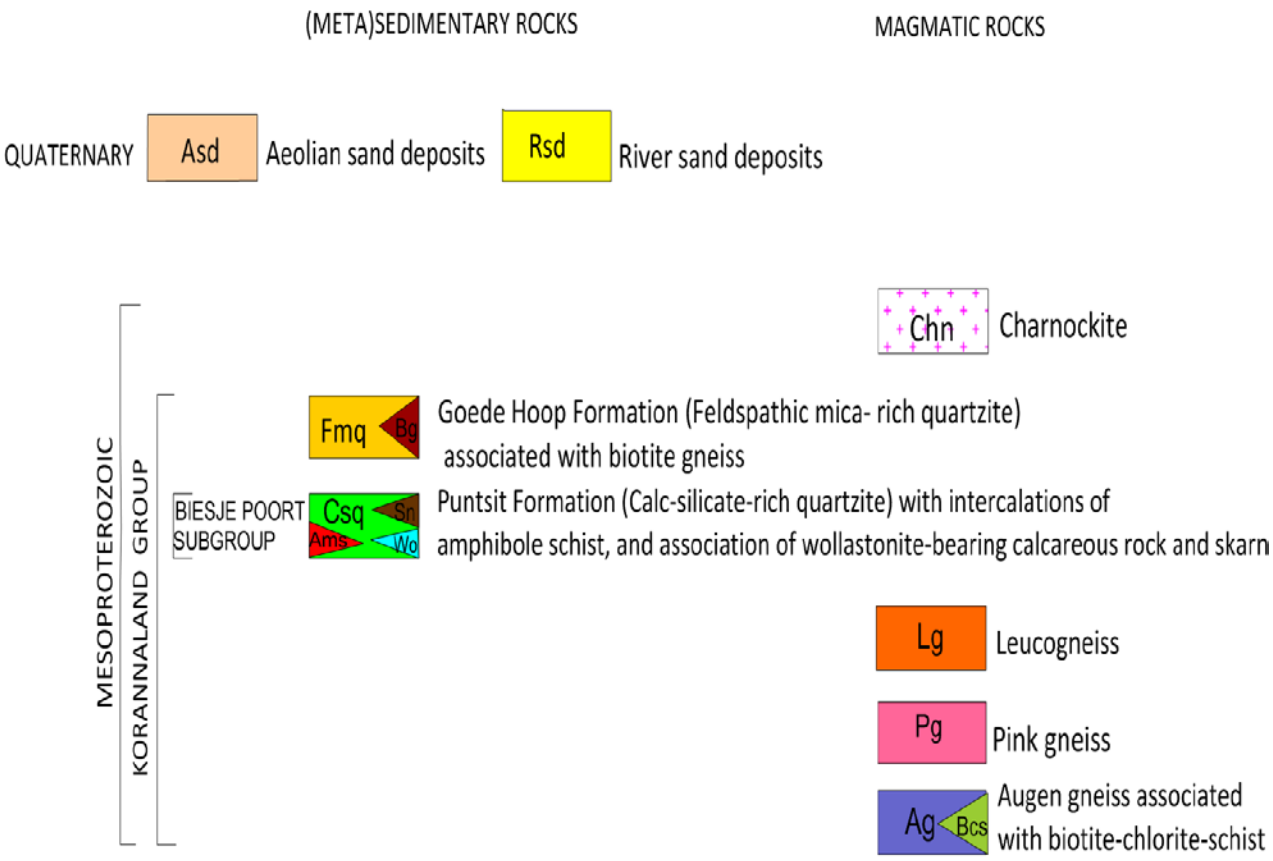

Figure 2.4: Lithostratigraphic column of the study area.

Table 2.1: Contrasting lithostratigraphic subdivisions of the southern Neusberg Mountain Range in the central part Kakamas Terrane according to Moen (2007) and van Bever Donker (1980)

							Moen (2007)				van Bever Donker (1980)	
Rocks type	**Formation**	**Lithology**	**Deformation**	**Metamorphic grade**	**Age (Ma)**	**Terrane**	**Group**	**Subgroup**	**Formation**	**Lithology**	**Formation**	**Lithology**
Metasedimentary rocks	Goede Hoop	Feldspathic mica-rich quartzite	D_1-D_2-D_3-D_4	Regional to contact	1220-1150	Kakamas	Korannaland		√	√	Neusberg	Neuspoort
	Puntsit	Calc-silicate-rich quartzite with intercalations of amphibole schist	D_1-D_2-D_3-D_4	Regional to contact				Biesje Poor	√	√		Baviaans krantz banded calc-silicate quartzite
Granitic gneisses		Augen	D_1-D_3	Regional								
		Biotite-chlorite-schist	D_1-D_3	Regional								
		Pink gneiss	D_3	Regional						Riemvasmaak gneiss		
		Leucogneiss	D_3	Regional								Wolfskop biotite gneiss
Intrusive rocks		Charnockite	D_4	Regional to contact	1113-1078					√		√
Contact rocks		Biotite gneiss		Contact								
		Skarn		Contact								
		Wollastonite-bearing calcareous rock		Contact								√

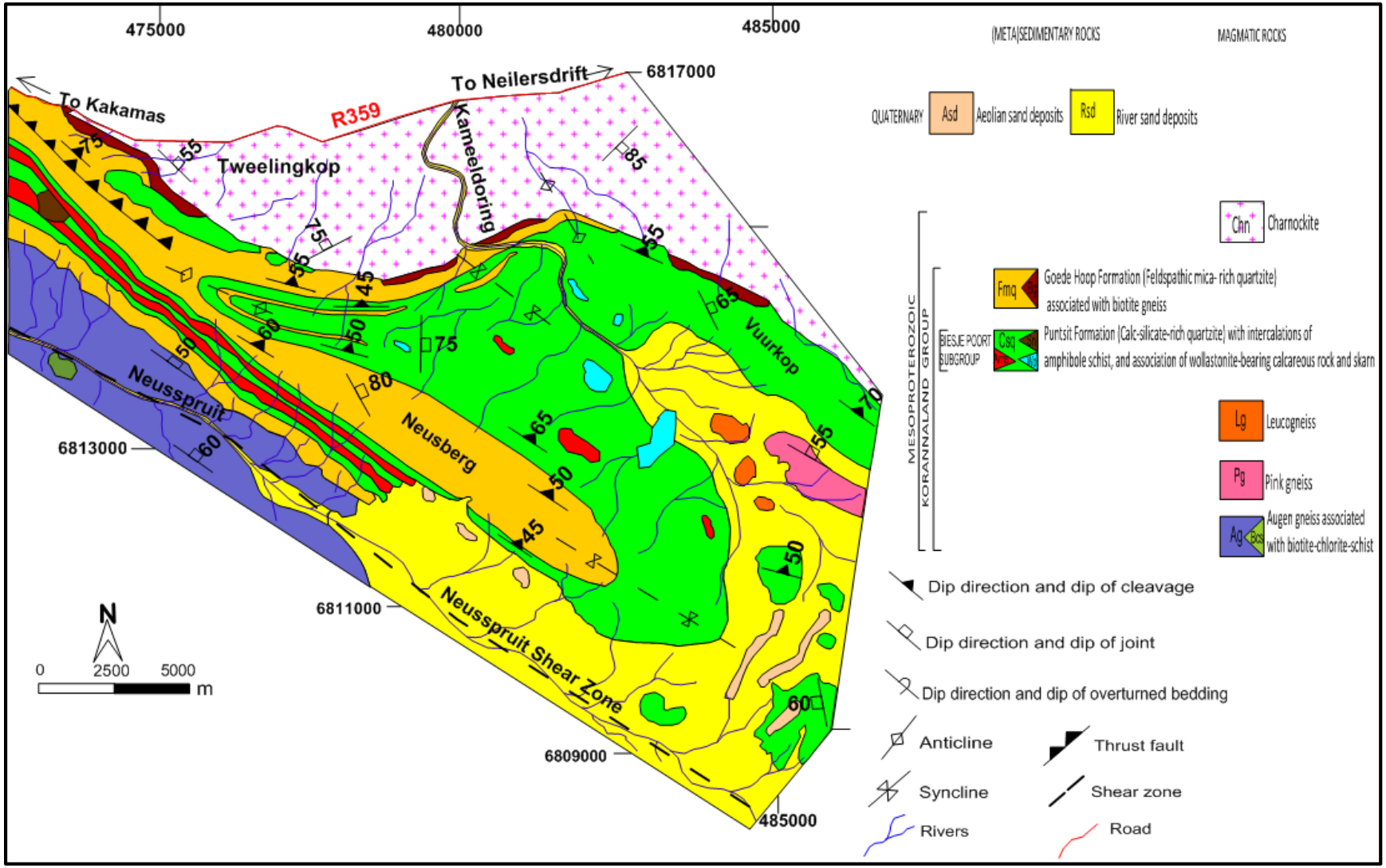

Figure 2.5: Geological map of the study area with location of the samples.

CHAPTER 3

PETROGRAPHY

3.1 Representative samples

The rocks in the area under investigation consist of metasedimentary rocks, granitic gneisses, metasomatised contact and hybrid rocks, and an intrusive granitoid rock. The granitoid forms a prominent hill called Tweelingkop, and extends to the north, northeast and east in the study area (Figure 2.5). The metasedimentary rocks of the Korannaland Group are widespread in the study area where they are consistently trending northwest and dipping northeast. The metasomatised and hybrid rocks occur locally within the metasedimentary rocks and at the contact with the granitoid.

Various samples (20 in total) were selected for petrographic examination with the two-fold aim of firstly determining the mineralogy of the rocks and secondly understanding the deformation recorded in the minerals. An attempt is made to determine the protolith of each unit petrographically, so as to facilitate the correct interpretation of the geological history of the area. An approximate metamorphic grade of each rock type is determined while doing this analysis. All features observed in the thin sections are identified and described. These descriptions have been ordered according to the lithostratigraphy of the rocks in the study area (Figure 2.4). The rocks are described as they appear in the field and hand specimen, as well as microscopically. Some mineral abbreviations are adopted for this study and others are in accordance with Schmid et al. (2007).

3.2 Lithostratigraphic description of the rocks in the study area

A comprehensive description of the various lithological units is developed to serve as a basis for the rock analysis in the study area. Due to the ongoing process of deposition of Quaternary sand in the study area, the sand deposits are described first prior to the metasedimentary

rocks, contact rocks, granitic gneisses, and intrusive rock. The metasedimentary rocks are described from the youngest to the oldest, where the feldspathic mica-rich quartzite is considered to be the youngest unit in the Korannaland Group (Figure 2.5).

3.3 Korannaland Group

In accordance with the recommendation of SACS (1980), the Korannaland Group, formerly known as the Korannaland Supergroup, was downgraded to group status to bring it in line with other units of similar rank (Moen, 2007). The Korannaland Group lies in the hanging wall of the Hartbees River Thrust Zone (Humphreys et al., 1991), a westerly vergent nappe pile that marks the boundary between the Gordonia Subprovince and the Bushmanland Subprovince (Joubert, 1986; Harris, 1988). The Korannaland Group is restricted to the Gordonia Subprovince and occurs as a northwest-trending belt, which extends from an area north of Kenhardt to the eastern boundary of the Riemvasmaak area where it disappears under undeformed sediments of the Neoproterozoic Nama Group (Moen, 2007). The metasedimentary rocks of the Korannaland Group are represented by the Biesje Poort Subgroup, which is overlain by the Goede Hoop Formation, considered the youngest formation of the Korannaland Group (Moen, 2007).

3.3.1 Metasedimentary rocks

3.3.1.1 Feldspathic mica-rich quartzite (Fmq)

Outcrop to hand specimen description

The term feldspathic mica-rich quartzite is adopted for these rocks, which are similar to the Goede Hoop Formation in composition as well as appearance (Geringer, 1973; Moen, 2007). The feldspathic mica-rich quartzite builds prominent linear ridges to the east of the Neusspruit Shear Zone (Moen, 2007). It is the youngest formation of the Korannaland Group and overlies

the Biesje Poort Subgroup, which is represented in the study area by the calc-silicate-rich quartzite, which has intercalations of amphibole schist, and is known as the Puntsit Formation (Moen, 2007). No Mesoproterozoic rocks are known to overlie the feldspathic mica-rich quartzite in the study area.

Primary sedimentary structures, such as cross-bedding (Figure 3.2), have been preserved despite the intense deformation in the study area. Kink folds are partly developed in the feldspathic mica-rich quartzite (Figure 3.1A). Joints of up to 5 m length are present in some places. Some joints crosscut (Figure 3.1B), and are filled, in places, with quartz veins varying from a few millimeters to meters in length. The feldspathic mica-rich quartzite is intruded by the charnockite, whereby the contact or reaction zone between the feldspathic mica rich quartzite and charnockite, particularly to the north of Vuurkop Mountain (Figure 2.5) is comprised of biotite gneiss.

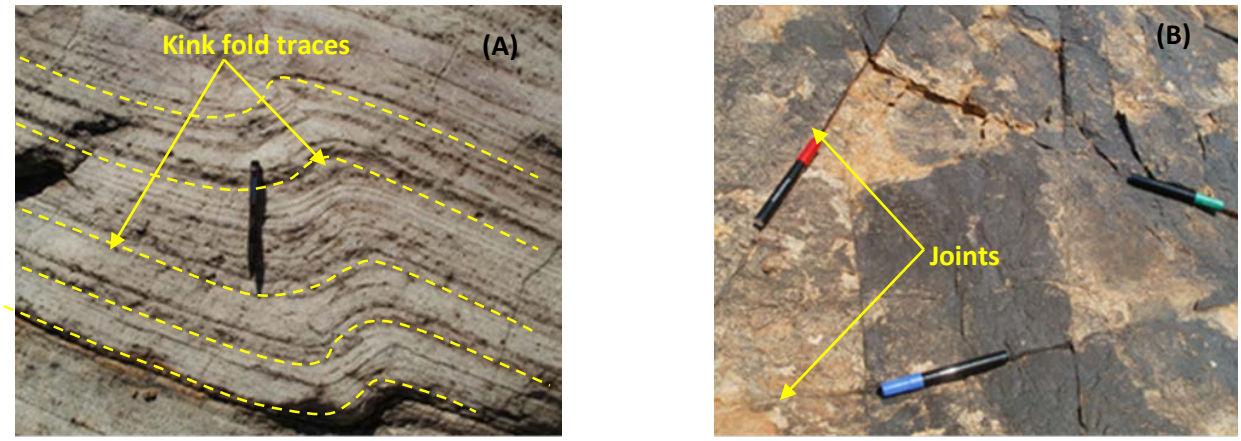

Figure 3.1: A) Kink folds in the feldspathic mica-rich quartzite. B) Feldspathic mica-rich quartzite crosscut by joints.

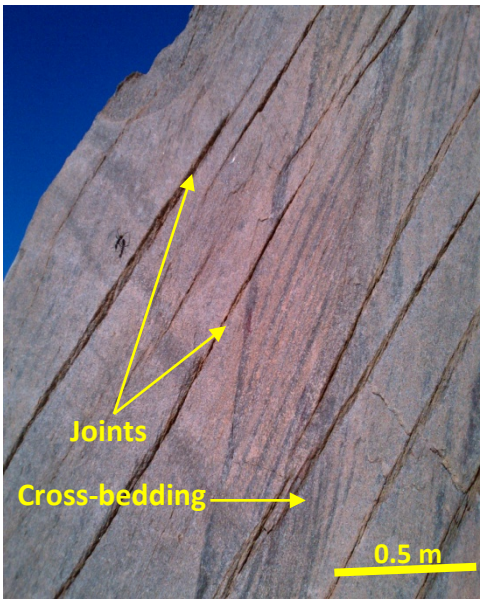

Figure 3.2: Outcrop of feldspathic mica-rich quartzite showing cross-bedding and joints.

By definition, breccias are fault rocks composed of angular fragments or clasts of rock set in a finer-grained matrix of crushed wall rock material (Davis and Reynolds, 1996). They have been identified in the north of the study area, as a marker of the Neusberg Thrust Fault (Figure 2.5). The breccia clasts in the field are mainly composed of feldspathic mica-rich quartzite (Figure 3.3).

Breccia classification has four main varieties based on the size of clasts (Twiss and Moores, 1992; Davis and Reynolds, 1996; Fossen, 2010). According to the classification schemes, and the observations made in the field, it appears that the size of the clasts corresponds to the interval 1 mm < clast size < 0.5 m. This confirms that the clasts of the feldspathic mica-rich quartzite observed along the western side of the Neusberg Mountain Range (NMR) correspond to the breccia variety (Figure 3.3). The presence of the breccia reflects a brittle deformation event related to the development of the Neusberg Thrust Fault and is linked to the third deformational event (D_3) in the study area.

Figure 3.3: Breccia showing a mixture of fragments of feldspathic mica-rich quartzite.

Pebbles identified in this formation have been preserved despite the strong deformation in the area. Flattened and fractured pebbles of quartz have their long axis oriented in the northwest-southeast direction (Figure 3.4A). Weathering patterns are observed in the rocks in certain places (Figure 3.4B).

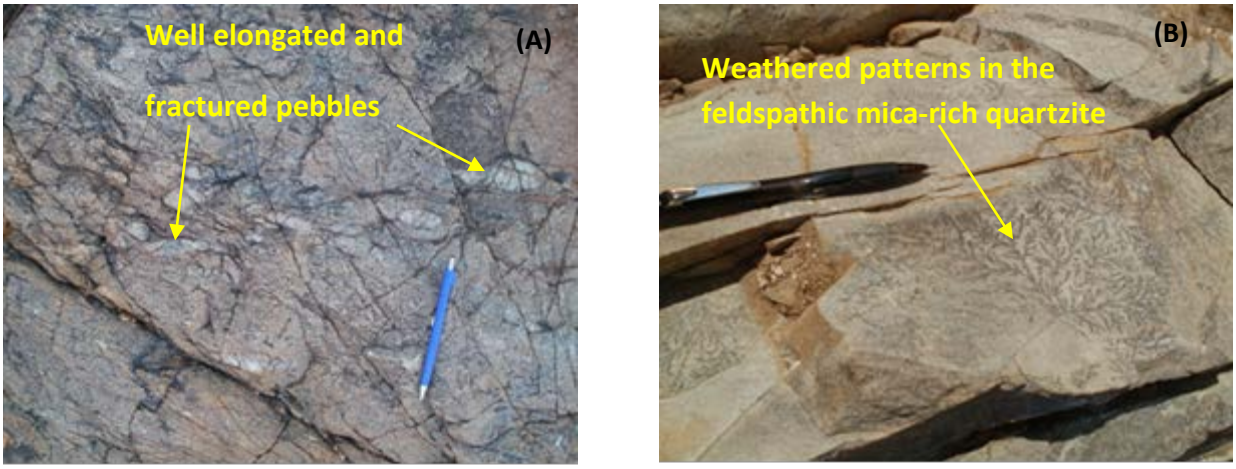

Figure 3.4: A) Strongly deformed, elongate and fractured pebbles in the feldspathic mica-rich quartzite unit. B) Weathering patterns in the feldspathic mica-rich quartzite.

Microscopic description

The thin sections of samples Fmq S7, Fmq S8, and Fmq S271 of the feldspathic mica-rich quartzite are composed of quartz grains as a major mineral constituting about 40vol.% of the rock volume. Other minerals are: orthoclase (31vol.%), muscovite (23vol.%), plagioclase (3vol.%), perthite (2vol.%) and opaques (1vol.%). The shape of the grains is generally subhedral to anhedral, and the overall texture of the grain aggregates is mostly granular (Figures 3.5A and B). The schistosity is weakly developed and the deformational texture in the feldspathic mica-rich quartzite is illustrated by strongly interlocking minerals suggesting intense phases of deformation and recrystallisation.

Quartz grains are colourless with an anhedral shape, and are of approximately 0.05-0.4 mm in size. Recrystallization features, such as intergrowth boundaries, and inclusions of muscovite are present. Some grains of quartz show weak to moderate undulose extinction. **Orthoclase** grains are randomly distributed (Figure 3.4A). They appear colourless, subhedral in shape, and are about 0.3-1 mm in size. Minor perthitic exsolution appear within the orthoclase. These occur as medium grained porphyroblasts (0.1-0.6 mm in size), anhedral to subhedral in shape, and with varying degrees of alteration into both sericite and clay minerals. The grain boundaries of the alkali feldspar are weakly curved, and the porphyroblasts of orthoclase are partially replaced by sericite. **Muscovite** appears as disseminated colourless flakes of about 0.8-1.5 mm size. The muscovite grains are in contact with quartz grains and opaque minerals. **Plagioclase** grains are anhedral in shape, and are about 0.3-0.8 mm in size in the groundmass. Porphyroblasts of 1.1-1.9 mm in size display vague twinning and form interlocking textures with grains of orthoclase. The plagioclase has been moderately subjected to sericitic alteration. **Perthite** grains are anhedral to subhedral and form small to medium porphyroblasts of about 0.2-1 mm in size. Smaller anhedral grains of perthite are found within the groundmass (0.02-0.08 mm). Perthite grains are extensively altered to sericite in some places. **Opaques** are accessory minerals, with euhedral shape. They are in contact with muscovite and orthoclase.

The presence of the cross-bedding in the feldspathic mica-rich quartzite suggests a sedimentary precursor.

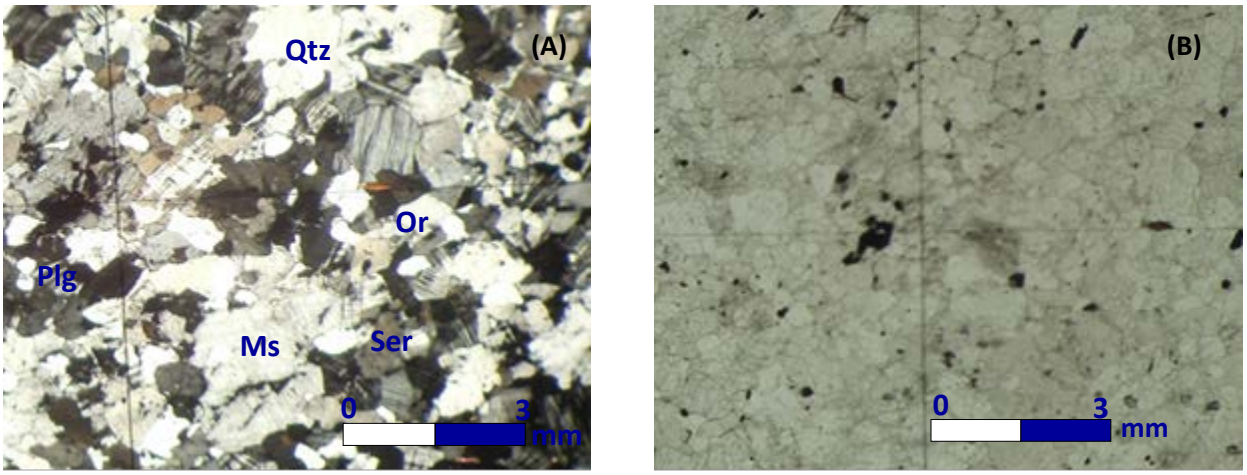

Figure 3.5: Photomicrographs of the feldspathic mica-rich quartzite displaying a granoblastic texture. Abbreviations: Qtz= Quartz; Or= Orthoclase; Ms= Muscovite; Plg= Plagioclase; Ser= Sericite. A) Crossed polars; B) Plane polarized light.

Interpretation

Cross-bedding is commonly preserved in the feldspathic mica-rich quartzite but is not easily identifiable, probably due to obliteration and overprinting by the different deformational phases that occurred in the study area. The presence of kink folds (Figure 3.1A) in the study area is interpreted to be as a result of an intense ductile deformation event. The undulatory extinction observed in quartz reflects partial recovery from the ductile deformation events in the study area. The development of joints and thrust faulting in the study area is the result of brittle deformation in the study area. The presence of orthoclase and quartz are generally useless for indicating metamorphic grade, except that the presence of muscovite indicates low to medium grade metamorphism but cannot exclude higher grade of metamorphism (Frey and Robinson, 1999).

3.4 Biesje Poort Subgroup

The term "Biesje Poort Formation" was first introduced by Geringer (1973) for a succession consisting mainly of calc-silicate-rich quartzite rocks. Subsequent workers (van Bever Donker, 1980; Slabbert, 1987; Slabbert et al., 1999) have shown a close relationship amongst the calc-silicate-rich quartzite rocks and the rocks resulting from contact metamorphism, of which rocks, such as the skarn and prominent wollastonite-bearing calcareous rock, are prominent. The number and complexity of the interrelated units led to the upgrading of the "Biesje Poort Formation" to the subgroup status (Moen, 2007).

3.4.1 Calc-silicate-rich quartzite (Csq) with intercalation of amphibole schist (Ams)

Outcrop to hand specimen description

The Calc-silicate-rich quartzite with intercalation of Amphibole schist is similar to the Puntsit Formation, as described by Moen (2007). It was first described as "granulite containing lenses of calc-silicate rock" by von Backström (1964), while van Bever Donker (1980) referred to it as the "Baviaanskrantz banded calc-silicate-rich quartzite". The calc-silicate-rich quartzite is intercalated with amphibole schist in the Neusberg Mountain Range and is overlain by the feldspathic mica-rich quartzite. The calc-silicate-rich quartzite on Koekoeb farm can be traced around the northern and southern closures of the Neusberg Mountain Range, and builds the topmost unit of Vuurkop Mountain (Figure 2.5), where it forms a rocky ridge.

The Calc-silicate-rich quartzite with intercalation of Amphibole schist, in the study area has dip direction NW-SE and dips to the NE. The calc-silicate-rich quartzite is weakly to moderately foliated, and shows a parting at irregularly spaced intervals parallel to the foliation. The contact between the calc-silicate-rich quartzite and amphibole schist is not clear due to the fact that the dark weathering colour at the surface of the calc-silicate-rich quartzite (Figure 3.6A) makes it difficult to differentiate it from the amphibole schist in the field. The unweathered amphibole schist is, however, brown to dark green in colour, whereas the calc-silicate-rich quartzite varies

in colour from light grey or green to almost white on fresh surfaces (Figure 3.6B). The amphibole schist is moderately cleaved with bands varying in thickness from a few millimetres to about 2 cm. Primary sedimentary structures are not observed in the amphibole schist, compared to the overlying feldspathic mica-rich quartzite.

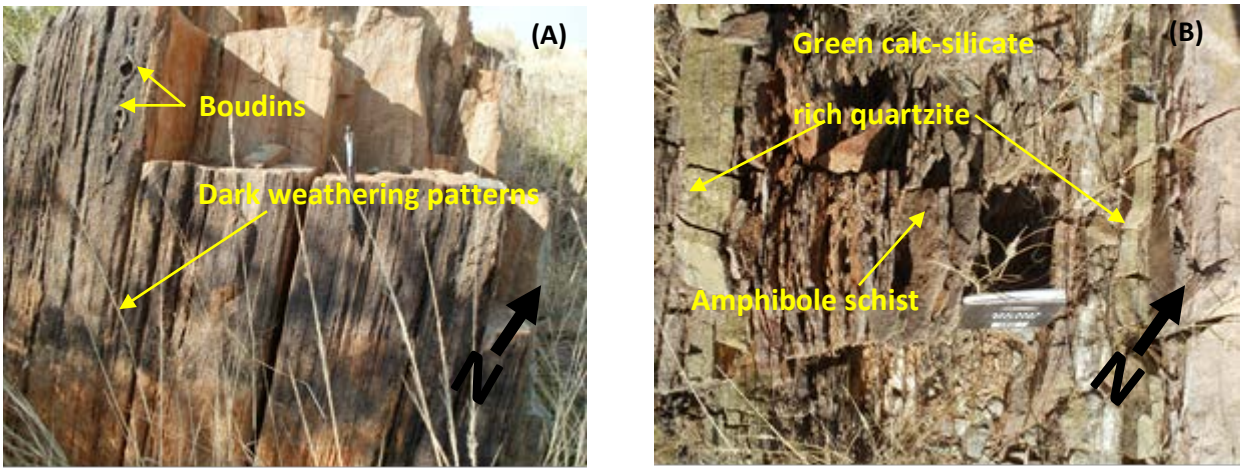

Figure 3.6: A) Dark weathering surface of the calc-silicate-rich quartzite displaying boudins with their long axis oriented in the same direction as the plane of foliation. B) Green layers of calc-silicate-rich quartzite intercalated with brown amphibole schist.

Some spots of white to brown wollastonite-bearing calc-silicate-rich quartzite are found south of the Neusberg Mountain Range and on Vuurkop Mountain (Figure 2.5). Furthermore, a skarn is also observed west of the Neusberg Mountain Range (Figure 2.5). Some structures have been observed in this lithology, where the competency contrast between the carbonate and the enclosing silicate-rich rock has given rise to intense small scale folds in the calc-silicate-rich quartzite with their fold axes parallel to each other and oriented NW-SE. The pronounced pinch-and-swell morphology or boudinage and tight fold appearance within the calc-silicate-rich rocks occur west of the Neusberg Mountain Range along the Neusspruit Shear Zone (Figure 3.7A). Mesoscopic folds are displayed at the base of the Vuurkop Mountain Range and some are locally crosscut by fractures (Figure 3.7B). Localised spots of amphibole schist are found between Vuurkop Mountain and the Neusberg Mountain Range.

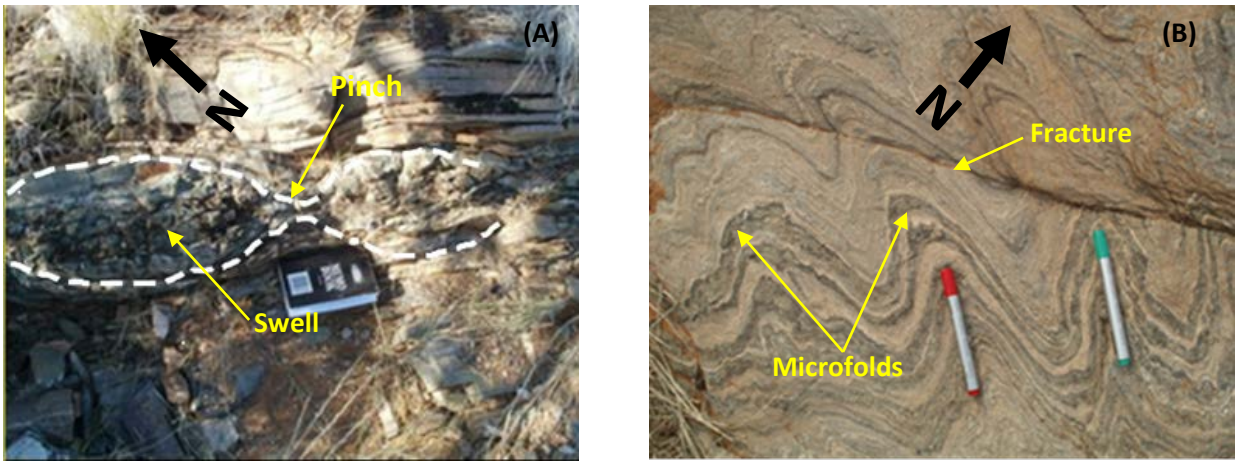

Figure 3.7: A) Pinch and swell displayed in the calc-silicate-rich quartzite layer on Vuurkop Mountain. B) Microfolds in the calc-silicate layer, with the fold axis shown by the markers and orientated NW-SE.

Microscopic description

Samples Csq S48 and Csq S465 of the calc-silicate-rich quartzite are chiefly composed of quartz grains of about 1.2 to 1.5 mm in size comprising about 40vol.% of the rock volume. Other minerals are: calcite (21vol.%), orthoclase (14vol.%), epidote (9vol.%), plagioclase (8vol.%), allanite (6vol.%), opaques (1vol.%) and accessory mineral such as zircon (below 1vol.%). The shape of the grains is generally subhedral to anhedral, and the grain aggregates have a granular texture (Figures 3.8A and B).

Quartz occurs as colourless grains with undulose extinction. Quartz grains are about 0.02-0.3 mm in size and display polygonal texture. Recrystallization features are present. **Calcite** grains appear subhedral to anhedral in shape and are about 0.5-0.8 mm in size and can reach 1.3 mm at the largest. Minor talcose alteration is present. The boundaries locally display a straight calcite-alkali feldspar boundary. Long axes are generally oriented in one direction which is prevalent only in the more elongate calcite grains. Twinning lamellae are present in the calcite. **Orthoclase** occurs as large subhedral to anhedral grains about 1-5 mm in size. Alteration of orthoclase to sericite has occurred to varying degrees along cleavage planes. Long axes are aligned parallel to the foliation direction in the rock. Orthoclase grains are in contact with

calcite. **Plagioclase** is subhedral in shape and approximately 0.3-1.3 mm in size. Larger plagioclase laths up to 2.7 mm in size are also present. Plagioclase grains are sericitised to varying degrees. **Epidote** grains occur as the Fe-rich variety, and are pleochroic green to olive green, subhedral to anhedral in shape and about 0.1-0.3 mm in size. They are in contact with calcite. **Allanite** appears as pale to dark brown grains with anhedral shape of about 0.2-0.3 mm in size. They are pleochroic with inclined extinction and are found in contact with orthoclase or quartz. **Opaque** grains are euhedral in shape, and about 0.2-2 mm in size. They are in contact with quartz and epidote.

The mineral assemblage of quartz + calcite + alkali feldspar + epidote suggests an impure siliceous carbonate as protolith (Philpotts and Ague, 2010).

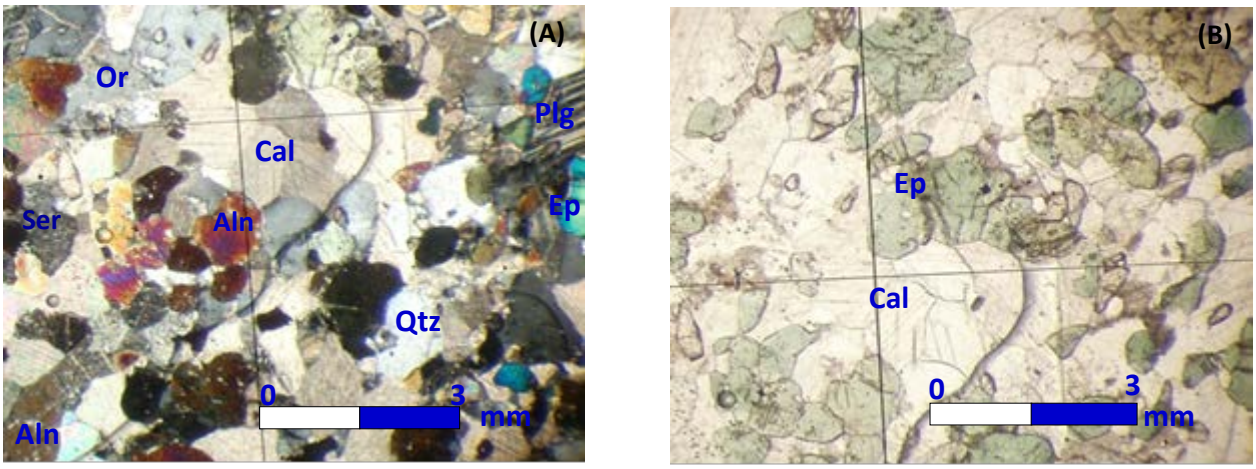

Figure 3.8: A) Photomicrographs of the calc-silicate-rich quartzite displaying sets of deformation twins in calcite (crossed polars). B) Calc-silicate-rich quartzite showing granular green epidote (plane polarized light). Abbreviations: Aln= Allanite; Cal= Calcite; Ep= Epidote; Or= Orthoclase; Plg= Plagioclase; Qtz= Quartz; Ser= Sericite.

Microscopic description

The thin sections of samples Ams S15 and Ams S481 of the amphibole schist are composed of hornblende grains constituting about 50vol.% of the rock volume. Other minerals are:

plagioclase (18vol.%), quartz (11vol.%), biotite (8vol.%), epidote (6vol.%), enstatite (4vol.%), opaques (2vol.%), and zircon (below 1vol.%). The grains are mainly subhedral to anhedral in shape (Figures 3.9A and B), and display well aligned minerals (schistosity texture).

Hornblende is subhedral in shape, with larger laths of about 2-5 mm in size. Hornblende grains are pleochroic displaying a light olive green to dark green colour. They are elongated parallel to the plane of foliation, and contain inclusions of opaques. Hornblende grains are in contact with enstatite, biotite, orthoclase and opaques. **Plagioclase** occurs as anhedral to subhedral grains of about 0.5-3 mm size. Extensive sericitic alteration is present along cleavage planes. Long axes are aligned parallel to foliation. **Quartz** appears as colourless subhedral to anhedral grains of approximately 0.5-1 mm size. Quartz grains display weak undulose extinction. **Biotite** occurs as flakes oriented parallel to the foliation plane. Biotite grains are euhedral to subhedral in shape and about 0.1-0.3 mm in size. Biotite grains show brown to light green pleochroism. They are in contact with hornblende, orthoclase, enstatite and opaques. **Epidote** is anhedral to subhedral in shape and about 0.1-0.2 mm in size. Epidote grains are pleochroic and display dark grass green to olive green colour. They occur between the parallel and elongated grains of hornblende. **Enstatite** appears as anhedral to subhedral grains of approximately 0.4-1.3 mm size. Enstatite grains are pleochroic and show brown to tan brown colour. They occur along the foliation plane and appear to overgrow the hornblende. Enstatite grains are in contact with biotite and orthoclase. **Opaque minerals** are abundant and occur as euhedral to subhedral grains of about 0.09-2 mm in size. In some places, skeletal masses (of about 1 mm in size) of opaque grains are associated with biotite and hornblende and enstatite along the foliation plane. **Zircon** is euhedral to subhedral in shape and about 0.05-0.095 mm in size. The zircons are colourless in transmitted light. They are found aligned in the plane of foliation.

The mineral assemblage of hornblende + enstatite + biotite + quartz + orthoclase + plagioclase in the amphibole schists may suggest either a mafic magmatic or mafic sedimentary origin.

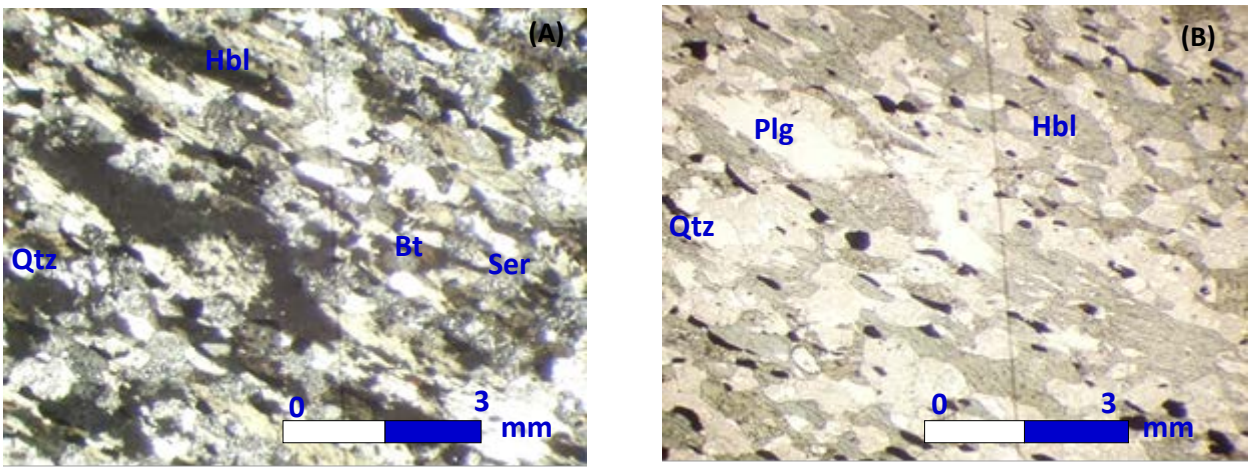

Figure 3.9: A) Photomicrograph of the amphibole schist showing a penetrative foliation (crossed polars). B) Photomicrograph of amphibole schist showing well elongated grains of hornblende (plane polarized light). Abbreviations: Plg= Plagioclase; Bt= Biotite; Hbl= Hornblende; Qtz= Quartz; Ser= Sericite.

Interpretation

The parallel alignment of the long axes of the orthoclase grains in the calc-silicate-rich quartzite relative to the plane of foliation implies either mechanical rotation into that plane or recrystallization into a preferred orientation. At high grade metamorphic conditions, dislocation glide is important in calcite, and grain boundary migration increases in importance with increasing temperature (Passchier and Trouw, 2005). Grain boundary sliding and 'superplastic' behaviour may be important in calcite if the grain size is very small (Schmid et al., 1987). The calc-silicate-rich quartzites are theoretically good grade indicators, but in practice there may be difficulties with the mineral identification needed as the major reactions in them do not coincide with grade category boundaries (Frey and Robinson, 1999). The assemblage of calcite, orthoclase, plagioclase and quartz reflects lower to medium grade metamorphism (Frey and Robinson, 1999). The presence of epidote is indicative that the Ca in the calc-silicate-rich quartzite contributed to its formation.

The presence of penetrative foliation indicates that the amphibole schist underwent some degree of deformation. The presence of orthopyroxene is indicative that the Mg in the

amphibole schist got taken up for its formation. The occurrence of retrogressive reaction from the granulite facies to amphibolite facies is illustrated along the foliation plane by the hornblende overgrowing the pyroxene. The presence of epidote reflects greenschist metamorphic facies conditions in the amphibole schists (Bucher and Grapes, 2011).

Table 3.2: Petrographic characterization of the metasedimentary rocks and amphibole schist.

Lithology	Colour	Grain size	Mineralogy and abundance	Texture	Specific features	Metamorphic grade	Contacts	Foliation	Folds	Faults	Fractures	Joints
Feldspathic mica-rich quartzite (Fmq)	Light grey to yellow brown	Medium to coarse	Qtz (40%); Or (31%) Ms (23%); Plg (3%) Perth (2%); Op (1%)	Granular; Sericitised to varying degrees	Dendritic weathering patterns; Flattened pebbles	High grade	Not exposed; Contact zone	Well Foliated	Kink folds	Thrust fault	Fractured pebbles	Quartz-filled joints; Presence of conjugate sets of joints
Calc-silicate-rich quartzite (Csq)	Light grey; Green to white	Fine to medium	Qtz (40%); Cal (21%) Or (14%); Ep (9%) Plg (8%); Aln (6%) Op (1%); Zrn (approximately 1%)	Granular; Epidotised and serici tised to varying	Green streaks of epidote; Boudins; Dark weathering	High grade	Intercalation with amphibole schist	Weakly to moderately foliated	Tight folds	Shear fault Thrust fault	Fractured microfolds	Epidote-filled joints
Amphibole schist (Ams)	Brown to dark green	Fine	Hbl (50%); An (18%) Qtz (11%); Bt (8%) Ep (6%); Ens (4%) Op (2%); Zrn (approximately 1%)	Schistosity texture	Well cleaved	Medium to high grade	Very foliated within Csq	Penetrative foliation	None	Shear fault	Cracks along the plane of foliation	None

Abbreviations: Ams= Amphibole schist; Csq= Calc-silicate-rich quartzite; Fmq= Feldspathic mica-rich quartzite; An= Anorthite; Aln= Allanite; Bt= Biotite; Cal= Calcite; Ens= Enstatite; Ep= Epidote; Hbl= Hornblende; Ms= Muscovite; Op= Opaques; Or= Orthoclase; Plg= Plagioclase; Perth= Perthite; Qtz= Quartz; Zrn= Zircon.

3.5 Contact Rocks

3.5.1 Biotite gneiss (Bg)

Outcrop to hand specimen description

The biotite gneiss is located in the northern portion of the study area and constitutes the reaction zone between the feldspathic mica-rich quartzite and the charnockite. The reaction zone has been mapped for about 10 km in the study area (Figure 2.5). The biotite gneiss displays a mortar weathering surface pattern (Figure 3.10).

Figure 3.10: Biotite gneiss containing a mafic xenolith, displaying a mortar weathering surface.

The biotite gneiss is dark brown in colour. It is medium grained, and contains inclusions of feldspathic quartzite and elongated xenoliths of mafic composition of about 3 to 5 cm in size (Figure 3.10). The biotite gneiss contains flakes of biotite (Figure 3.11). The foliation is displayed by oriented platy minerals (mica) in the rock sample.

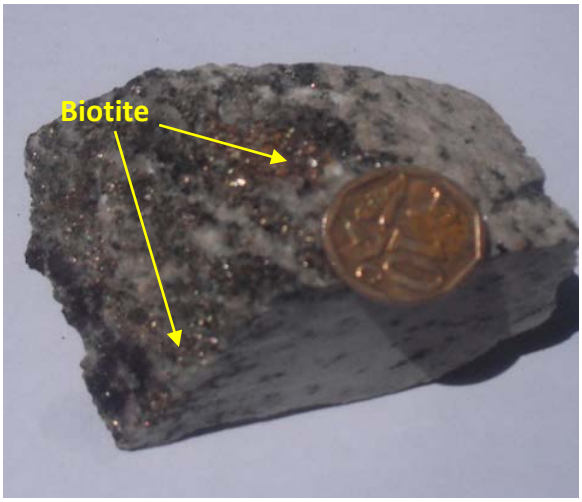

Figure 3.11: Sample of biotite gneiss showing biotite-rich patches. Scale is given by a coin of 1.7 cm diameter.

Microscopic description

Samples Bg S235 and Bg S422 of the biotite gneiss consist of biotite grains accounting for 40 % of the rock volume. Other minerals are: quartz (20vol.%), orthoclase (15vol.%), plagioclase (11vol.%), perthite (5vol.%), enstatite (4vol.%), hornblende (3vol.%), opaques (1vol.%), and piemontite (below 1vol.%) as an accessory mineral. The shape of the grains is generally subhedral to anhedral with the grain aggregates having a granular texture (Figures 3.12A and B). The foliation is defined by the alignment of both felsic and mafic minerals. The deformational texture in the biotite gneiss is shown by strong interlocking minerals displaying sutured boundaries.

Biotite grains are anhedral in shape and about 0.8-1.5 mm in size. The biotite grains are pleochroic red-brown to brown. The foliation is defined by the weak alignment of the biotite grains. Biotite grains are extensively chloritized, and are in contact with quartz and feldspar. **Quartz** grains are anhedral in shape, and variable in size, from sub-grains (0.02-0.09 mm), through larger grains (0.1-0.2 mm). They have interlocking boundaries and display moderate undulose extinction. Quartz grains are in contact with orthoclase. **Orthoclase** grains are cloudy

and anhedral to subhedral in shape. The orthoclase grains are 1.2 - 1.7 mm in size. Medium-grained bands (colourless, 1 mm width) of alkali feldspar and quartz occur within the rocks giving them a gneissic texture. The grain boundaries locally display a straight plagioclase-alkali feldspar boundary. Some grains of alkali feldspar are partially replaced by sericite. **Plagioclase** grains are subhedral in shape and are 0.2-0.5 mm in size. Larger laths up to 1.8 mm in size are also present. Some grains of plagioclase show myrmekitic intergrowth with quartz. The plagioclase grains occur in contact with orthoclase. Plagioclase grains are partially replaced by sericite (Figure 3.11A). **Perthite** appears as anhedral to subhedral grains and forms medium to large porphyroblasts of about 0.8-3 mm in size. Smaller anhedral grains of perthite are found within the groundmass (0.04-0.3 mm). Partial alteration of perthite grains to sericite is observed in the biotite gneiss. **Enstatite** grains are euhedral to anhedral in shape and of about 0.6-1 mm in size. Enstatite grains are seen locally. They are pleochroic and display a pale yellow brown to tan brown colour and are associated with biotite. Enstatite grains form a rim around opaque minerals (likely to be magnetite) and are in contact with biotite or hornblende. Fine inclusions (0.01 mm) of opaques are found within the enstatite grains. **Hornblende** grains are skeletal to subhedral in shape, and vary in size from 0.3-0.5 mm, through to larger grains (1.2 mm). Hornblende grains are pleochroic displaying a pale olive green to dark grass green colour, and are associated with biotite and opaques. In some places, inclusions of quartz of euhedral shape (0.05-0.09 mm in size) are found within the hornblende grains. Symplectic intergrowths with quartz are present in places. **Piemontite** appears as euhedral to anhedral grains displaying a dark red colour. Piemontite grains are about 0.7-1.5 mm in size. Numerous inclusions of opaques have been found within the piemontite grains, which is associated with biotite. **Opaque minerals** are euhedral to anhedral in shape. Opaque grains are found as inclusions within a number of minerals (biotite, enstatite and piemontite), and form part of the groundmass.

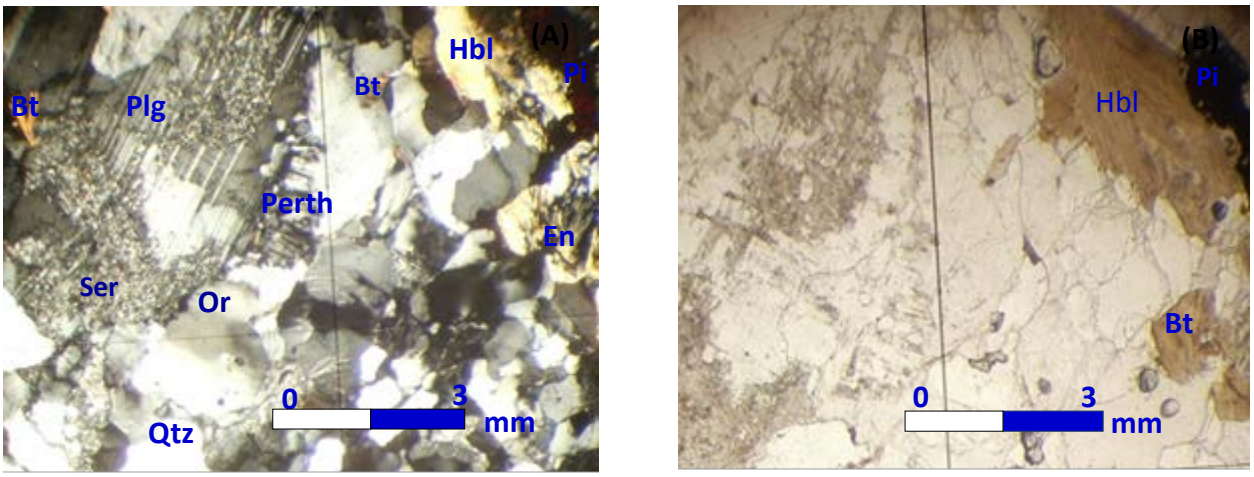

Figure 3.12: Photomicrographs of the biotite gneiss showing large grain of orthoclase and a cluster of biotite. Abbreviations: Bt= Biotite; En= Enstatite; Hbl= Hornblende; Or= Orthoclase; Plg= Plagioclase; Perth= Perthite; Pi= Piemontite; Qtz= Quartz; Ser= Sericite. A) Crossed polars; B) Plane polarized light.

Interpretation

The biotite gneiss appears to be a 'hybrid' or reaction zone between the intrusive charnockite and the metasedimentary feldspathic mica-rich quartzite. This is also supported by the presence of mafic xenoliths (Figure 3.10) in the biotite gneiss as observed also in the charnockite. The contacts between the charnockite and biotite gneiss and the biotite gneiss and feldspathic mica-rich quartzite are common in the field. The biotite gneiss in contact with the feldspathic mica-rich quartzite locally shows a less micaceous nature with a partially preserved foliation (Figure 3.12). The contact of the biotite gneiss with the charnockite locally shows the presence of mafic xenoliths similar to those observed in the charnockite. The occurrence of the biotite gneiss in the study area could be due to the fact that at the depth where the feldspathic mica-rich quartzite was intruded by the granitoid, the high grade metamorphic conditions were maintained, so that an ensuing reaction zone could be developed. A retrogressive reaction from the granulite facies to the amphibolite facies is identified in the biotite gneiss with the hornblende overgrowing the pyroxene.

3.5.2 Skarn (Sn)

Outcrop to hand specimen description

The word "skarn" is an old Swedish term that originally referred to the very hard rocks composed predominantly of calc-silicate minerals (Robb, 2005). It is also known as tactite (Winter, 2010). Skarn assemblages are typically the product of regional or contact metamorphism and metasomatism associated with the intrusion of granitoids into carbonate rocks (Winter, 2010). The skarn in the study area is located west of the Neusberg Mountain Range, where the contacts with the surrounding units are not exposed. The skarn appears as a dark-brown block of about 35 cm to 1 m in size within the calc-silicate-rich quartzite, with white inclusions of quartzite (Figure 3.13). The skarn is very hard and fine grained. The fresh rock contains patches of epidote. Sedimentary features, such as foliation, are not present in the skarn.

Figure 3.13: Massive dark-brown skarn with spots of quartzite.

Microscopic description

Sample Sn S19 of the skarn is composed of garnet comprising about 60% of the rock volume; other minerals are: enstatite (18vol.%), biotite (10vol.%), quartz (5vol.%), allanite (4vol.%), epidote (2vol.%), and opaque minerals (1vol.%). The minerals display a skeletal texture. The shape of the grains is amoeboid with strongly curved, lobate, and interlocking grain boundaries (Figures 3.14A and B).

Garnet is the most dominant mineral, and is 0.1-0.2 mm in size. Garnet grains are variably distributed and display a brown colour, and are in contact with enstatite, biotite and magnetite. **Enstatite** is euhedral to anhedral in shape and 0.06-1.1 mm in size. Enstatite grains occur as a symplectic intergrowth with garnet and quartz. In some places, they are in contact with epidote and opaques. **Biotite** occurs as euhedral to subhedral grains of about 0.08-1.3 mm size. Biotite grains also occur as inclusions in the garnet and do not show any preferred orientation. **Quartz** is present in the skarn as anhedral crystals of about 0.03-0.1 mm size. Quartz grains occur as inclusions in the garnet and develop symplectic intergrowth with enstatite and garnet. **Allanite** is anhedral in shape and about 0.08-1 mm in size. Allanite grains are pleochroic and show a dark grass green to olive green colour. They are in contact with biotite, garnet and magnetite. **Epidote** is anhedral to subhedral in shape and about 0.05-0.1 mm in size. Epidote grains are pleochroic and display dark grass green to olive green colour. Epidote grains are in contact with biotite and opaque minerals. **Opaque minerals** are euhedral in shape and about 0.07-1.8 mm in size. Opaque grains are found in contact with epidote, enstatite and quartz.

The mineral assemblage of the skarn suggests a calcareous protolith that has been metasomatized due to an igneous intrusion (Philpotts and Ague, 2010).

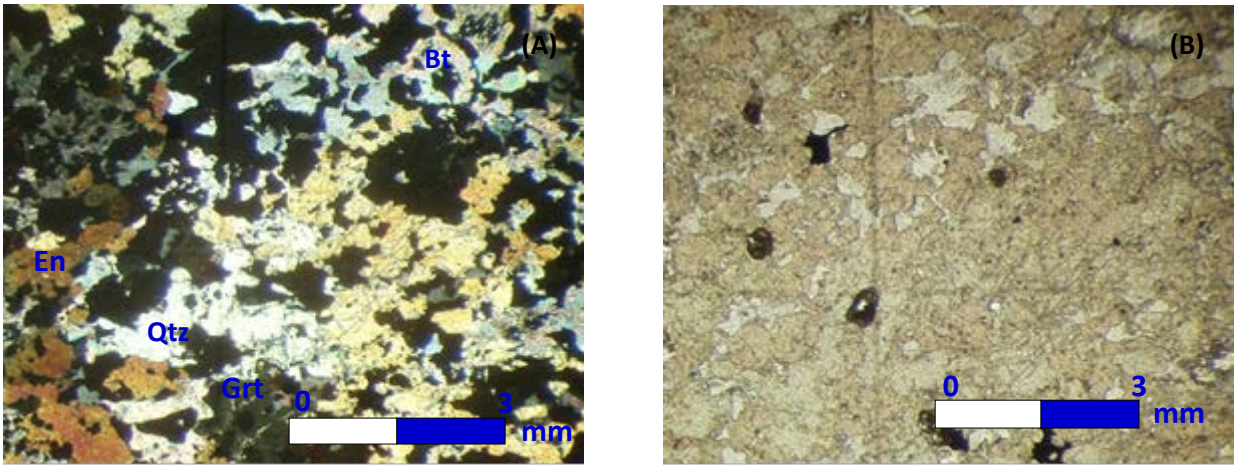

Figure 3.14: Photomicrographs of the skarn displaying pervasive garnet with skeletal texture. Abbreviations: Grt= Garnet; En= Enstatite; Qtz= Quartz; Bt= Biotite. A) Crossed polars; B) Plane polarized light.

Interpretation

The presence of a skarn in the study area is indicative of contact metamorphism and metasomatism associated with, and accompanied by igneous related hydrothermal input (Pertoldová et al., 2009). The minerals displayed in the photomicrographs do not show the foliation as observed in the metasedimentary rocks.

3.5.3 Wollastonite-bearing calcareous rock (Wbc)

Outcrop to hand specimen description

The white to greyish wollastonite-bearing calcareous rock is spottily distributed between the Neusberg Mountain Range and Vuurkop Mountain in the southern portion of the study area (Figure 2.5). It shows a folded structure and displays a brown to dark weathered pattern (Figure 3.15). The wollastonite-bearing calcareous rock consists of several bands of about 1.5 m length, and about 10 to 40 cm width (Figure 3.15). The contacts of the wollastonite-bearing calcareous rocks with the surrounding rocks are not seen in the field. A fresh sample of wollastonite-

bearing calcareous rock is composed of lath-like grains of wollastonite. They rarely have a euhedral shape, probably due to their unique cleavage properties (Hamilton et al., 2006).

Figure 3.15: Greyish wollastonite-bearing calcareous rock with a dark weathered surface.

Microscopic description

The thin section of sample Wbc S829 of the wollastonite-bearing calcareous rock is composed of wollastonite constituting about 55% of the rock volume; other minerals are: calcite (20vol.%), vesuvianite (15vol.%), diopside (5vol.%), grossular (3vol.%), quartz (2vol.%). The shape of the grains is euhedral to subhedral and they display an inequigranular texture (Figures 3.16A and B).

Wollastonite occurs as long, elongate grains 2.3-4 mm in length. Wollastonite grains are euhedral to subhedral in shape, with larger masses (up to 6 mm in size) also occur, but not as elongate grains. Twin lamellae are well developed in the wollastonite grains. Wollastonite grains are white to grey in colour and display a fibrous habit. **Enstatite** grains aggregate together, and form triple junctions in places. Grains are about 0.3-0.6 mm in size, with a few grains reaching up to 1.6 mm in size. **Calcite** occurs as subhedral grains, associated with the

wollastonite, and is about 1.2-1.5 mm in length. In some places, they are elongated parallel to the foliation defined by the wollastonite. **Vesuvianite** occurs as small, stubby grains associated with wollastonite. Vesuvianite grains are euhedral to subhedral in shape and about 0.2-0.4 mm in size, with a few grains reaching up to 1.5 mm in size. **Diopside** is euhedral to subhedral in shape and approximately 0.3-1.5 mm in size. Diopside grains aggregate together, and are associated with enstatite. They display second order green and orange interference colours. **Grossular** is subhedral in shape, and about 0.7 mm in size. Smaller (0.06 mm in size) inclusions of talc are present in the grossular and display very high birefringence. **Quartz** grains are anhedral shape, and are of about 0.05-0.1 mm in size. The grains of quartz are associated with calcite and wollastonite.

The mineral assemblage of the wollastonite-bearing calcareous rock reflects a carbonate protolith that has been subjected to the contact metamorphism and metasomatism related with, and likely associated to an igneous intrusion (Philpotts and Ague, 2010).

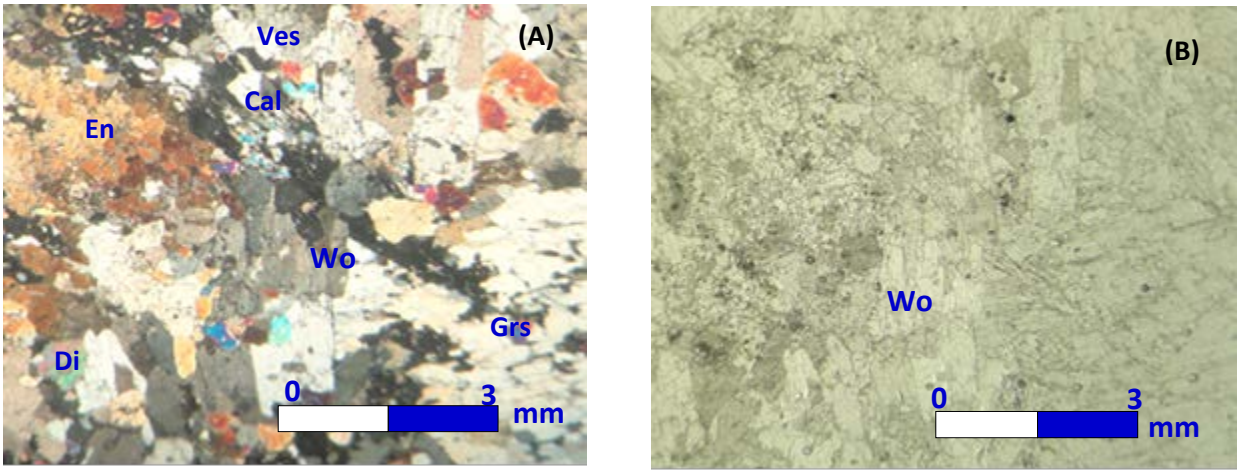

Figure 3.16: Photomicrographs of the wollastonite-bearing calcareous rock showing inequigranular texture and randomly distributed wollastonite. Abbreviations: Wo= Wollastonite; En= Enstatite; Cal= Cal; Ves= Vesuvianite; Di= Diopside; Grs= Grossular. A) Crossed polars; B) Plane polarized light.

Interpretation

The wollastonite-bearing calcareous rock in the study area likely formed where the calc-silicate-rich quartzite reacted with high temperature metasomatic fluids from an igneous source. This may reflect the reaction (Philpotts and Ague, 2010):

$$CaCO_3 + SiO_2 = CaSiO_3 + CO_2$$

(calcite) + (quartz) = (wollastonite) + (vapour)

The effect of metamorphism is therefore to transfer carbon dioxide progressively from the minerals to the vapour phase (Philpotts and Ague, 2010). Such a process is described as decarbonation wherein a certain amount of carbon dioxide is migrated out of the rock during high grade metamorphism. The CO_2 driven off depends on the prevalent pressure of CO_2 in the rock. The poorly developed calcite twinning lamellae may be a reflection of the partially completed process within the wollastonite-bearing calcareous rock (Passchier and Trouw, 2005). This probably reflects the state of deformation of the wollastonite-bearing calcareous rock. The presence of triple point junctions indicates full recovery and a strain free rock. The presence of wollastonite, diopside, enstatite and grossular in the wollastonite-bearing calcareous rock reflects granulite facies (Philpotts and Ague, 2010).

Table 3.3: Petrographic characterization of the contact rocks.

Lithology	Colour	Grain size	Mineralogy and abundance	Texture	Specific features	Metamorphic grade	Contacts	Foliation	Folds	Faults	Fractures	Joints
Biotite gneiss (Bg)	Dark brown	Medium	Bt (40%); Qtz (20%) Or (15%); Plg (11%) Perth (5%); En (4%) Hbl (3%); Op (1%) Pi (approximately1%)	Granular; Partially chloritized; Partially sericitised	Flakes of biotite; Elongated mafic xenoliths (3 to 5 cm in size)	High grade	Reaction zone between Fmq and Chn	Well foliated	None	None	None	None
Skarn (Sn)	Brown	Fine	Grt (45%); Ens (18%) Bt (10%); Qtz (6%) Aln (4%); Ep (2%) Op (1%)	Skeletal	White spots of quartzite; Patches of epidote	High grade	Not exposed	None	None	None	None	None
Wollastonite-bearing calcareous rock (Wbc)	Grey	Lath-like	Wol (55%); Cal (20%) Ves (15%); Di (5%) Grs (3%); Qtz (2%)	Equigranular	Patches of grossular and Fe-oxides; Weathered patterns	High grade	Not exposed	Disharmonic flow patterns	Kink bands	None	Well fractured	Cross-cutting joints

Abbreviations: Bg= Biotite gneiss; Chn= Charnockite; Fmq= Feldspathic mica-rich quartzite; Sn= Skarn; Wbc= Wollastonite-bearing calcareous rock; Grt= Garnet; Aln= Allanite; Bt= Biotite; Di= Diopside; Dol= Dolomite; En= Enstatite; Grs= Grossular; Hbl= Hornblende; Mag= Magnetite; Op= Opaques; Or= Orthoclase; Perth= Perthite; Plg= Plagioclase; Qtz= Quartz; Ves= Vesuvianite; Wo= Wollastonite.

3.6 Granitic gneisses

3.6.1 Leucogneiss (Lg)

Outcrop to hand specimen description

The leucogneiss in the study area outcrops well on Koekoeb farm between the Neusberg Mountain Range and Vuurkop Mountain. The leucogneiss is also known as the Riemvasmaak gneiss (van Bever Donker, 1980; Moen, 2007). Three major areas of Leucogneiss outcrop are present in the southern part of the study area, where they occur as small, separated hills in the study area (Figure 3.17A). Joints and fractures are present in the Leucogneiss (Figure 3.17B). The contacts with the surrounding rocks are not exposed in the field. The leucogneiss is light brown in colour. It is fine to medium grained, and foliation bands in the sample are not easily visible.

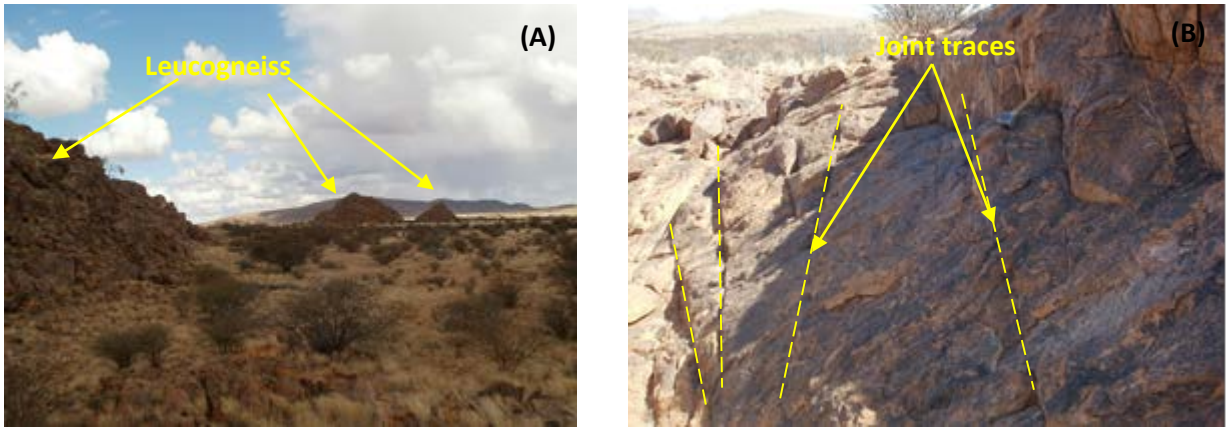

Figure 3.17: A) Distribution of the Leucogneiss as small, separated hills in the study area. B) Well jointed Leucogneiss with a brown colour. The joints are highlighted by dashed yellow lines.

Microscopic description

Samples Lg S754 and Lg S759 of the leucogneiss are composed of quartz constituting about 40 % of the rock volume. Other minerals present are: orthoclase (30vol.%), perthite (11vol.%), opaques (9vol.%), biotite (6vol.%), microcline (2vol.%), plagioclase (1vol.%), and goethite (below 1vol.%) as accessory mineral. The grains are euhedral to subhedral and display a granular texture (Figures 3.18A and B).

Quartz is subhedral to anhedral in shape, with recrystallised sub-grains (0.08-0.1 mm in size) in the groundmass displaying undulose extinction. Quartz grains show interlocking grain boundaries in contact with alkali feldspar and plagioclase. **Orthoclase** occurs as subhedral to anhedral grains of about 0.1-0.3 mm size, patchily altered to sericite. The grain boundaries of the orthoclase are curved, and locally display a straight quartz-orthoclase boundary. **Perthite** is anhedral to subhedral in shape, and of approximately 0.1-0.2 mm in size. Perthite grains are randomly distributed in the groundmass. **Opaque** grains are euhedral to subhedral in shape and about 0.05-0.1 mm in size. They are associated with quartz, orthoclase and biotite. **Biotite** is sparsely developed and appears as euhedral to subhedral grains about 0.1-0.3 mm in size. Biotite grains are pleochroic and display brown to olive green colour, and are associated with quartz and alkali feldspar. **Microcline** occurs as anhedral to subhedral grains of approximately 0.09-0.2 mm size. Microcline grains appear as cloudy masses and variably replace orthoclase. **Plagioclase** occurs as subhedral grains of about 0.1-0.2 mm in size. Plagioclase grains are variably altered to sericite, and are associated with quartz and orthoclase. **Goethite** is dark brown in colour. It occurs along fractures, as illustrated in Figure 3.17B.

The mineral assemblage of biotite + quartz + orthoclase in the leucogneiss could reflect a sedimentary precursor (Black et al., 2005), or a granitic (Praekelt, 1984), rhyolitic or felsic volcano-plutonic origin (Saad, 1987).

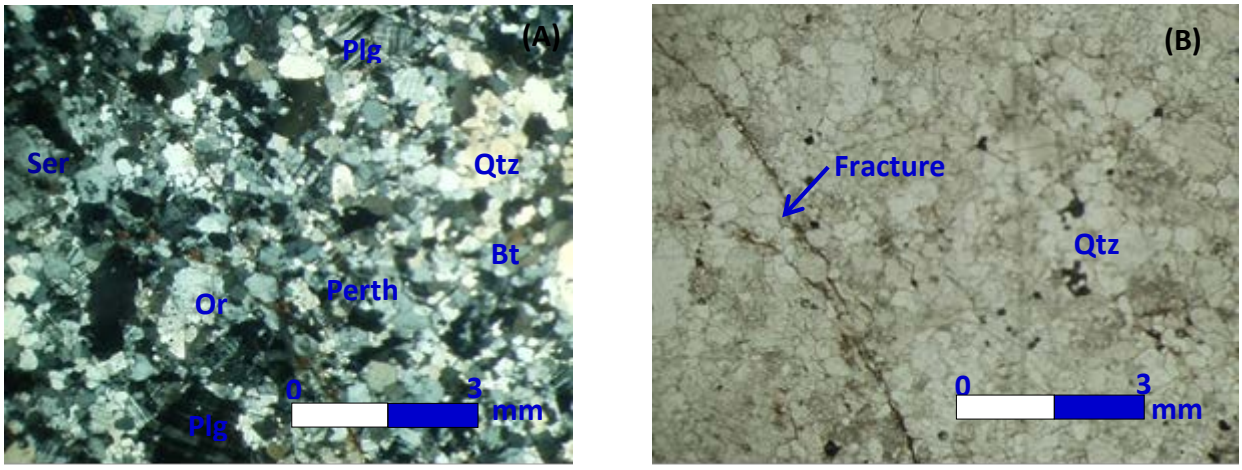

Figure 3.18: A) Photomicrograph of the Leucogneiss displaying a granoblastic texture. B) Photomicrograph of the Leucogneiss displaying a fracture. Abbreviations: Qtz= Quartz; Or= Orthoclase; Perth= Perthite; Plg= Plagioclase; Bt= Biotite; Mc= Microcline; Ser= Sericite. A) Crossed polars; B) Plane polarized light.

Interpretation

The state of deformation of the quartz grains is denoted by the presence of cracks and undulose extinction. The grain boundaries of the quartz grains are curved, and the development of undulose extinction may be due to deformation at high strain rates possibly with a large component of solid-state diffusive mass transfer such as Coble or Nabarro-herring creep (Gower and Simpson, 1992). The mineral assemblage in the leucogneiss is useless for indicating the metamorphic grade, except that the presence of biotite reflects low to medium grade metamorphism but higher grade metamorphism should not be excluded (Frey and Robinson, 1999).

3.6.2 Pink gneiss (Pg)

Outcrop to hand specimen description

The Pink gneiss is identifiable in the study area by its characteristic pinkish colour. Joints and fractures are observed in this rock (Figure 3.19). Good exposure of the Pink gneiss is seen south of Vuurkop Mountain. The contact with the metasedimentary rocks is not exposed in the study area. Ductile features such as folds or boudins have not been observed in the Pink gneiss in the study area. The pink gneiss is medium to coarse grained and moderately foliated. A fresh sample of the pink gneiss shows streaks of mafic minerals.

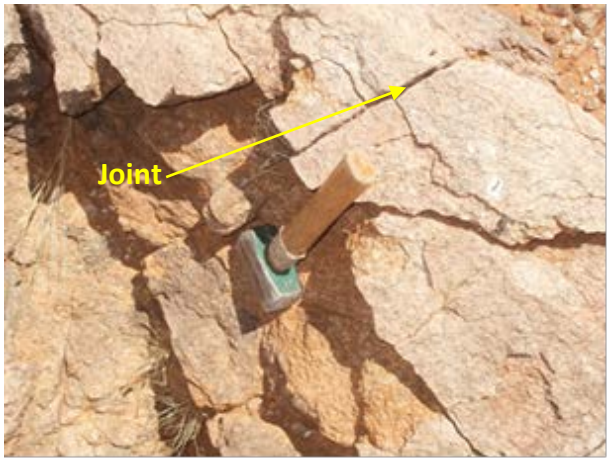

Figure 3.19: Pink gneiss transected by joints and fractures.

Microscopic description

Sample Pg S761 of the pink gneiss is composed of quartz grains accounting for about 45 % of the rock volume. Other minerals are: orthoclase (27vol.%), hornblende (8vol.%), biotite (7vol.%), plagioclase (5vol.%), microcline (3vol.%), opaques (2vol.%), perthite (2vol.%), and accessory mineral such as zircon (below 1vol.%). All the minerals in the pink gneiss display an

inequigranular texture. Foliation is developed in the pink gneiss and defined by alternating felsic and mafic minerals (Figure 3.20A and B).

Quartz grains are anhedral in shape, and variable in size, from small recrystallised sub-grains (0.05-0.1 mm - some sub-grains of quartz show triple junctions), through larger grains (0.2-0.3 mm), to aggregates and more elongate grains of about 1.5-2.5 mm with interlocking grain boundaries and initiation of sub-grain formation displaying undulose extinction in some sub-grains of quartz. **Orthoclase** grains are anhedral to subhedral in shape and approximately 0.7-0.8 mm in size. They are variably and partially altered to sericite. Orthoclase grains show an elongated orientation and display alignment with the overall rock foliation. **Hornblende** is anhedral to subhedral in shape and about 0.6-1 mm in size. Hornblende grains are pleochroic and display light olive green to dark green colour, and are commonly associated with biotite. **Biotite** occurs as euhedral to subhedral grains of approximately 0.1-0.5 mm in size. Biotite grains are pleochroic and display dark brown to dark olive green colour. Biotite flakes define a foliation in the groundmass. **Plagioclase** is anhedral in shape and approximately 0.2 mm in size. Plagioclase grains are partially altered to sericite. **Microcline** is subhedral to anhedral in shape and about 0.4-0.8 mm in size. Microcline grains are unaltered and show varying degrees of deformation in their twinning. **Opaques** are euhedral to subhedral in shape and about 0.1-0.2 mm in size. Some opaque grains are sub-cubic and are associated with biotite. **Perthite** occurs as anhedral to subhedral grains. Large porphyroblasts (2-4 mm in size) are present; smaller, anhedral grains (1.2-2 mm in size) occur within the groundmass, and are more randomly oriented than the quartz. **Zircon** is euhedral in shape and 0.2 mm in size, and is associated with orthoclase and quartz.

The mineral assemblage of hornblende + biotite + quartz + orthoclase in the pink gneiss could possibly reflect a sedimentary precursor (Black et al., 2005), or a granitic (Praekelt, 1984), rhyolitic or felsic volcano-plutonic origin (Saad, 1987).

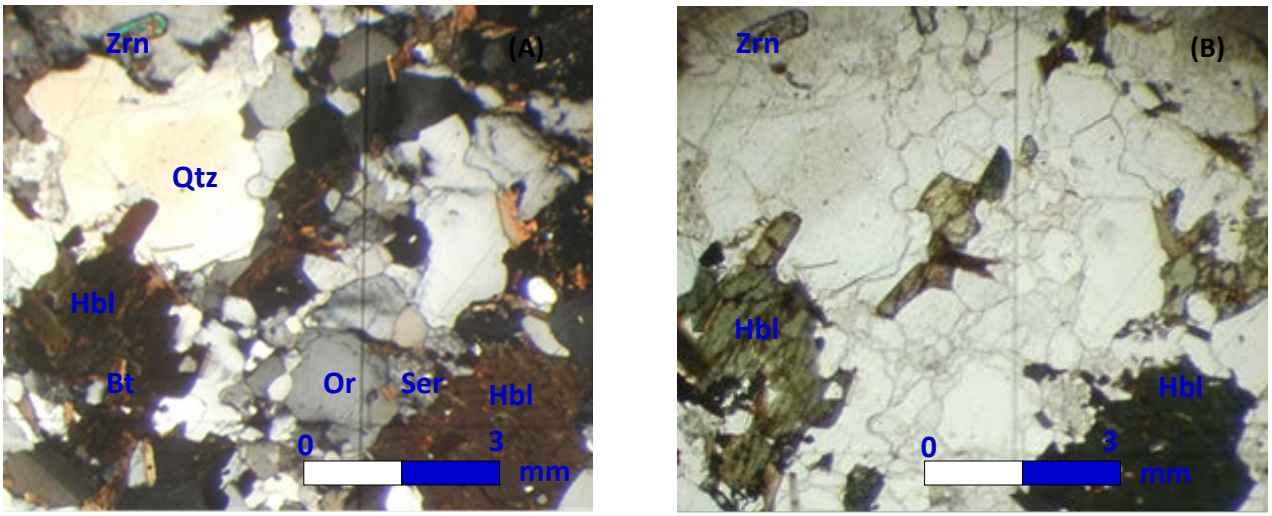

Figure 3.20: Photomicrographs of well foliated Pink gneiss. Abbreviations: Qtz= Quartz; Or= Orthoclase; Bt= Biotite; Hbl= Hornblende; Zrn= Zircon; Ser= Sericite. A) Crossed polars; B) Plane polarized light.

Interpretation

The undulose extinction observed in quartz suggests a bending or straining of quartz crystals due to a dislocation originating from a high strain rate probably related to the compressional events in the study area. The mild foliation in the pink gneiss is denoted by semi-aligned hornblende and biotite, and the axes of some elongate quartz and orthoclase grains suggest that this rock was subjected to some degree of deformation. The presence of fractures in the zircon grains is likely due to differential metamictization of the zircon, which is a natural process that occurs as the rock is exhumed from great depth (Woodhead et al., 1991). The euhedral shape of the zircon suggests a possible magmatic protolith. The mineral assemblage of hornblende and biotite denotes low to medium grade metamorphism in the pink gneiss, but higher grade metamorphism should not be excluded (Frey and Robinson, 1999).

3.6.3 Augen gneiss (Ag)

Outcrop to hand specimen description

Augen is a German word meaning 'eye'. Augen gneiss is a general term for gneissic rocks containing oval or lenticular crystals or their aggregates usually composed of feldspars (Buriánek et al., 2009). The augen gneiss appears in the study area west of the Neusberg Mountain Range. The augen gneiss is strongly foliated in a NW direction with foliation dipping NE. Augen structures are present in the augen gneiss (Figure 3.21). The augen gneiss is medium to coarse grained and is strongly foliated displaying discontinuous and alternating light and dark bands. It contains medium to large porphyroblasts of alkali feldspar of about 1 cm in size.

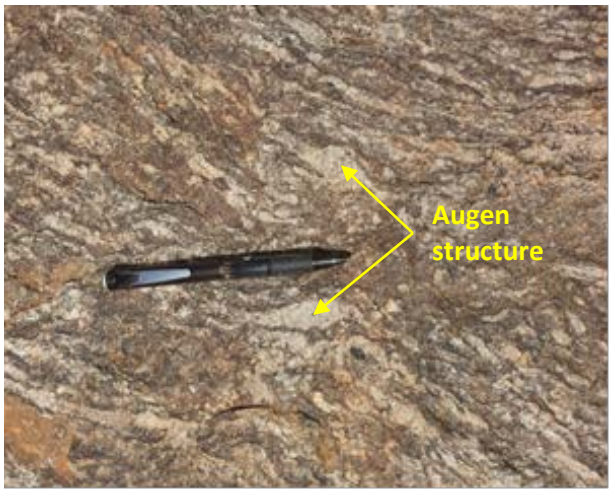

Figure 3.21: Augen gneiss displaying an augen structure.

Microscopic description

The thin sections of samples Ag S2, Ag S6 and Ag S11 of the augen gneiss are composed of grains of quartz comprising about 40 % of the rock volume. Other minerals are: orthoclase (26vol.%), biotite (17vol.%), hornblende (7vol.%), microcline (4vol.%), plagioclase (3vol.%), opaques (2vol.%), and accessory minerals such as zircon and apatite (below 1vol.%). The grains

are subhedral to anhedral and display an augen texture (Figure 3.22A). The fabric is inequigranular with grains of orthoclase embedded in a finer-grained matrix. Strong foliation with an augen structure is formed by biotite wrapped around quartz and orthoclase porphyroblasts.

Quartz appears colourless; it is coarser grained where in the 'augen' and finer grained elsewhere. It is mostly anhedral with a variable grain size from 0.05 mm, through 0.2-0.3 mm and 0.5 mm to larger grains of about 3 mm showing evidence of the start of sub-grain formation and partial undulose extinction. The 'augen' are dominated by quartz, whereas the surrounding groundmass is comprised predominantly of alkali feldspars. In some places, triple junction grain boundaries are present. **Orthoclase** occurs as subhedral grains of about 0.3-0.5 mm size. Orthoclase grains are altered in the groundmass to clay minerals, so that grain boundaries are indistinct. In the 'augen' structure, orthoclase is also extensively altered to sericite and displays a subhedral shape of approximately 0.3-0.4 mm to 1 mm in size. The grain boundaries of orthoclase are curved, and locally the grains contain biotite inclusions. **Biotite** appears as euhedral to subhedral grains of approximately 0.2-0.5 mm in size. Biotite grains are pleochroic and display red brown to dark green colour. Strong foliation is displayed by biotite grains wrapping around quartz or orthoclase and defining the 'augen'. **Hornblende** occurs as anhedral grains about 0.6-0.8 mm in size. Hornblende grains are pleochroic dark green to light olive green in colour, and are associated with biotite. **Microcline** is anhedral in shape and 1-4 mm in size. Microcline grains display undulose extinction and are associated with orthoclase and quartz. **Plagioclase** appears as subhedral grains of about 0.1-0.5 mm in size. Plagioclase grains are variably altered to sericite, and are associated with quartz and orthoclase. **Opaque minerals** are anhedral in shape and are disseminated throughout the groundmass, where they are mainly of variable size from small (0.05 mm) to large grains (0.5-1 mm), with larger irregularly shaped blebs (2 mm) present. **Zircon** is euhedral in shape and about 0.4 mm in size, and is included in the biotite. **Apatite** appears as euhedral grains of approximately 0.05 mm in size, associated with orthoclase.

The mineral assemblage of quartz, orthoclase, biotite and hornblende and the presence of disordered orthoclase augen in the augen gneiss may be derived from a porphyritic granite (Reid, 1969; Brinkmann, 1976).

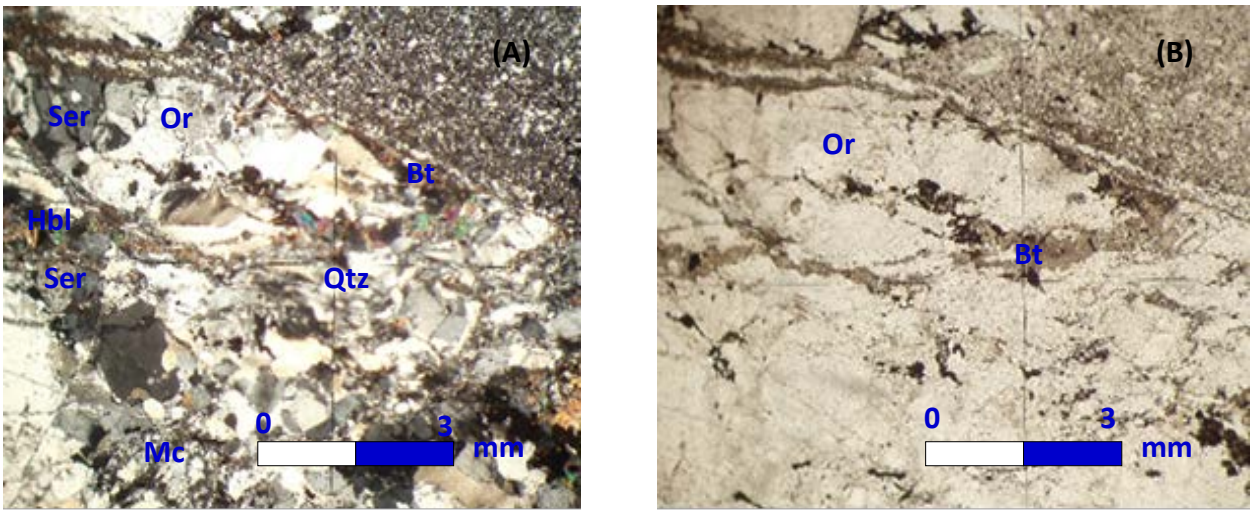

Figure 3.22: A) Photomicrograph of the Augen gneiss displaying a large grain of orthoclase surrounded by biotite. B) Photomicrograph of the Augen gneiss showing a mixture of fine grained crystals (top right hand) with larger augen in the centre to lower left. Abbreviations: Qtz= Quartz; Or = Orthoclase; Bt= Biotite; Hbl= Hornblende; Mc= Microcline; Ser= Sericite. A) Crossed polars; B) Plane polarized light.

The mixture of fine-grained crystals (Figure 3.22A; top right side) is similar to a mortar texture, which provides evidence of a high strain rate along the Neusspruit shear zone. The development of large crystals of alkali feldspar is due to the difference in rheology between the constituent minerals, with the relatively competent minerals (alkali feldspar) forming the large crystals, while the relatively incompetent ones (biotite) form part of the surrounding matrix (Figure 3.22A). The alkali feldspar (orthoclase) or 'augen' (orthoclase and quartz) are porphyroblasts, so that they were most likely formed earlier and subsequently deformed.

Mylonites are observed in the Augen gneiss and, according to Passchier and Trouw (2005), are classified with regard to the grade at which deformation took place, and the lithotype or mineralogy in which they are developed. Another commonly used mylonite classification is

based on the percentage of matrix compared to large crystals of alkali feldspar (Sibson, 1977). The augen gneiss has been subjected to extensive deformation. The large crystals of alkali feldspar account for between 10 and 50% of the rock, which classifies the augen gneiss as a protomylonite (Passchier and Trouw, 2005). Anastomosed foliation observed in the augen gneiss is related to shearing. Finely recrystallised quartz (0.1 mm in size) occurs along a quartz vein sub-parallel to the shearing orientation.

3.6.4 Biotite-chlorite-schist (Bcs)

Outcrop to hand specimen description

The biotite-chlorite-schist is located within the augen gneiss along the Neusspruit in Die Mas farm, west of the Neusberg Mountain Range. It displays a greyish colour on weathered surfaces. The biotite-chlorite-schist in the study area is locally weathered (Figure 3.23). The biotite-chlorite-schist is fine to medium grained and cleaves easily.

Figure 3.23: Extensively weathered outcrop of the biotite-chlorite-schist.

Microscopic description

Sample Bcs S5 of the biotite-chlorite-schist is composed of flakes of mica (biotite) which comprise about 40 % of the rock volume. Other minerals present are: chlorite (23vol.%), orthoclase (15vol.%), quartz (10vol.%), hornblende (4vol.%), plagioclase (3vol.%), microcline (3vol.%), and opaques (2vol.%). The shape of the grains is subhedral to anhedral and they display an 'augen' texture (Figure 3.24A). The fabric is composed of inequigranular grains of orthoclase surrounded by thin bands of mica displaying an anastomosing foliation.

Biotite appears as flakes of euhedral to subhedral shape of about 0.3-0.6 mm size. Biotite grains are pleochroic and display red brown to dark green colour. Strong anastomosing foliation is displayed by biotite surrounding quartz or orthoclase grains describing an eye-shaped or 'augen' structure (Figures 3.24A and B). **Chlorite** occurs as euhedral grains of approximately 0.2-0.4 mm size. Chlorite grains display pleochroic patches of green to yellow colour. They are in contact with biotite, orthoclase and quartz. **Orthoclase** occurs as subhedral grains of about 0.2-0.5 mm – 1 mm in size. Orthoclase grains are highly altered to sericite in the groundmass (0.05-0.08 mm). In the "augen" structures orthoclase grains are also altered to sericite and display a subhedral shape of approximately 0.5-1 mm in size in places. The grain boundaries of orthoclase are strongly curved in contact with quartz. **Quartz** appears as subhedral to anhedral grains which are colourless and about 0.1-0.4 mm-1mm in size. Quartz grains display moderate undulose extinction in the 'augen' structure; boundaries with alkali feldspar are curved. Quartz sub-grains (0.04-0.08 mm) are found in the groundmass mostly in contact with alkali feldspar or biotite. **Hornblende** appears as laths of anhedral shape of about 0.3 to 0.5 mm in size. Hornblende grains are pleochroic dark green to light olive green in colour and are mostly associated with chlorite or biotite in places along the anastomosed bands surrounding the quartz grains. **Plagioclase** occurs as subhedral grains of about 0.1-0.4 mm in size. Plagioclase grains are variably altered to sericite, associated with quartz and orthoclase. **Microcline** is subhedral to anhedral in shape and 0.5-2 mm in size. Microcline grains display undulose extinction and are associated with orthoclase and quartz. **Opaque minerals** are anhedral in

shape and are distributed throughout the groundmass, and are of different size from the smallest (0.05 mm) to large grains (0.5-2 mm), along with larger irregular shaped blebs (3 mm).

Sample Bcs S5 of the biotite-chlorite-schist shows a similar mineral content to the augen gneiss denoting a porphyritic granite (Reid, 1969; Brinkmann, 1976).

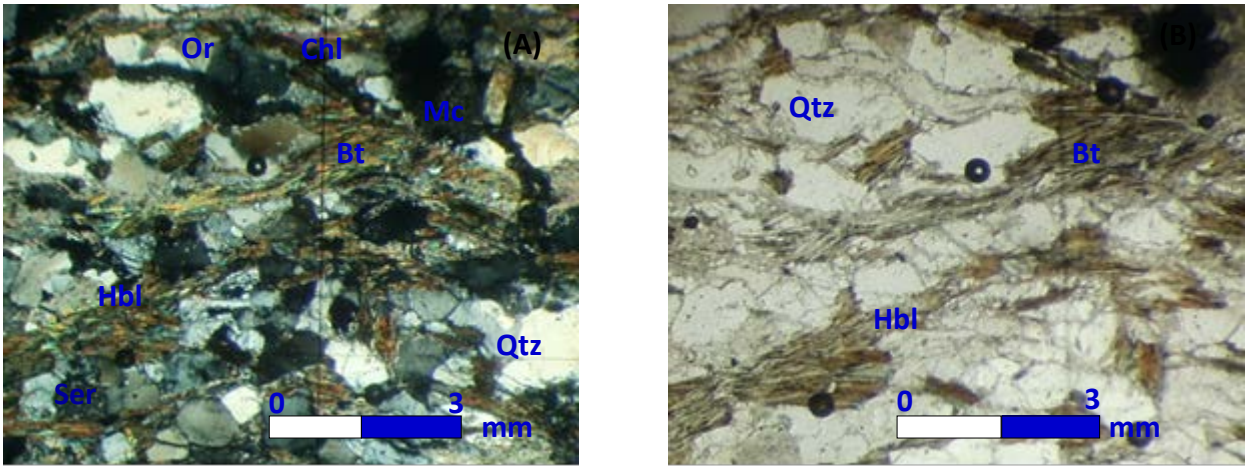

Figure 3.24: A) Photomicrograph of the Biotite-chlorite-schist showing a relatively fine grained, and biotite – rich version of the augen gneiss. B) Photomicrograph of the biotite-chlorite-schist with porphyroblasts of quartz surrounded by biotite. Abbreviations: Bt= Biotite; Chl= Chlorite; Qtz= Quartz; Or= Orthoclase; Hbl= Hornblende; Mc= Microcline; Ser= Sericite. A) Crossed polars; B) Plane polarized light.

Interpretation

The curved boundaries of orthoclase are evidence for high strain and high metamorphic grade conditions (Passchier, 1982; Gower and Simpson, 1992). The biotite-chlorite-schist has suffered similar shearing and fracture characteristics as the augen gneiss. Deformation and formation of sub-grain domains in quartz and alkali feldspar grains reflect extensive shearing. Biotite is altered to chlorite and the orthoclase is replaced by sericite reflecting retrograde metamorphism.

Table 3.4: Petrographic characterization of the granitic gneisses.

Lithology	Colour	Grain size	Mineralogy and abundance	Texture	Specific features	Metamorphic grade	Contacts	Foliation	Folds	Faults	Fractures	Joints
Leucogneiss (Lg)	Light brown	Fine to medium	Qtz (40%); Or (30%) Perth (11%); Op (9%) Bt (6%); Mc (2%) Plg (1%) Gt (approximately 1%)	Granular; Patchilly sericitised	None	Medium to high grade	Not exposed	Poorly foliated	None	None	Microfractures filled with Fe-oxides	Cross-cutting joints
Pink gneiss (Pg)	Pink	Medium to coarse	Qtz (45%); Or (27%) Hbl (8%); Bt (7%) Plg (5%); Mc (3%) Op (2%); Perth (2%) Zrn (approximately 1%)	Inequigranular; Partially sericitised	Streaks of mafic minerals	Medium to high grade	Not exposed	Moderately foliated	None	None	Presence of cracks at the surface	Cross-cutting joints
Augen gneiss (Ag)	Alternating dark and light bands	Medium to coarse	Qtz (40%); Or (26%) Bt (17%); Hbl (7%) Mc (4%); Plg (3%) Op (2%); Zrn and Ap (approximately 1%)	Inequigranular; Extensively sericitised	Augen and surfboard structures	Medium to high grade	Not exposed	Strongly foliated	S-vergence folds	Shear fault	Microfractures around the augen structure	Quartz-filled joints
Biotite-chlorite-schist (Bcs)	Greyish	Fine to medium	Bt (40%); Chl (23%) Or (15%); Qtz (10%) Hbl (4%); Plg (3%) Mc (3%); Op (2%)	Inequigranular; Extensively sericitised	Well weathered	Medium to high grade	Not exposed	Strongly foliated	None	None	None	None

Abbreviations: Ag= Augen gneiss; Bcs= Biotite-chlorite-schist; Lg= Leucogneiss; Pg= Pink gneiss; Ap= Apatite; Bt= Biotite; Chl= Chlorite; Hbl= Hornblende; Mc= Microcline; Op= Opaques; Or= Orthoclase; Perth= Perthite; Plg= Plagioclase; Qtz= Quartz; Zrn=Zircon.

3.7 Intrusive Rock

3.7.1 Charnockite (Chn)

Outcrop and hand specimen description

The charnockite is well exposed along the R359 gravel road where large and continuous bodies of it occur to the northwest, northeast and east in the study area. It is recognizable by the prominent hill named Tweelingkop where exfoliated boulders are observed (Figure 3.25A). The charnockite is highly jointed, where joints locally show epidote mineralization (Figure 3.25B). The charnockite contains elongated xenoliths of felsic and mafic composition of about 2 to 6 cm in size (Figure 3.26A). The weathered charnockite shows onion skin exfoliation (Figure 3.26B). The contact between the charnockite and the metasedimentary rocks is well exposed in the field and is represented by the biotite gneiss. The charnockite is dark grey to brown in colour. It is medium to coarse grained and faintly foliated. Blue opalescent quartz is present in the charnockite

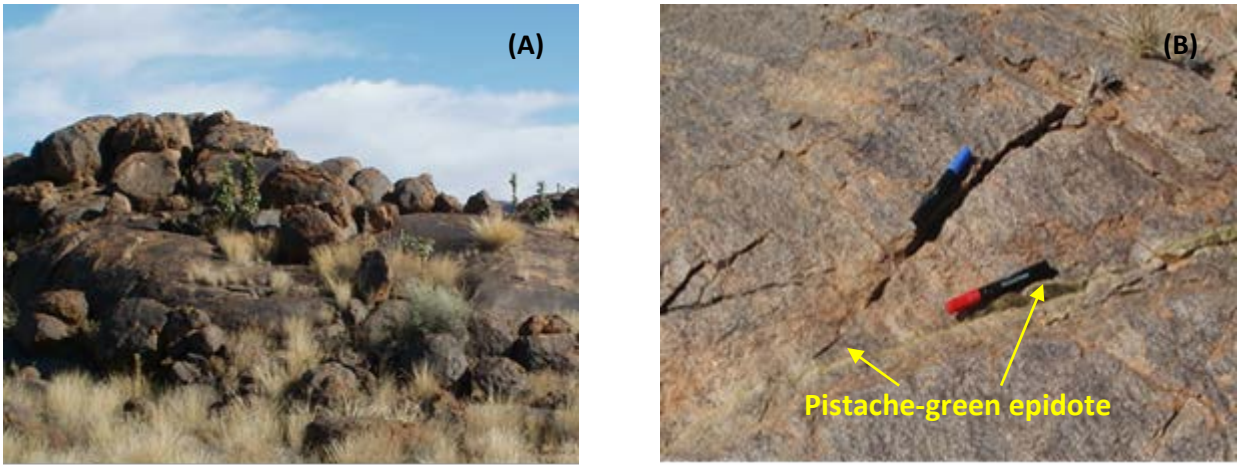

Figure 3.25: A) Exfoliated tor outcrop of charnockite. B) Joints filled with pistache – green epidote mineralization.

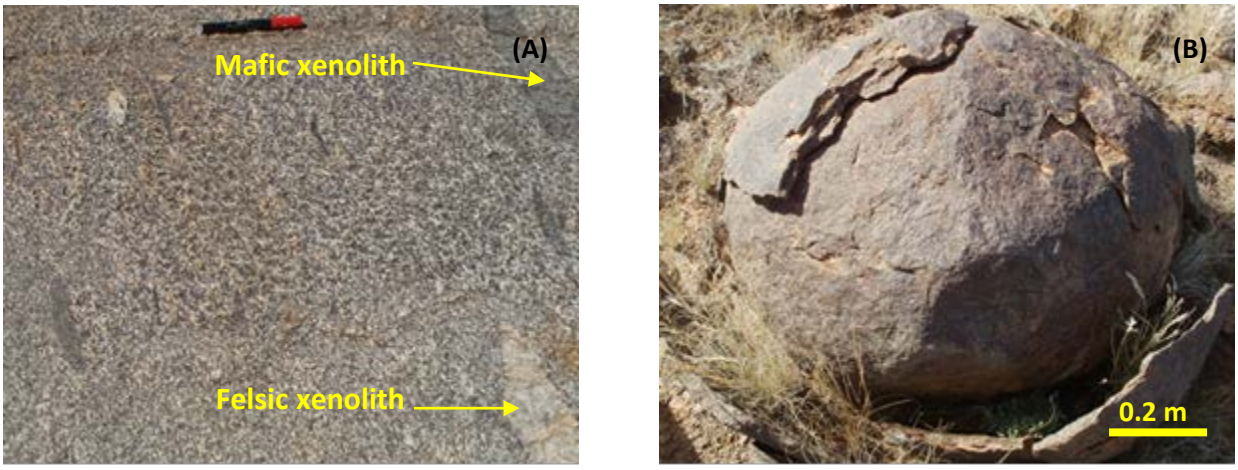

Figure 3.26: A) Mortar texture with xenoliths of mafic and felsic composition. B) Charnockite displaying onion skin weathering.

Microscopic description

Samples Chn S367 and Chn S815 of the charnockite are composed of quartz grains constituting about 40vol.% of the rock. Other minerals are: orthoclase (25vol.%), microcline (10vol.%), biotite (8vol.%), hornblende (7vol.%), enstatite (5vol.%), plagioclase (3vol.%), opaques (1vol.%), and accessory minerals such as zircon and apatite accounting for 1vol.%. The shape of the grains is generally subhedral to anhedral, and the texture is inequigranular (Figure 3.27A).

Quartz grains form glomeroporphyritic masses 1.5-1.8 mm in size composed of grains 0.8-1.0 mm in size forming triple junctions; elsewhere, however, this glomeroporphyritic mass (3 mm in size), is composed of anhedral interlocking grains varying from 0.2-2.0 mm in size. **Orthoclase** occurs mostly as phenocrysts having a plagioclase rim of 0.05-0.1 mm in size. Orthoclase grains locally form rapakivi texture. They are subhedral to anhedral (rounded) of about 1.0-1.3 mm in size displaying partial and variable alteration to sericite. **Microcline** occurs as phenocrysts of subhedral to anhedral shape of about 1.0-2.0 mm in size; the grains are partially altered to clay minerals. **Biotite** is subhedral in shape forming clusters of approximately 0.2-0.3 mm in size; biotite grains are pleochroic pale yellow brown to dark brown in colour, and are associated with opaques and hornblende. **Hornblende** is subhedral to skeletal in shape and about 0.5-0.6 mm –

1.5 mm in size. Hornblende grains are pleochroic pale olive green to dark grass green, associated with biotite; it has numerous inclusions of quartz (of euhedral shape of approximately 0.05-0.1 mm size) within it. **Enstatite** appears as euhedral, short, stubby, four side diamond-shaped prisms (0.5 mm) to more anhedral, irregular grains (0.9-1 mm in size). Enstatite grains are pleochroic pale yellow brown to tan brown in colour; they are associated with biotite and opaques and display fine inclusions of euhedral (0.01 mm or less in size) opaques within them. In some places, enstatite envelopes or surrounds opaque 'blebs' and in places these opaque minerals form the 'core' of the enstatite. **Plagioclase** occurs as phenocrysts of euhedral to subhedral shape of about 2.7-3 mm in size; other smaller more subhedral grains of approximately 1-1.5 mm in size also occur. Plagioclase grains display Carlsbad twinning in places; partial alteration to sericite is present. **Opaques** are abundant euhedral to subhedral grains, 0.2-0.4 mm in size, with smaller grains 0.1 mm, together forming clusters 0.8-1.0 mm in size, as well as forming skeletal masses enveloping euhedral quartz grains 0.1 mm in size, and are associated with biotite and hornblende. **Zircon** occurs as transparent, euhedral to subhedral grains of about 0.075-0.1 mm size with high relief; they are associated with biotite. **Apatite** occurs as elongate, clear, euhedral grains ranging from 0.3-0.4 mm at the largest, but typically 0.05-0.1 mm in size; they are associated with orthoclase.

The whole rock modal composition corresponds to the composition of monzonite, and the presence of orthopyroxene makes it charnockitic (Gliko et al., 1999; Frost and Frost, 2008).

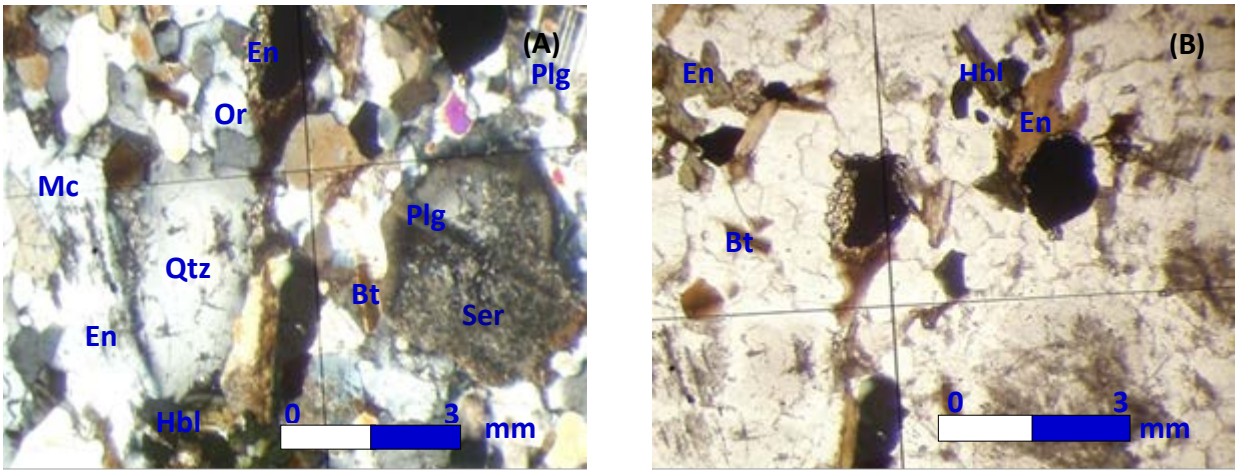

Figure 3.27: A) Photomicrograph of charnockite showing inequigranular texture with sericitised plagioclase. B) Photomicrograph of charnockite showing opaque grains associated with hornblende. Abbreviations: Qtz= Quartz; Or= Orthoclase; Mc= Microcline; Bt= Biotite; Hbl= Hornblende; En= Enstatite; Plg= Plagioclase; Ser= Sericite. A) Crossed polars; B) Plane polarized light.

Interpretation

Orthoclase and plagioclase have been partially or extensively sericitised, reflecting a secondary mineral growth after initial growth. The faint foliation in the charnockite is defined by semi-aligned biotite and the axes of some elongate quartz grains and suggests that this rock was subjected to some degree of deformation and metamorphism.

The reaction creating both characteristic minerals of charnockite - orthopyroxene and orthoclase is called the "charnockite reaction" (Gliko et al., 1999; Frost and Frost, 2008):

$$K(Mg, Fe)_3AlSi_3O_{10}(OH)_2 + 3\,SiO_2 = 3\,(Fe, Mg)\,SiO_3 + KAlSi_3O_8 + H_2O$$

biotite + quartz = orthopyroxene + orthoclase + fluid

Table 3.5: Petrographic characterization of the intrusive rock.

Lithology	Colour	Grain size	Mineralogy and abundance	Texture	Specific features	Metamorphic grade	Contacts	Foliation	Folds	Faults	Fractures	Joints
Charnockite (Chn)	Dark grey to brown	Medium to coarse	Qtz (40%); Or (25%) Mc (10%); Bt (8%) Hbl (7%); En (5%) Plg (3%); Op (1%) Zrn and Ap (1%)	Inequigranular; Partially sericitised	Elongated (2 to 6 cm in size) xenoliths of felsic and mafic composition; Onion peel exfoliation	High grade	Well exposed; Reaction zone between Fmq and Chn	Faintly foliated	None	None	Fractures are displayed in places	Cross-cutting joints filled with epidote

Abbreviations: Fmq= Feldspathic mica-rich quartzite; Chn= Charnockite; Ap= Apatite; Bt= Biotite; En= Enstatite; Hbl= Hornblende; Mc= Microcline; Op= Opaques; Or= Orthoclase; Plg= Plagioclase; Qtz= Quartz; Zrn= Zircon.

3.8 Metamorphic grade indicators

The ternary ACF diagram was proposed by Eskola (1915) as a way to illustrate metamorphic mineral assemblages on a simplified three-component triangular diagram (Winter, 2010). This diagram is used to show mineral parageneses of Ca-, Al-, Mg- and Fe-bearing minerals, i.e., of minerals occurring in mafic rocks (Winter, 2010). A bulk geochemical pilot analysis was done on the amphibole schist by the author, as it is the only appropriate lithology of mafic composition in the study area which can be plotted on the ternary ACF diagram (Figure 3.28), to indicate the parageneses acting as indicators of metamorphic grade. The other lithologies are all quartzofeldspathic in nature, and therefore not particularly helpful in estimating the P-T conditions of the study area. The ACF diagram of Eskola (1915) groups several chemical species and represents a projection into a reduced number of components (Winter, 2010). The three pseudo-components A, C, and F are all calculated on a molecular basis (Winter, 2010), as follows:

$$A = Al_2O_3$$

$$C = CaO$$

$$F = FeO + MgO$$

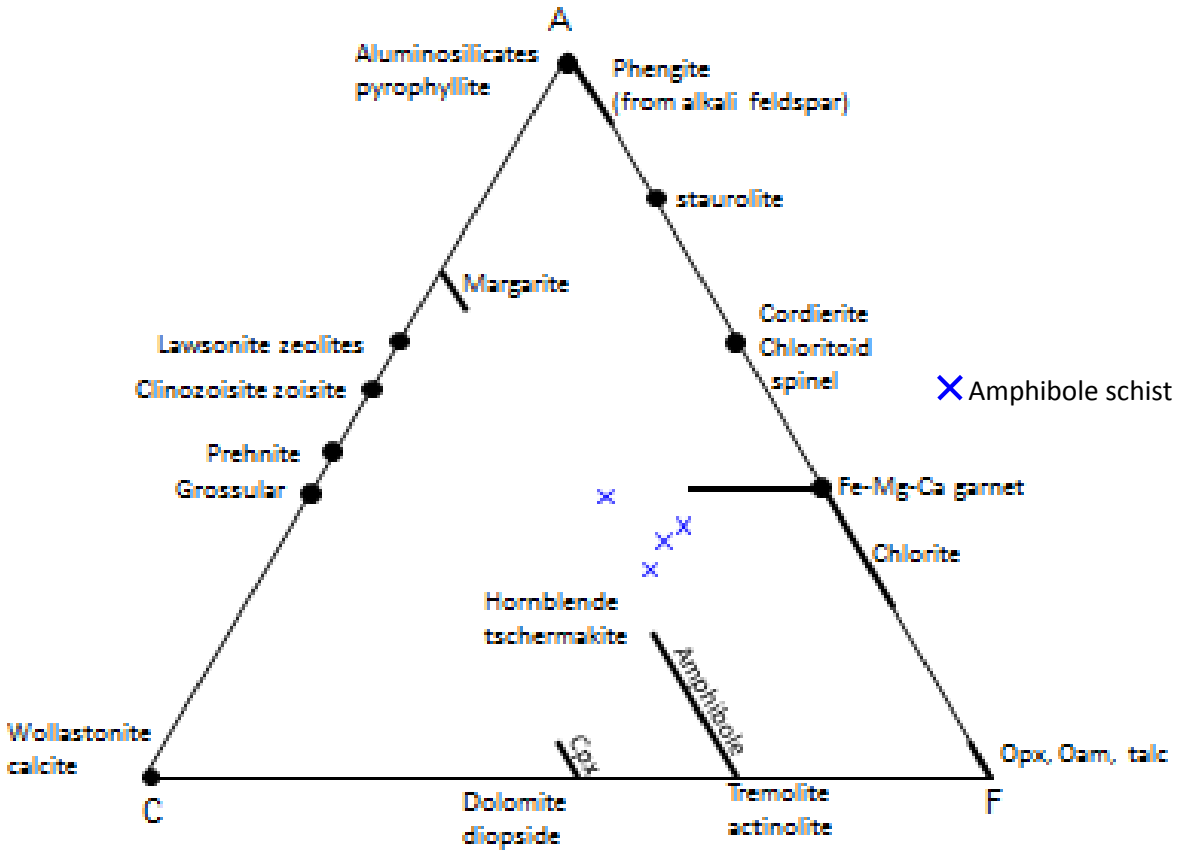

Figure 3.28: Modified ternary ACF diagram to show the plotted compositions of the amphibole schist of the Korannaland Group. Abbreviations: Cpx= Clinopyroxene; Opx= Orthopyroxene; Oam= Orthoamphibole (after Bucher and Frey, 2002).

The petrographic analysis of the metasedimentary rocks (feldspathic mica-rich and calc-silicate-rich quartzites), granitic gneisses (leucogneiss, pink gneiss, augen gneiss, and biotite-chlorite-schist), and intrusive rock (charnockite) shows that the mineral assemblage of these various rocks compared to the AFC diagram of the amphibole schists (Figure 3.28), is not informative enough to indicate the metamorphic grade. The mineral assemblage of hornblende-anorthite-quartz-biotite-epidote-enstatite-zircon-opaques in the amphibole schist is represented in the shaded field by biotite, epidote and hornblende illustrated in the orange circle reflecting greenschist-amphibolite facies transition grade (Figure 3.29). Staurolite and garnet are rare in the thin sections of the amphibole schist, the former more common in the kyanite zone in pelitic rocks at the same equivalent metamorphic grade or in mafic rocks (Bucher and Grapes, 2011), the latter assuming the role of an important constituent only in the highest grade of

plagioclase zone rocks (Cooper, 1972). The transition from greenschist to amphibolite facies grade in the amphibolite schist involves major mineralogical change, such as the transition from a sodic plagioclase (albite) to a more calcic plagioclase (anorthite) with increasing temperature (Winter, 2014). Such reaction is suggested to occur at the temperature of approximately 500 °C and pressure of about 5 kbar in the amphibole schist (Figure 3.29).

The presence of contact rocks, such as the wollastonite-bearing calcareous rock, is indicative of contact metamorphism (Winter, 2014), reflecting a change of metamorphic conditions (Bucher and Grapes, 2011). When carbonate is subordinate to other clastic material (quartz, feldspar, clays, and other silicates or oxides), it may be largely consumed by decarbonation reactions, and the metamorphic rocks, particularly at medium and high grades, are then composed solely of Ca-Mg-Fe-Al-Na-K silicate minerals (Winter, 2014), such as the mineral assemblage of wollastonite-calcite-vesuvianite-diopside-grossular in the wollastonite-bearing calcareous rock. Some calc-silicate minerals (e.g., vesuvianite and grossular) have been demonstrated to be stable in H_2O-rich fluids, whereas others (e.g., anorthite) are stable in CO_2-rich fluids (Winter, 2014). It is important to mention that the AFC diagram proposed by Burger and Grapes (2011) was set up for mafic rocks. The application of the AFC diagram on the wollastonite-bearing calcareous rock is to show the change of metamorphic grade in the study area. The mineral assemblage of the wollastonite-bearing calcareous rock is illustrated in the AFC diagram in the green circle (Figure 3.29) corresponding to a pyroxene hornfels as proposed by Bucher and Grapes (2011), reflecting a change of metamorphic grade from the greenschist-amphibolite transition to the granulite facies, in general, as also shown by the transition from the kyanite zone to the sillimanite zone in metapelitic rocks (Bucher and Grapes, 2011). The metamorphic conditions of the occurrence of the wollastonite-bearing calcareous rock could be at the temperature of about 800 °C and a pressure of approximately 3 kbar (Bucher and Grapes, 2011). The temperature-pressure conditions for the wollastonite-bearing calcareous rock are very dependent on the X_{co_2} (Winter, 2014), with the temperature varying accordingly relative to the amount of CO_2 fluxing through the rocks (Winter, 2014). The mineral assemblages given for the compositions are sufficient to estimate approximate P-T conditions.

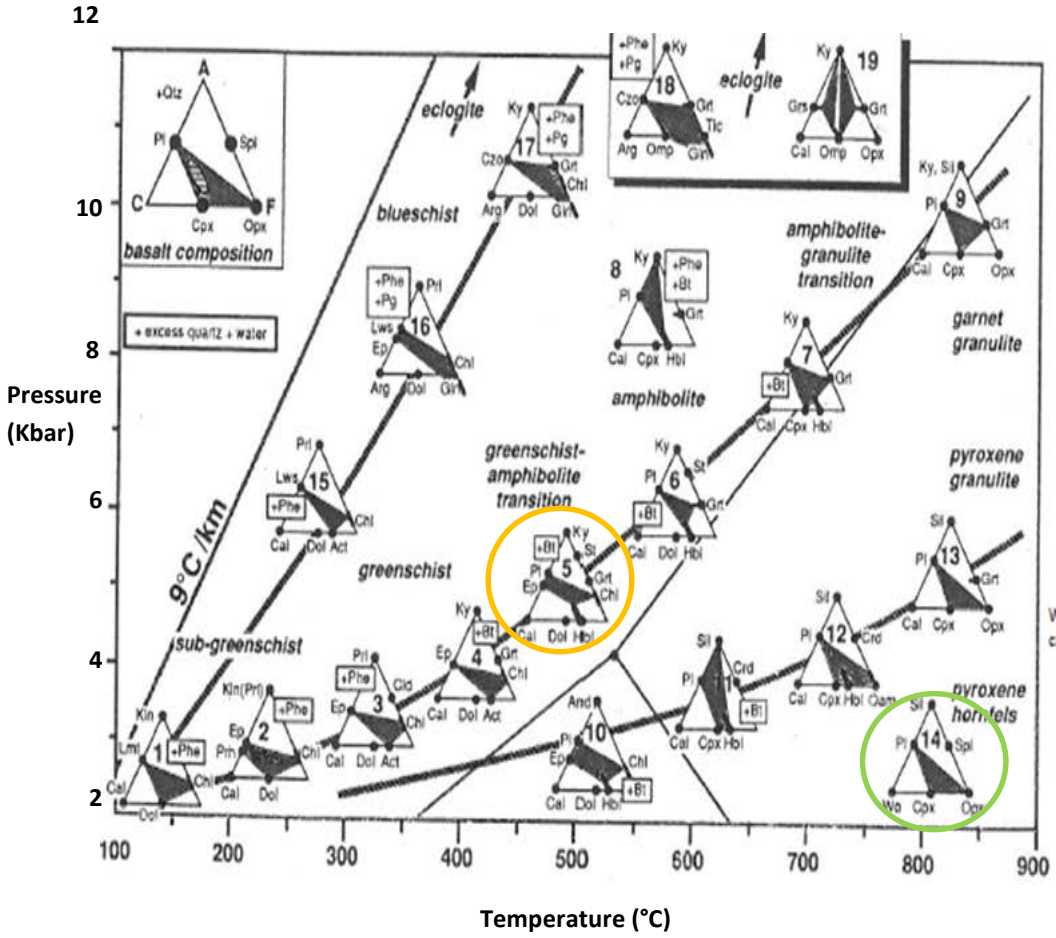

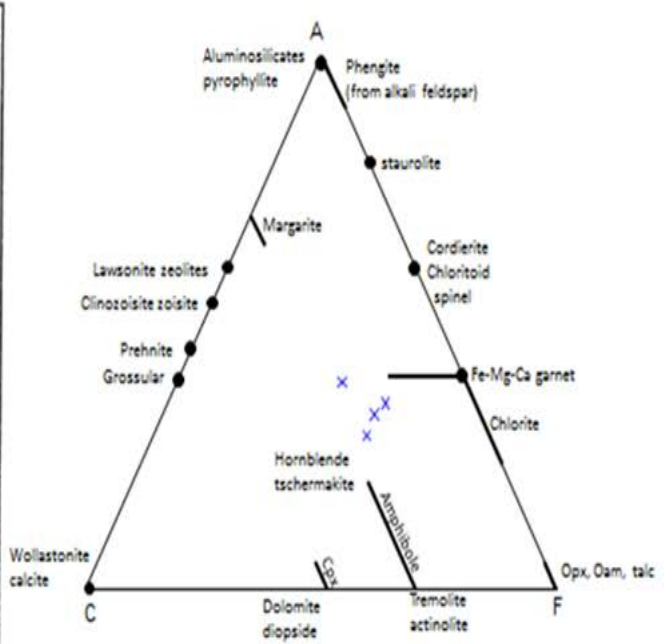

Modified ternary AFC diagram of the amphibole schists.

Figure 3.29: **A generalised pressure and temperature diagram for the metamorphism of mafic rocks (after Bucher and Grapes, 2011) represented by AFC diagrams for varying P-T conditions. In the orange circle is the metamorphic mineral assemblage of the greenschist-amphibole facies transition, with an approximate temperature of ≈ 500 °C and pressure of ≈ 5 kbar. In the green circle is the metamorphic mineral assemblage of the pyroxene hornfels (Temperature: ≈ 800 °C; Pressure: ≈ 3 kbar). The diagram to the right represents a modified ternary AFC diagram showing the compositions of the amphibole schist samples.**

Summary

The break down of orthoclase and plagioclase into sericite in the Goede Hoop and Puntsit Formations could reflect a low grade metamorphism or deuteric alteration in the study area. The presence of enstatite and hornblende in the amphibole schist reflects an upper medium to high grade metamorphism (Bucher and Grapes, 2011). The presence of enstatite and hornblende parageneses in the biotite gneiss, and garnet and enstatite parageneses in the skarn along with wollastonite, diopside and grossular in the wollastonite-bearing calcareous rock denotes high grade metamorphism in the contact rocks (Bucher and Grapes, 2011).

The mineral assemblage of hornblende, biotite, and chlorite in the biotite-chlorite-schist occurring within the augen gneiss reflects low to medium grade. The presence of biotite altering to chlorite and hornblende breaking down to chlorite along with orthoclase altering to sericite denotes a low grade metamorphism reflecting greenschist facies. The presence of augen features in the biotite-chlorite-schist shows that it was highly sheared.

Apart from the presence of goethite in the leucogneiss and zircon and apatite in the augen and pink gneisses, the granitic gneisses have similar mineral assemblages. The occurrence of apatite in the augen gneiss suggests low to medium grade metamorphism related to the flow of hydrothermal fluid along the Neusspruit Shear Zone. High grade metamorphism is expressed by the presence of hornblende in these granitic gneisses. The augen gneiss and leuco-pink gneisses are called granitic gneisses in this study based on the presence of alternating mafic and felsic layers. Field work and petrography analysis have shown varying degrees of foliation in the granitic gneisses from faintly to strongly foliated. The contact between the augen gneiss and leuco-and pink gneisses is not exposed in the field. The development of recrystallized quartz is thought to have occurred due to the peak metamorphic conditions and intense deformation in the area. Shearing is identified by the presence of the augen structures in the augen gneiss along the Neusspruit Shear Zone west of the Neusberg Mountain Range in the study area.

Various metamorphic events have taken place in the study area resulting to different metamorphic assemblages. Regional metamorphism (M_1) reached medium to high grade

conditions in the amphibole schists. The mineral assemblage of hornblende + enstatite + biotite + quartz + orthoclase + plagioclase in the amphibole schists reflects medium to high grade metamorphism due to tectonic and/or magmatic reasons.

The second event (M_2) is illustrated by high grade metamorphism that was reached in the vicinity of the charnockite. Good examples of contact metamorphism are the metasomatic rocks (skarn to the west of the Neusberg Mountain Range, and wollastonite-bearing calcareous rock between the Neusberg Mountain Range and Vuurkop Mountain) (Figure 2.5). The mineral assemblages that were formed as result of M_2 occur in the skarn (garnet + enstatite + biotite + quartz + Allanite + epidote) and the wollastonite-bearing calcareous rock (wollastonite + enstatite + calcite + vesuvianite + diopside + grossular + quartz). The presence of garnet and enstatite parageneses in the skarn along with wollastonite, diopside and grossular in the wollastonite-bearing calcareous rock denotes high grade metamorphism in the contact rocks (Bucher and Grapes, 2011). As shown in Figure 3.29, the paragenesis in the wollastonite-bearing calcareous rock reflects the one in the green circle defining contact metamorphism (Bucher and Grapes, 2011).

Low grade metamorphism (M_3) has occurred throughout the area and is expressed by the late growth of minerals such as biotite, chlorite and sericite. For example the occurrence of epidote in the joints affecting the charnockite, and the mineral assemblage in the Goede Hoop Formation (quartz + orthoclase + muscovite + plagioclase + perthite) occurs frequently. Apart from the obviously late grown low grade minerals occurring throughout the area. It is important to mention the lack of medium to high grade minerals. Low grade assemblage is contradicted by the presence of hornblende and enstatite suggesting that medium to higher conditions may have prevailed. Supporting evidence is the amphibole schist intercalated in the Puntsit Formation in direct contact with the Goede Hoop Formation indicates medium grade metamorphism. It is likely the apparent low grade assemblage is misleading and most of the area reached medium grade metamorphism (van Bever Donker, 1980).

CHAPTER 4

STRUCTURE

4.1 Overview of the study area

The deformation of the rocks in the area has been described in several previous studies (van Bever Donker, 1980, 1983; Moen, 2007). These earlier works were regional studies which did not have sufficient details and this study will fill the gaps based on the observation of various structural elements such as foliations, lineations, joints, faults and shear sense indicators which were carefully observed, described and analyzed for better comprehension of the structural evolution of the study area. The megascopic structure in the field is best understood by dividing the entire structure in the study area into homogeneous sub-areas whereby the individual description of each sub-area is of great importance. The analysis and related interpretation of structural elements within each sub-area are compared and correlated in order to produce a common and comprehensive deformational history for the entire structure in the study area.

4.2 Subdivision of the study area

Both ductile and brittle tectonic structures are present in the study area. The structural pattern is mostly dominated by: (1) a regional scale northwest striking foliation; (2) a northwest striking shear zone; (3) a northwest striking thrust fault; (4) mesoscale folds in the metasedimentary rocks in various localities; and (5) joints and fractures in both metasedimentary and intrusive rocks. The metasedimentary rocks are characterised by a pervasive foliation, whereas the charnockite is faintly foliated. The geological map of the study area (Figure 4.1) is characterised by a structural feature that occupies the entire area of 5x14 kilometres together with a shear zone of regional extent defining its western boundary.

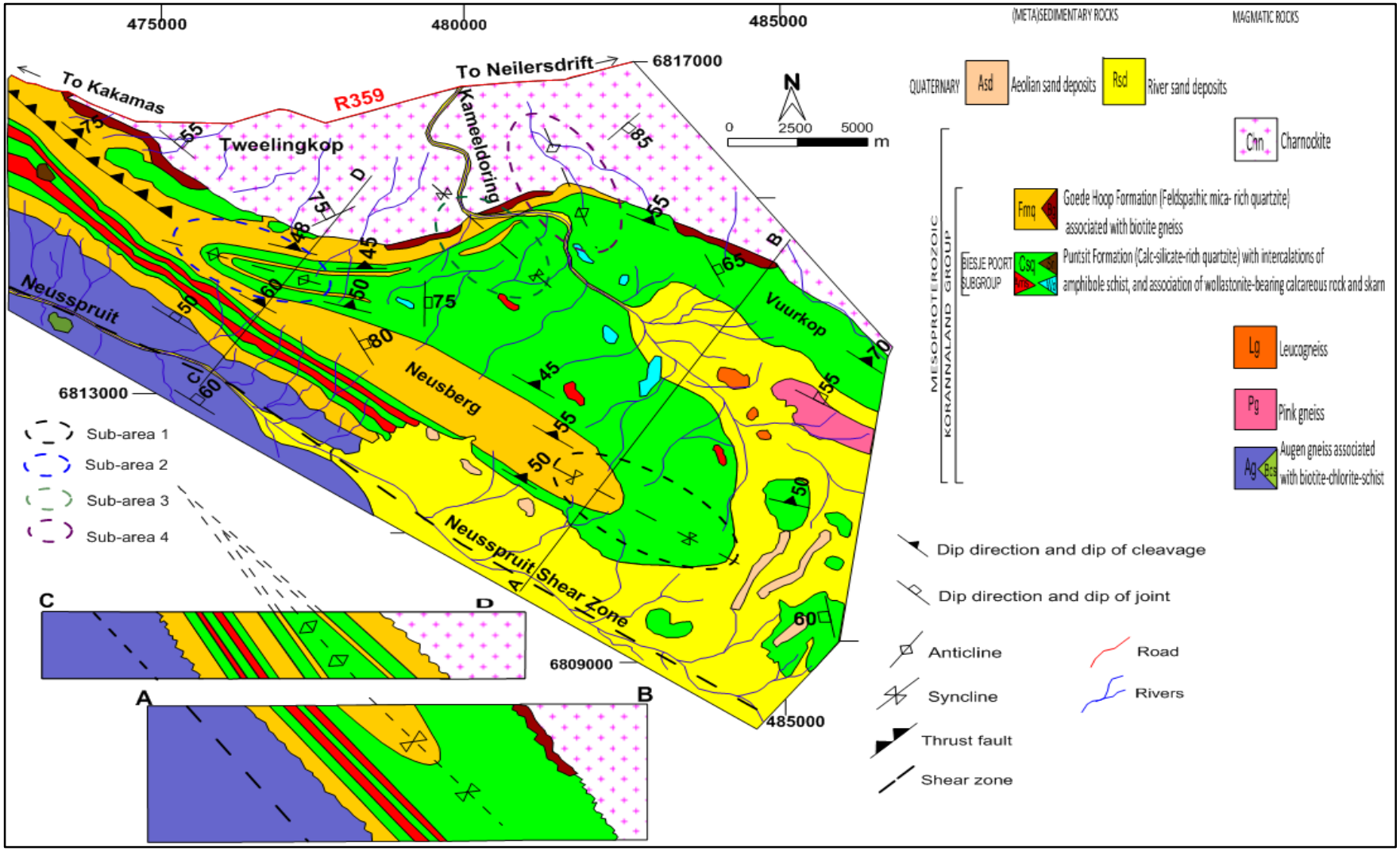

Figure 4.1: Geological map of the study area displaying the four structural sub-areas.

The division of a large heterogenous structure into homogeneous sub-areas is done in order to distinguish the various stages of deformation that took place (Fossen, 2010). It is noteworthy to mention that an objective description of the structure on a large scale is well constrained when the entire area under investigation is subdivided into homogeneous sub-areas (Davis and Reynolds, 1996). The study area is divided into four homogeneous sub-areas, as indicated in Figure 4.1. The area marked as a sub-area on the map encloses the essential structural feature of that particular sub-area, but the full extent of each individual sub-area is not shown to avoid cluttering the map.

According to Ramsay and Huber (1987), folds are unlikely to be perfectly cylindrical and it would seem a good idea to develop some practical terminology and simple testing procedure to define whether a fold is cylindrical or not. Suggestions made by Ramsay and Huber (1987) are as follows:

''Taking into account that if more than 90 % of the π-poles fall within an angle of 10° from the constructed π-circle the fold should be termed cylindrical for the purposes of geological description. If less than 90 % lie in this zone, and more than 90 % of data points fall within 20° of the π-circle the fold is then termed sub-cylindrical. Folds with data outside this limit are termed non-cylindrical. A scheme like this is a comparatively rapid process to construct small circles at 10° and 20° from the best fit great circle''.

It is important to note that the eigenvectors (e_1, e_2, and e_3) (Woodcock, 1977), in this study can be considered as representing the three principal stress vectors (σ_1, σ_2, and σ_3), but as the study area has been subjected to various deformational events, the eigenvectors obtained from the fold analysis of each sub-area are not taken into account based on following assumptions:

- Supposing that there has been subsequent re-orientation of the D_1 folds, this would imply that the D_2 event, which would have involved simple shear forming the Neusberg Thrust Fold, had effect on the D_1 folds in the area.
- Considering that the deformation in the study area was by pure shear (non-rotational or coaxial strain), the presence of thrusting (Neusberg Thrust Fault) shows that a simple

shear (rotational or non-coaxial strain) had occurred, implying that the axial plane may have rotated relative to the principal axes of maximum compressional stress. Therefore the orientation of the axial plane cannot be used to obtain the σ_1 stress direction (Figure 4.2A).

- Prior to deformation the layer that was to be deformed was lying in the σ_1-σ_3 plane. It is most unlikely that after D_1 event all the layers in the area were parallel to this plane. They would have had different orientations so the orientation of a fold axis cannot be used to obtain the orientation of σ_2 (Figure 4.2B).

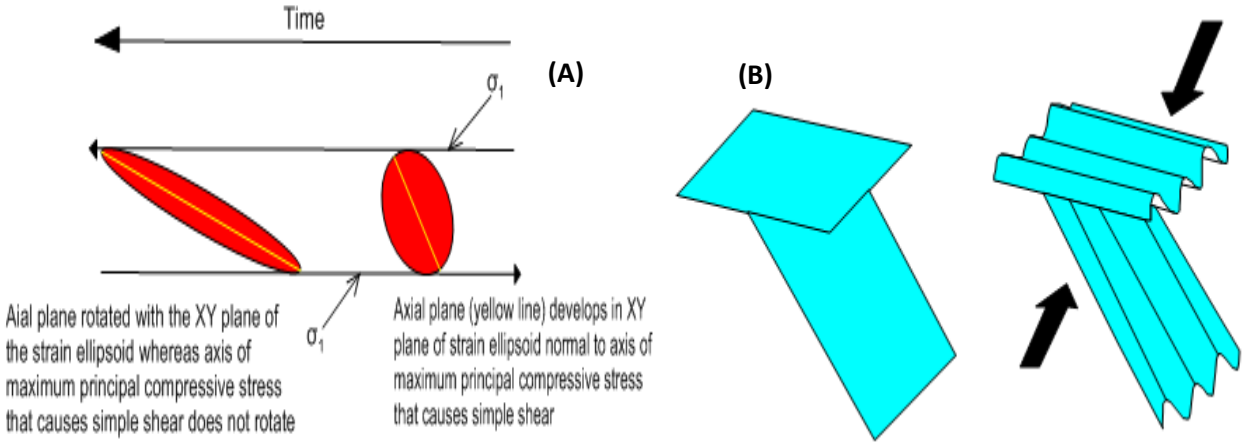

Figure 4.2: A) Sketch of rotation of axial plane during simple shear with time, and the maximum compressional stress direction remains consistent. B) Sketch of two layers with different orientations deformed in the same event produce fold axes of different orientations. This shows that the orientation of fold axes cannot be considered as the orientation of σ_2.

4.3 Foliation

The most obvious structural feature is the intense, pervasive foliation (S_0) developed in the metasedimentary rocks. Foliation is also observed in the granitic gneisses. The dip direction of the foliation in the four sub-areas is towards NE, with dips mostly directed to the NE along the Neusberg Thrust Fault (Figure 4.1). The orientation of the foliation to the SW is well displayed by displaced rocks of feldspathic mica-rich quartzite along the Neusberg Thrust Fault (Figures 4.3A and B).

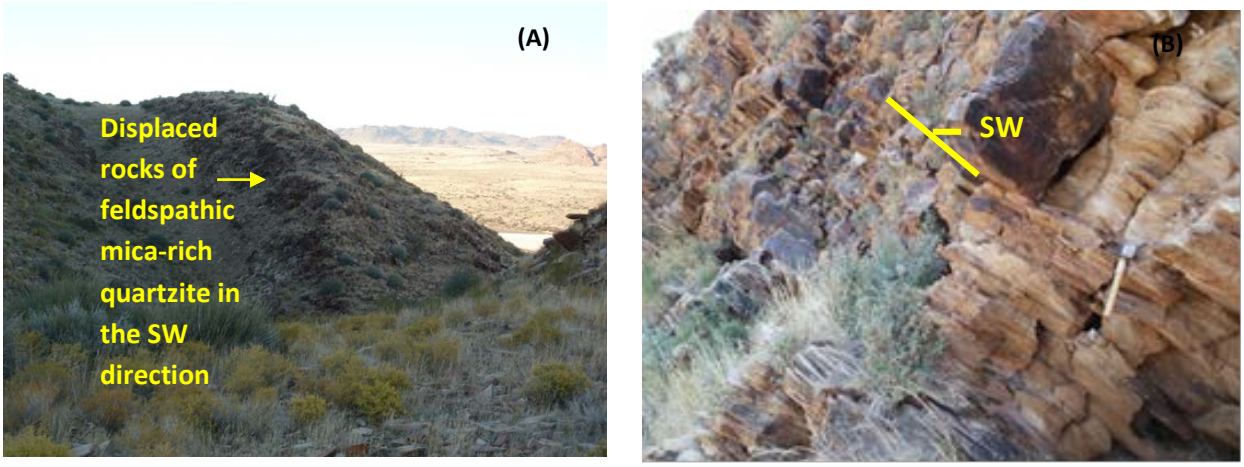

Figure 4.3: A) Displaced rocks of feldspathic mica-rich quartzite towards southwest as indicated by the yellow arrow in sub-area 2. B) Part of the feldspathic mica-rich quartzite along the Neusberg dipping to the southwest. The direction of view is towards the southeast.

4.4 Linear features

Elongated pebbles define linear features in the study area (Figure 4.4) with their long axes trending in the NW direction. Such features are sporadically found in the feldspathic mica-rich quartzite and are not considered for lineation analysis as they are statistically too few for proper interpretation. The presence of elongated pebbles in sub-area 2 only constitutes evidence for compressional deformation in the study area. The orientation of the long axis of the flattened pebbles is parallel to the foliation S_0. Mineral lineation (L_1) is an important feature that reflects the recrystallization or reorientation during deformation, but can also arise from a solution/precipitation process (Fossen, 2010). Such fabric (L_1) has been identified in sub-areas 1 and 2, with a trend mostly towards NE with a plunge to the NE similar to the S_0 orientation.

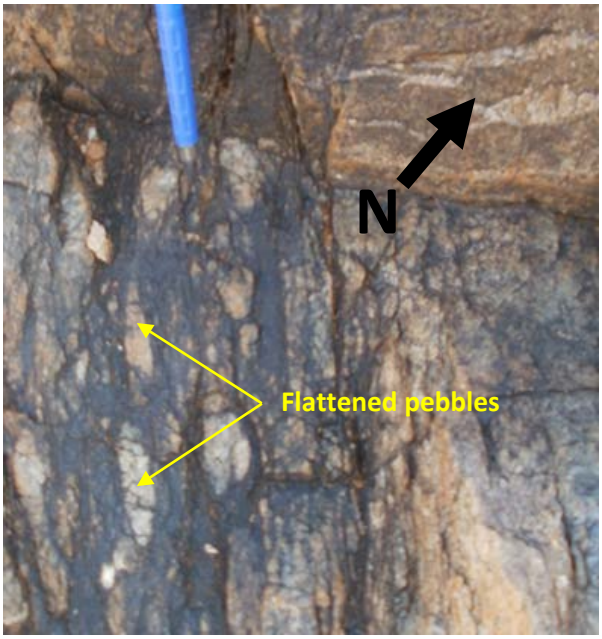

Figure 4.4: Linear feature defined by elongated pebbles in sub-area 2.

4.5 Analysis of each sub-area

4.5.1 Sub-area 1

Sub-area 1 is characterised by a closure with limbs dipping mostly towards NE as illustrated by the strike and dip symbols in yellow in Figure 4.5. This sub-area contains the southern closure of the Neusberg Mountain Range which is easily identified on the geological map and in the field by the well deformed calc-silicate-rich quartzite (Figure 4.5).

Figure 4.5: Closure displayed by the calc-silicate-rich quartzite in sub-area 1. The direction of view is towards the southeast. The white dotted line indicates how the calc-silicate-rich quartzite forms a fold closure.

4.5.1.1 Fold analysis in sub-area 1

According to Ramsay and Huber (1987), for more than 90 % of the π-poles located within an angle of 10° (defined by two red π-circles; Figure 4.6A) from the π-circle shows that the closure in sub-area 1 is a cylindrical fold. The stereographic plot of the foliation (S_0) displays one cluster describing an isoclinal fold with an interlimb angle of 0° according to the classification of Rowland et al. (2007). Derived values show that the axial plane dips 69° towards 033° describing a steeply inclined fold (Fleuty, 1964). Derived fold axis is plunging 34° and trending 047° describing a moderately plunging fold (Fleuty, 1964). The southern closure is classified as a moderately plunging and steeply inclined isoclinal fold defining a synform (Figure 4.1). The plot of data points of lineation (L_1) of sub-area 1 show cluster trending to the NE (Figure 4.6B) likely the orientation of the fold axis in the southern closure. From field observations together with derived values, the southern closure of the Neusberg Mountain Range represents a synformal structure.

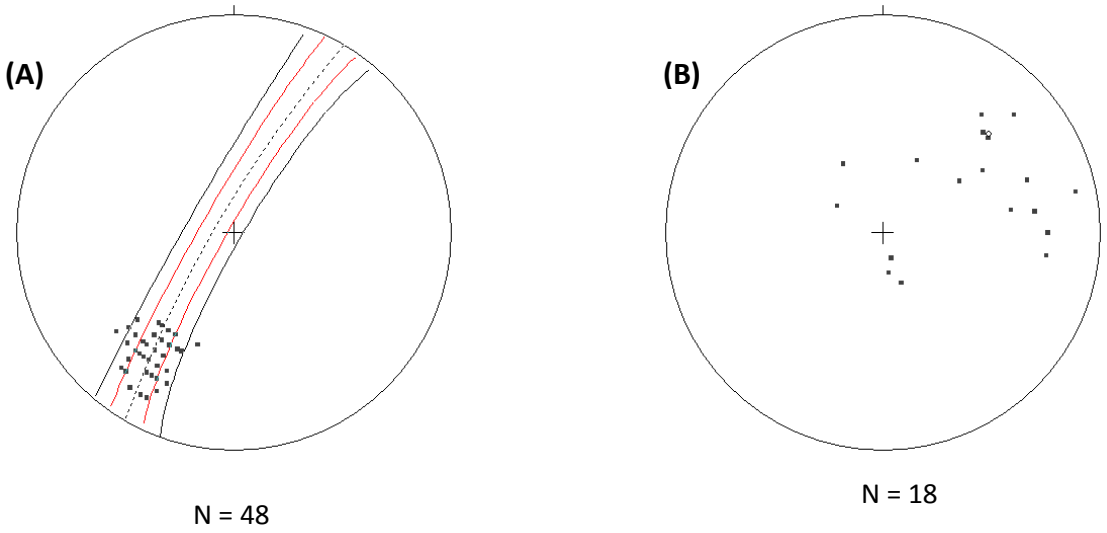

Figure 4.6: A) Stereographic plot of the foliation (S_0) of sub-area 1. B) Stereographic plot of the mineral lineation (L_1) of the southern closure. The red lines in Figure 4.6A take show that more than 90 % of the π-poles fall within an angle of 10°. From the constructed π-circle the fold is termed cylindrical for the purposes of geological description.

Mesoscopic structures:

The structures in sub-area 1 consist of synformal closure displayed by the calc-silicate rich quartzite rocks forming the southern closure in the study area. A synformal structure is also displayed in the feldspathic mica-rich quartzite in sub-area 1 (Figure 4.7). From field observations and actual measurements, the closure in the calc-silicate-rich quartzite is steep with an axial plane dipping 70° towards 050° similar to that in feldspathic mica-rich quartzite with an axial plane dipping 80° towards 030° suggesting a synformal structure. The actual measurements are confirmed by the derived values, defining a moderately plunging, steeply inclined isoclinal fold (Figure 4.8), according to the classification of Fleuty (1964).

Microscopic features:

The microscopic features are observed in the calc-silicate-rich quartzite and feldspathic mica-rich quartzite, where the quartz grains in the feldspathic mica-rich and calc-silicate-rich quartzites display undulose extinction (Chapter 3; Sections 3.3.1 and 3.4.1; Figures 3.5A and 3.8A). As a result of the physical rearrangement of a crystallographic lattice by the migration of dislocations, crystals may show strain effects, with the crystals within aggregates commonly having a shape orientation and a preferred orientation of their lattices (Ramsay and Huber, 1983). The crystalline aggregates of the rock undergo, or are subjected to, various deformation mechanisms leading to the overall deformation features of the rock (Ramsay and Huber, 1983). Features such as undulose extinction suggest that the recovery process in the rocks of sub-area 1 has not been completed and can be considered to be 'frozen' thus giving insight into the deformation processes that have taken place (Passchier and Trouw, 2005).

Figure 4.7: Synformal mesoscopic D_2 structure in the feldspathic mica-rich quartzite at the southern closure of the Neusberg Mountain Range.

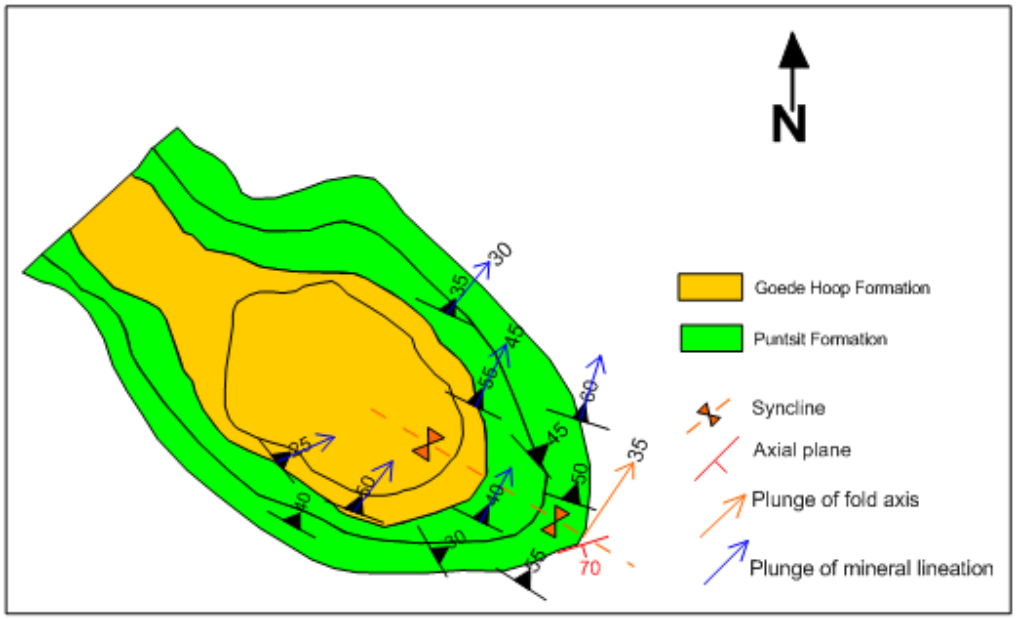

Figure 4.8: Detailed mapping of the southern closure of the Neusberg Mountain Range.

4.5.1.2 Joints analysis of sub-area 1

The joints in sub-area 1 are locally mineralized with quartz. The stereographic projection of the joints shows the concentration of one cluster denoting steeply dipping joints (Figure 4.9). The orientation of the joints in sub-area 1, as shown in Figure 4.10 shows two dominant trends trending northeast (55°± 5°) and northwest (310°± 5°) respectively. There is a slight trend of E-W too, and, to some extent N-S. The two joint sets trending northwest and northeast crosscut at about 90° (Figure 4.10). The joints and fractures are well developed in the feldspathic mica-rich quartzite (Figure 4.11).

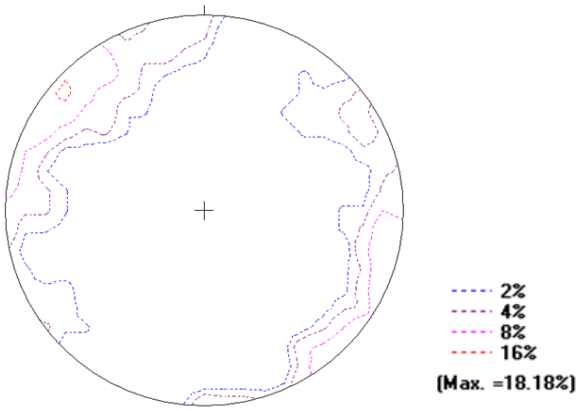

Figure 4.9: Stereographic plot of the joints for sub-area 1 displaying one cluster with a density of 16 % trending NE-SW, and a lesser cluster defining joints trending NW-SE with a density of 4%.

For the purpose of calculating the principal stress directions from these joints, a conjugate set has been identified in the field. This is based on the fact that joints parallel to the joints in sub-area 1 have been seen to mutually displace each other in sub-area 2.

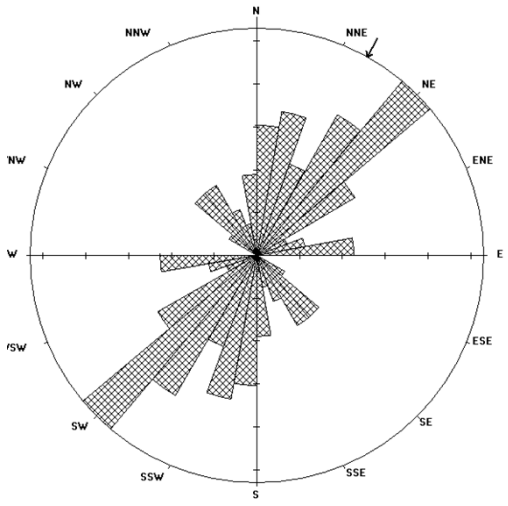

Figure 4.10: Rose diagram of trends of joints as recorded in sub-area 1. The arrow reflects the statistical maximum.

Number of data points = 84

Axial (non-polar) data

Sector angle = 10°

Scale: tick interval = 3%

Maximum = 16 %

Stress vectors:

σ_1 = 12/029

σ_2 = 76/210

σ_3 = 02/122

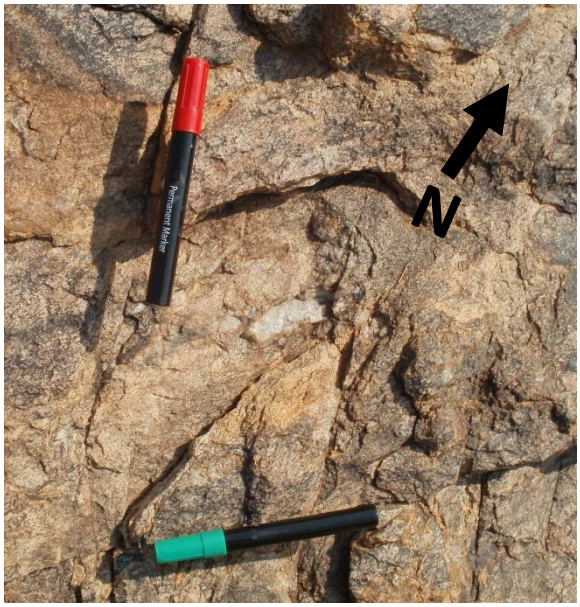

Figure 4.11: Sets of joints crosscutting the feldspathic mica rich-quartzite in sub-area 1.

4.5.2 Sub-area 2

Sub-area 2 is characterised by a closure in the calc-silicate-rich quartzite (Figure 4.1) illustrated by the yellow strike and dip symbols in Figure 4.12. The closure is also identified on aerial photographs and in the field; it is well delineated by the calc-silicate-rich quartzite.

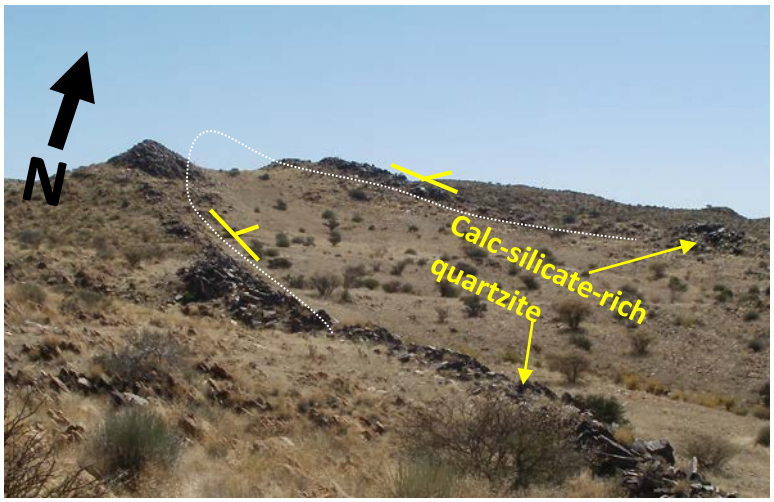

Figure 4.12: Calc-silicate-rich quartzite displaying the northern antiformal closure in sub-area 2 illustrated by the white dotted line.

4.5.2.1 Fold analysis in sub-area 2

The data points in sub-area 2 show majority of the π-poles at an angle of 10° (illustrated by two red π-circles; Figure 4.13A) from the π-circle defining the closure in sub-area 2 as a cylindrical fold based on technique of Ramsay and Huber (1987). The stereographic projection of foliation (S_0) in sub-area 2 shows one cluster (Figure 4.13A) defining an isoclinal fold with an interlimb of 0° (Rowland et al., 2007) similar to that in sub-area 1. The axial plane in sub-area 2 dips 52° towards 038° NE defining a moderately inclined fold (Fleuty, 1964). The fold axis plunges 54° towards 028° describing a moderately plunging fold (Fleuty, 1964). The structure in sub-area 2 is classified as a moderately plunging and moderately inclined isoclinal fold defining an antiform in the study area (Figure 4.1). The stereographic projection of mineral lineation (L_1) of sub-area 2 shows cluster trending to the NE (Figure 13B) similar to the orientation of the fold axis belonging to same deformation event in this sub-area. Field observations together with derived values confirm the structure in sub-area 2 as an antiform.

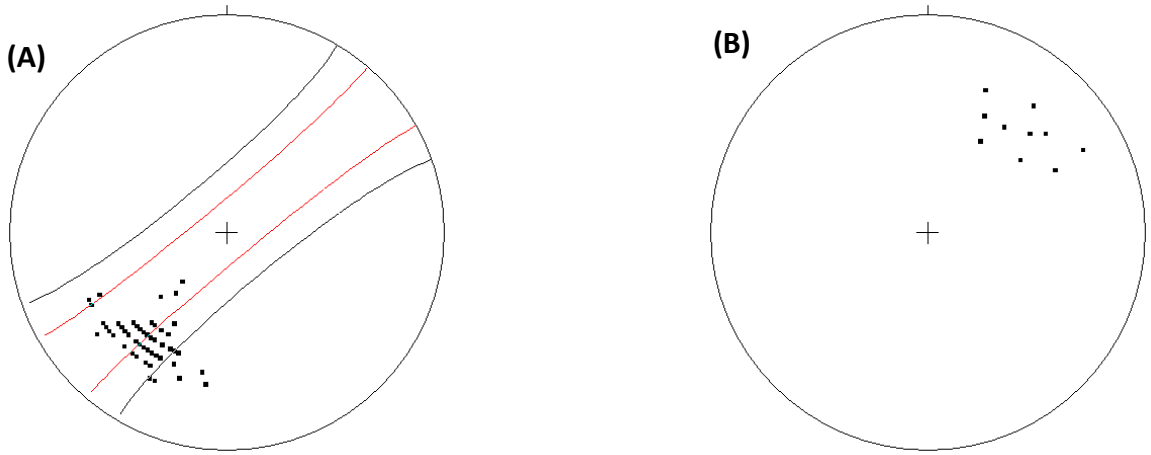

Figure 4.13: A) Stereographic plot of the foliation (S_0) of sub-area 2. B) Stereographic plot of the mineral lineation (L_1) of sub-area 2.

Mesoscopic features:

Mesoscopic structures in sub-area 2 are denoted by flattened pebbles with their long axes trending parallel to the plane of foliation (Figure 4.14A). Parasitic structures are displayed in the feldspathic mica-rich quartzite in sub-area 2 (Figure 4.14B). Field observations together with actual measurements in sub-area 2 show a steep axial plane dipping 72° towards 025° (Figure 4.15) compare to the derived values of the axial plane dipping 54° towards 028° obtained from the calc-silicate-rich quartzite forming the closure in this sub-area (Figure 4.12). Measurements of mineral lineation confirm the trend towards NE as illustrated on the detailed mapping of the structure in sub-area 2 (Figure 4.15).

Microscopic features:

The study of thin sections has revealed the presence of twinning lamellae in calcite which is used as an indicator of deformation (Passchier and Trouw, 2005). Dissolution and reprecipitation due to deformation induced pressure has been observed in the calc-silicate-rich quartzite in the form of elongated grains of calcite (Chapter 3; Section 3.4.1; Figure 3.8A). A strong compressive stress is evident in the amphibole schist. This is based on the presence of a strong penetrative foliation (Chapter 3; Section 3.4.1; Figure 3.9A) defined by aligned amphibole grains. The compressive patterns identified in thin sections of the calc-silicate-rich quartzite and amphibole schist confirm the interpretation of flattened pebbles observed in the feldspathic mica-rich quartzite in the northern closure as described above.

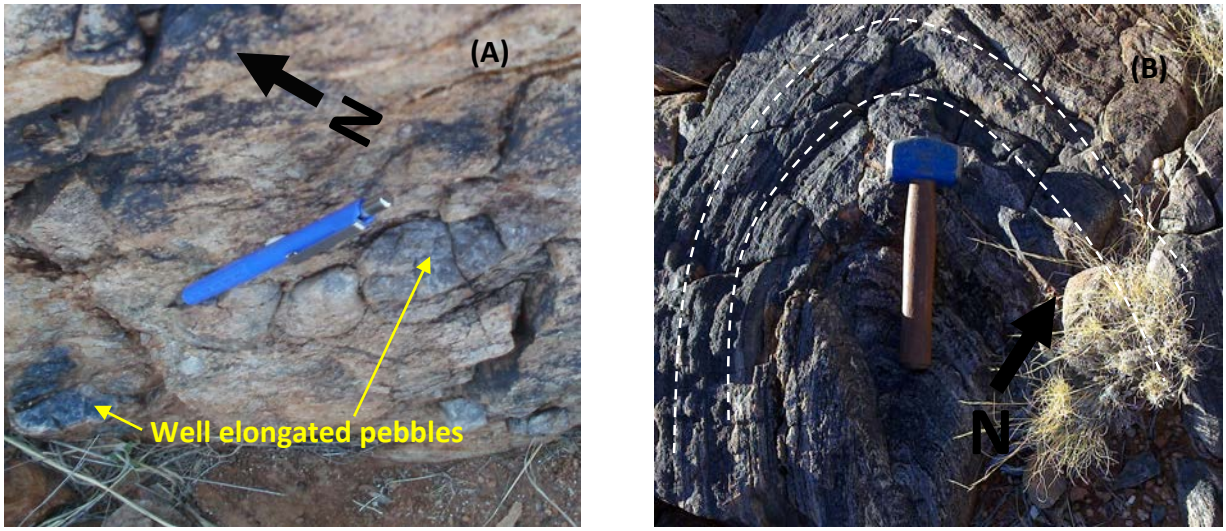

Figure 4.14: A) Feldspathic mica-rich quartzite showing highly flattened pebbles trending NW-SE. B) Parasitic structure in the feldspathic mica-rich quartzite at the closure in sub-area 2.

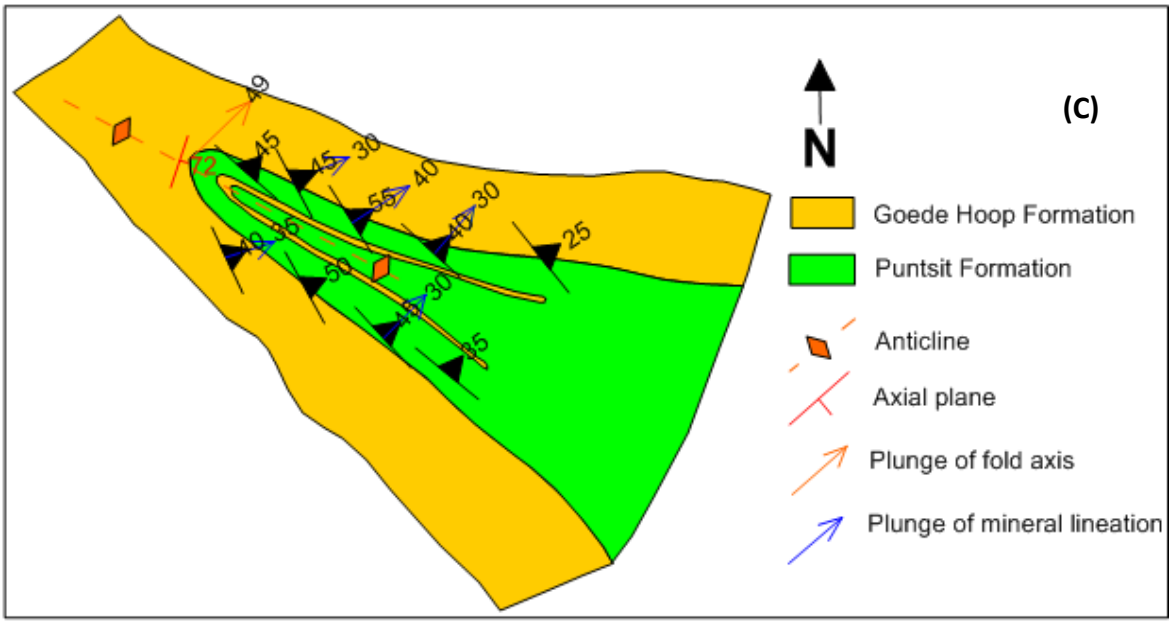

Figure 4.15: B) Parasitic structure in the feldspathic mica-rich quartzite at the northern closure of the Neusberg Mountain Range. C) Detailed mapping of the antiformal closure in sub-area 2.

4.5.2.2 Joints analysis in sub-area 2

Sub-area 2 is affected by joints and fractures. In some places the joints are filled with quartz. The joints identified in various places were individually described. A total number of 71 joint readings were recorded in sub-area 2. In order to determine the attitude of the joints and to ascertain the number of sets present, the poles to the joint planes were plotted on the lower hemisphere of the Schmidt's Equal Area net (Figure 4.16). As illustrated on Figure 4.16, the concentration of poles indicates that the joints are steeply dipping. As in sub-area 1, the stereographic projection of the joints shows two clusters (Figure 4.16). The eigenvectors are considered as stress vectors and were obtained by plotting representative joints on a stereonet and obtaining σ_2 from the intersection of two great circles representing the two most frequently occurring directions, and σ_1 and σ_3 from the acute and obtuse bisectrix respectively (Davis and Reynolds, 1996).

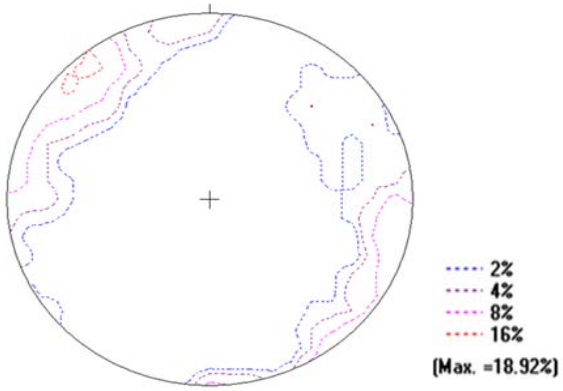

Figure 4.16: Stereographic plot of the joints for sub-area 2 displaying two clusters with a density of 16 % trending NE-SW and one trending E-W.

The orientation of the joints shows two dominant trends, a spread of joints between N-S and NE-SW are considered as one set (45°± 5°), and the second set is oriented E-W (90°± 5°) (Figure 4.17) respectively. The rose diagram of the joints in sub-area 2 confirms the sets of joints crosscutting at about 45°. A conjugate set of joints is observed in the feldspathic mica-rich quartzite of sub-area 2, where one joint, indicated in Figure 4.18 by a red marker, is displaced by another joint, indicated by a blue marker and vice versa, proving that these joints formed simultaneously and hence form a conjugate set, which allows for the determination of the three principle stress directions (Twiss and Moores, 1992; Fossen, 2010).

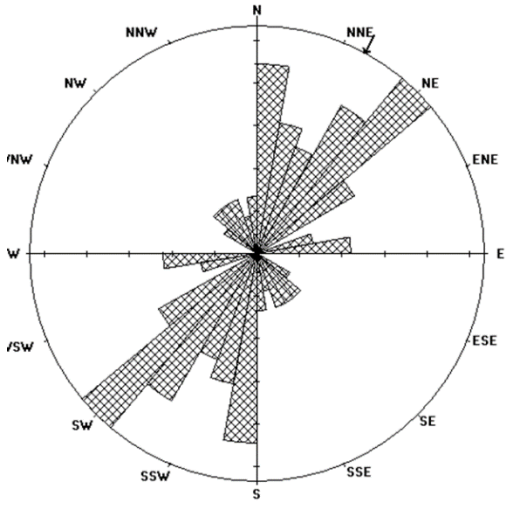

Figure 4.17: Rose diagram of the trends of the joints as recorded in sub-area 2. The arrow reflects the statistical maximum.

Number of data points= 71	Stress vectors:
Axial (non-polar) data	σ_1= 13/246
Sector angle= 10°	σ_2= 74/090
Scale: tick interval= 3 %	σ_3= 06/346
Maximum= 16 %	

Based on their geometry, the conjugate set of joints (Figure 4.18) reveals a composite mechanism for their formation. The red and blue markers define a conjugate set with a set of stresses caused by a dextral strike-slip system. Anderson (1951) has drawn attention to the relationship between joints and stress directions. Three principal stresses acted in sub-area 2 where the magnitude of the three principal stresses (σ_1, σ_2 and σ_3) are considered to be $\sigma_1 > \sigma_2 > \sigma_3$. From the derived values of the eigenvectors, the maximum (σ_1) and minimum (σ_3) stresses are horizontal and the medium stress (σ_2) is vertical. In such situations, shearing planes, being either faults or joints, may develop in planes parallel to the median stress direction and make an acute angle bisected by the maximum stress direction (σ_1), whereas tension joints are trending parallel to the maximum stress and perpendicular to the minimum stress (van der Pluijm and Marshak, 2004). Application of this theory to the joint systems in sub-area 2 would suggest that the maximum stress (σ_1) has acted in the NE-SW direction, and the minimum stress is directed perpendicular to the direction of the maximum stress. The joint analysis in this sub-area reflects a strike-slip environment according to Anderson's classification (1951). The interpretation of the relationship between the orientation of the principal stresses and operating fractures in the shear system will be done while dealing with the Neusspruit Shear Zone in order to understand if the fractures are the response to shearing in the study area.

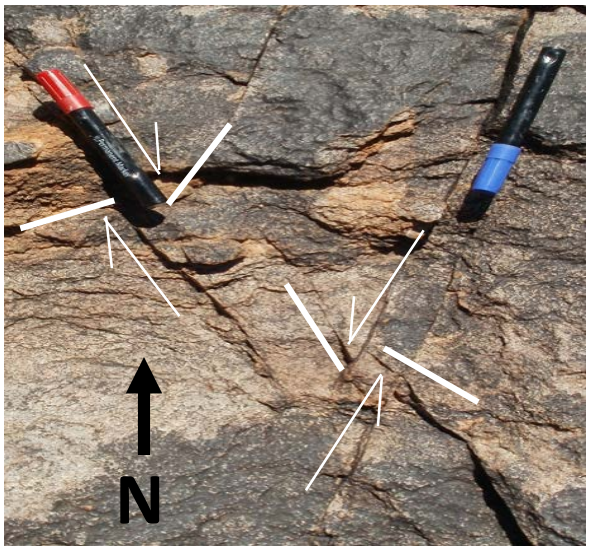

Figure 4.18: Conjugate sets of joints in the feldspathic mica-rich quartzite in sub-area 2.

4.5.2.3 Neusberg Thrust Fault (NTF)

The Neusberg Thrust Fault (NTF) is a northwest trending brittle feature that cuts the calc-silicate-rich quartzite and feldspathic mica-rich quartzite and is located north of sub-area 2 (Figure 4.1). The NTF extends for approximately 150 m in length, and is identified by the old rocks of the Puntsit Formation placed on top of the younger Goede rocks of the Hoop Formation (Figure 4.22B). The presence of a mixture of fragments of different types of rock units (Figure 4.19). The size of the clasts is comprised between 1 mm < clast size < 0.5 m. This corresponds to a breccia (Twiss and Moores, 1992; Davis and Reynolds, 1996; Fossen, 2010). This breccia is located along a valley (Figure 4.20), which defines the trace of the Neusberg Thrust Fault. It is thought that the thrust fault continues to the north of the Orange River (van Bever Donker, 1980), suggesting that it is of regional extent for both the southern and northern portions of the Neusberg Mountain Range.

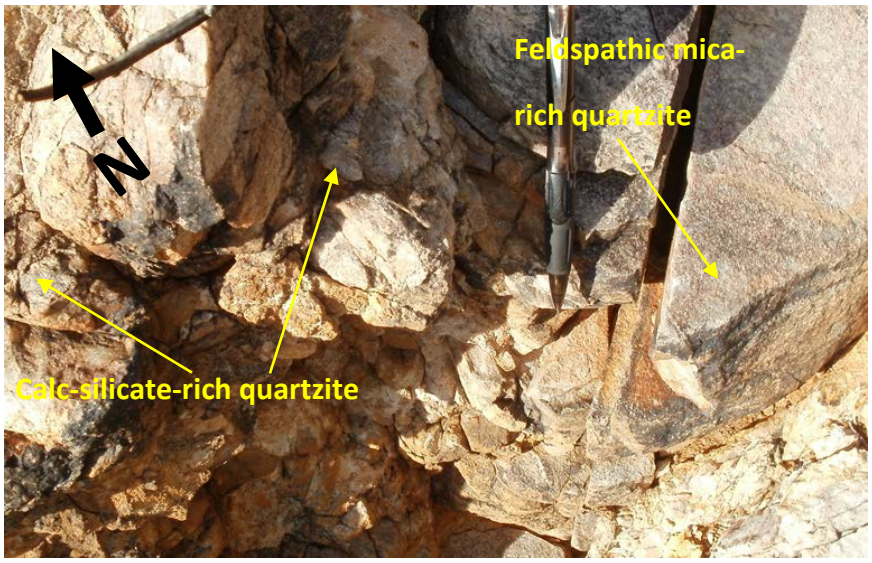

Figure 4.19: Breccia in the Neusberg Thrust Fault showing a mixture of fragments of feldspathic mica-rich quartzite and calc-silicate-rich quartzite.

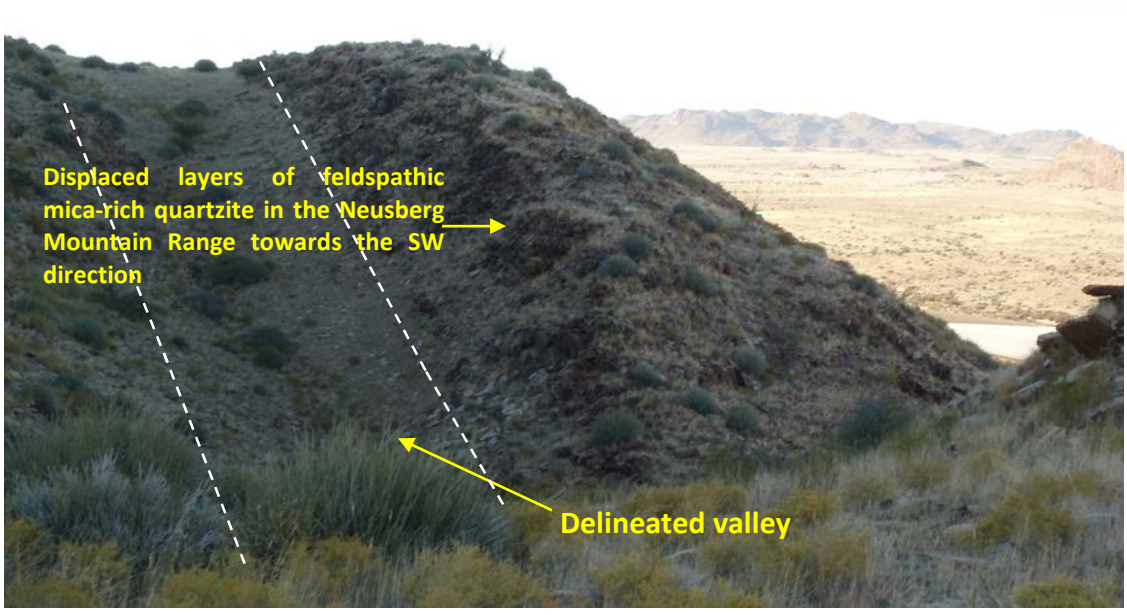

Figure 4.20: Portion of the valley along the Neusberg Thrust Fault. The direction of view is towards the southwest.

Kink bands of about 30 to 50 cm wide are developed in the feldspathic mica-rich quartzite in the vicinity of the Neusberg Thrust Fault (Figure 4.21A). Kink bands are typically related to kink folds (Figure 4.21B), which are well displayed in outcrops of the feldspathic mica-rich quartzite. The existence of kink folds could be related to the development of the thrust fault in the Neusberg Mountain Range.

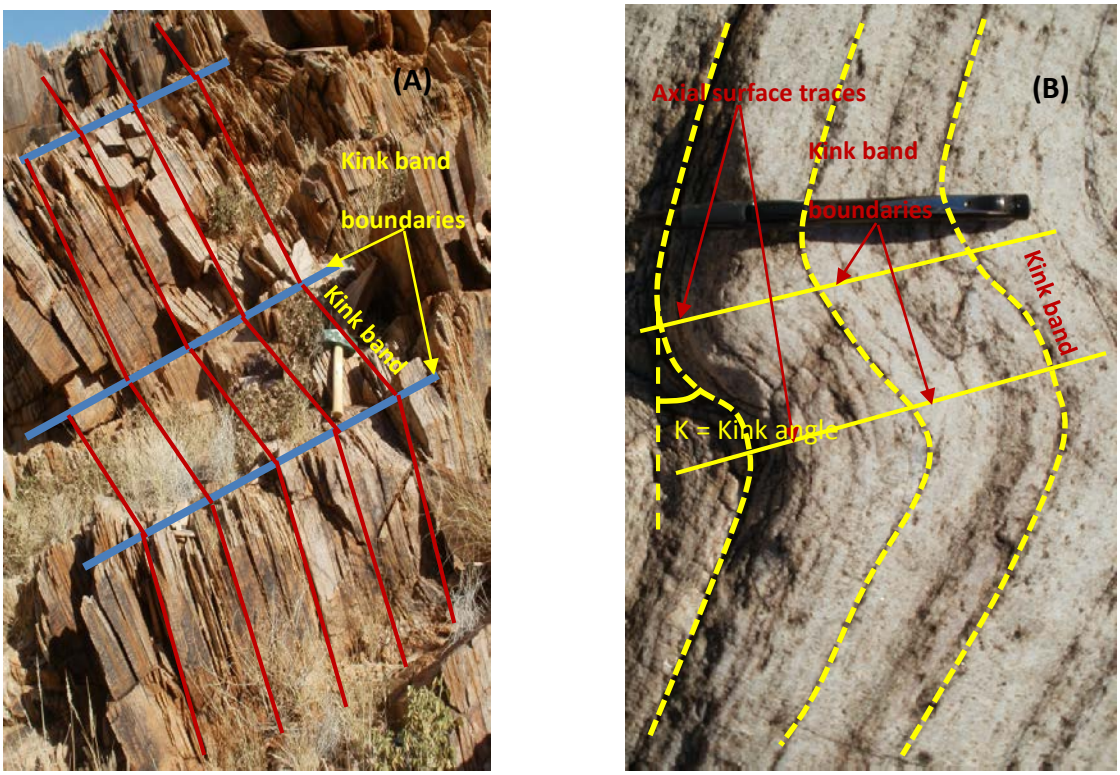

Figure 4.21: A) Kink bands deelopped in the feldspathic mica-rich quartzite. The direction of view is towards the southwest. B) Kink folds in the feldspathic mica-rich quartzite displaying the simplified geometryof a kink band. The pencil is trending north.

A model for the development of the kink bands as a result of the Neusberg Thrust Fault movement is proposed in Figure 4.21. The following assumptions were made by Fossen (2010):

1. Kink bands are cm- to dm wide zones.

2. Kink bands are bands with sharp boundaries across which the foliation is abruptly rotated.

3. Kink bands are oblique to σ_1.

4. Kink bands may develop in conjugate sets, in which case σ_1 bisects the sets of joints.

5. When kink bands occur as single sets, σ_1 is known to be oblique to the band, but its precise orientation is unknown.

An explanation for the development of kink bands and kink folds, as put forward by Twiss and Moores (2007) and displayed in the feldspathic mica-rich quartzite is as follows:

''*Assume that two phases in the development of the fault-bend fold have taken place at a ramp connecting horizontal decolléments. During the initial increment of displacement on the fault, the kink bands form, with kink band boundaries A and A' for one and B and B' for the other (Figure 4.22A). In the first phase of development, axial planes A' and B' are fixed at X' and Y', respectively, in the hanging wall block, and they migrate with the block as displacement accumulates on the fault. Axial planes A and B are fixed at X and Y, respectively, in the footwall block. Thus as displacement continues, material in the hanging wall block migrates through the axial surfaces A and B, and the kink folds grow (Figure 4.22B). This phase of development continues until the point Y' in the hanging wall block, to which axial plane B' is attached, and reaches the point X at the top of the ramp (Figure 4.22B). At this instant, the fold reaches its maximum amplitude, the axial surface B' becomes fixed at the point X in the footwall block, and the axial surface A becomes fixed to the point Y' in the hanging wall block.*''

It is of importance to highlight that the top of the fault-bend fold in the study area has been eroded away, and the breccia is composed of the mixture of the fragments of the feldspathic mica and calc-silicate-rich quartzites easily identified along the Neusberg Thrust Fault.

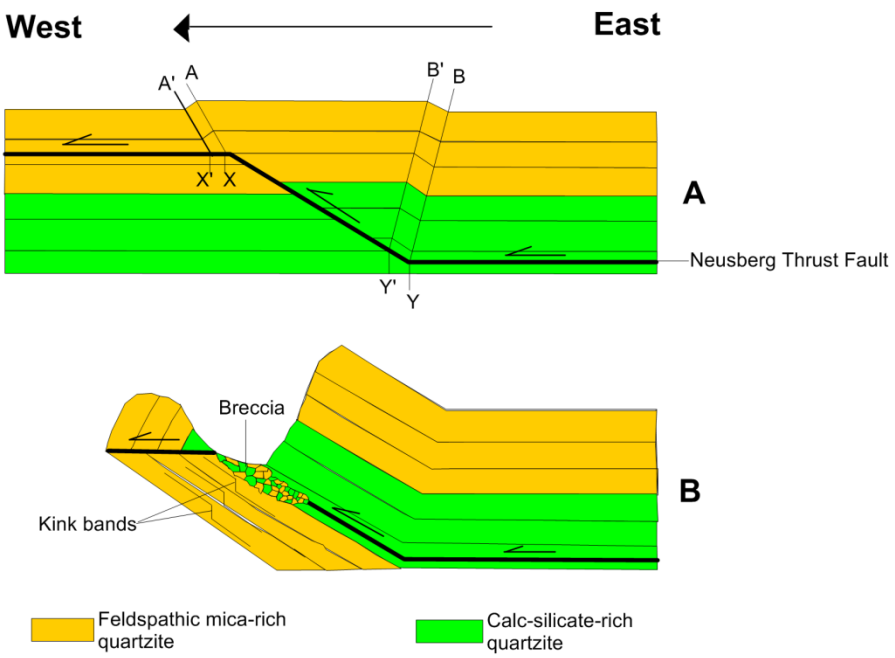

Figure 4.22: Kink model for the development of a fault-bend fold as developed in the feldspathic mica-rich quartzite (after Suppe, 1983).

4.5.3 Sub-area 3

This sub-area is delimited by the Neusberg Mountain Range (NMR) to the west and Vuurkop Mountain (VM) to the east (Figure 4.1). Sub-area 3 is underlain by deformed feldspathic mica-rich quartzite, wollastonite-bearing calcareous rocks and calc-silicate-rich quartzite (Figure 4.1). The pervasive regional foliation is present in the calc-silicate-rich quartzite and feldspathic mica-rich quartzite alike. Brittle deformation features are seen in this portion of the study area in the wollastonite-bearing calcareous rock (Figure 4.23).

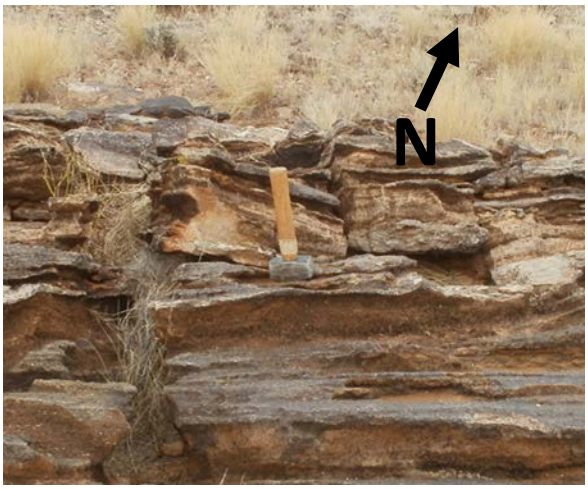

Figure 4.23: Well jointed and fractured outcrop of the wollastonite-bearing calcareous rock.

4.5.3.1 Fold analysis in sub-area 3

The number of data points for the analysis of the foliation (S_0) in sub-area 3 is not enough to apply a pi diagram with countours. With only 30 data points for sub-area 3, it is better to show a plot without countours and/or a beta diagram (Figure 4.24). The stereographic projection of the structure in sub-area 3 shows that the foliation (S_0) describes an open fold with a degree of tightness defined by an interlimb angle of 100° which is classified according to Rowland et al. (2007). Derived values from the stereographic projection show that the axial plane dips 49° towards 043° describing a moderately inclined fold according to the classification of Fleuty (1964). The fold axis plunges 36° towards 092° defining a moderately plunging fold (Fleuty, 1964). The structure in sub-area 3 is described as a moderately plunging and moderately inclined open fold defining a synform (Figure 4.1). No actual measurements of fold axis and axial plane were taken as opposed to sub-areas 1 and 2.

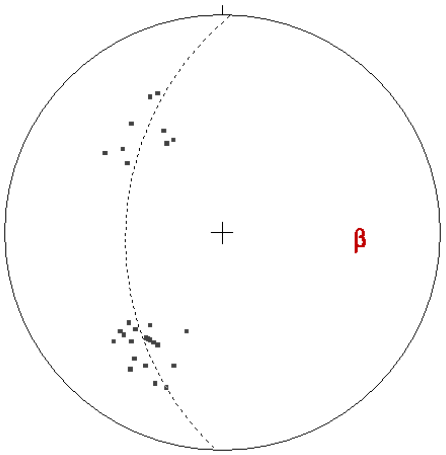

Figure 4.24: Stereographic plot of the foliation (S_0) of sub-area 3. Only nine points cluster yet significantly different from the southern cluster.

Mesoscopic structures

Sub-area 3 contains pinch-and-swell structures, boudins, faults and joints. Pinch-and-swell structures (Figure 4.25A) occur within the calc-silicate-rich quartzite. They form when a stiff layer (quartzite) in a weaker matrix (calc-silicate) is subject to layer-parallel extension, or, equivalently, layer-normal shortening (Kidan and Cosgrove, 1996). The competency contrast between the silicate and the carbonate is evident in sub-area 3, with the direction of the long axis of the swells (Figure 4.25A) or boudins (Figure 4.25B) trending NW-SE. This is similar to that identified along the Neusspruit Shear Zone in the calc-silicate-rich quartzite located west of the Neusberg Mountain Range, and similar to the Neusberg itself in sub-area 1. It is suggested that the pinch-and-swell structures form by continuous extension, while discrete boudins commonly form after extension and subsequent disruption of layers, bodies or foliation planes within a rock mass (Ramberg, 1955; Goscombe et al., 2004; Pollard and Fletcher, 2005; Figures 4.25A and B). The separation into individual boudins means that the extension exceeded the strength of the competent band causing it to fail. Small scale fractures occur in the quartzite (Figure 4.25A). The presence of discrete ''Z-shaped boudins'' (Figure 4.25A) could be the result of drag along a Riedel shear (Twiss and Moores, 1992). Another interpretation is that the boudins are

slightly rotated which would happen if the extension is not layer parallel. A displacement of approximately 3 to 4 millimetres has been recorded along the truncated boudins and quartz veins (Figure 4.25B). This can be related to the brittle deformation (D_1) in the study area. Some joints in the feldspathic mica-rich quartzite are filled with quartz crystals of about 1 to 3 centimeters long (Figure 4.25C). The quartz crystals are oriented perpendicular to the wall of the joint indicating that these joints are extension joints.

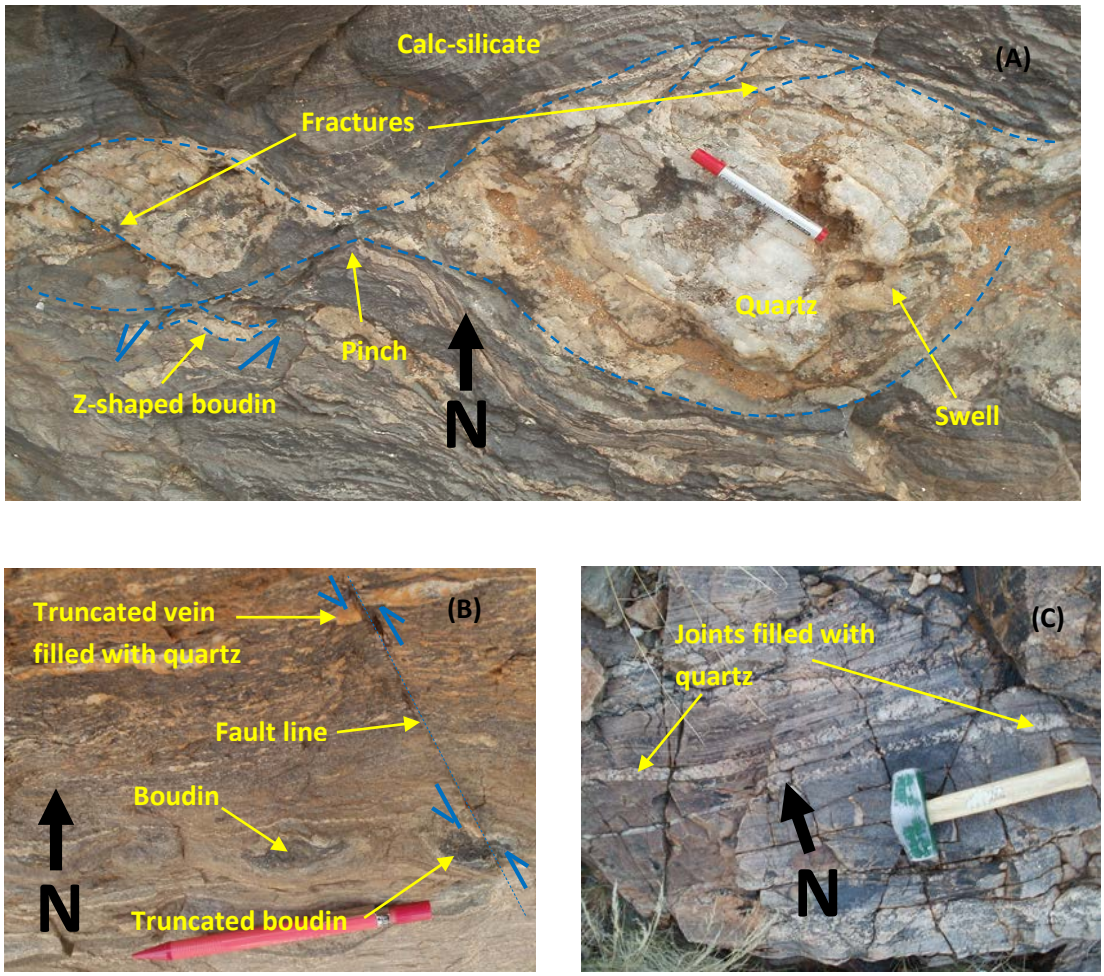

Figure 4.25: A) Outcrop of calc-silicate-rich quartzite displaying pinch-and-swell structure and a "Z-shaped" boudin. Refer to text for explanation. B) Truncated boudin and quartz vein in the calc-silicate-rich quartzite. C) Outcrop of feldspathic mica-rich quartzite displaying joints filled with quartz crystals.

Microscopic structures

Microscopic structures are present in the calc-silicate-rich quartzite, but are restricted to undulose extinction in quartz grains and twinning lamellae in calcite respectively. This shows that the recovery process in these rocks has been halted probably to decreasing temperature or releasing stresses (Passchier and Trouw, 2005).

4.5.3.2 Joints analysis of sub-area 3

Field observation, combined with satellite imagery and data analysis of orientation data obtained on the outcrops provided a better understanding of the deformation in sub-area 3. The stereographic projection of the joints in this sub-area (Figure 4.26) shows various clusters which are interrelated and correlated with the orientations displayed by the rose diagram (Figure 4.27). Joint orientations for sub-area 3 show two dominant steeply dipping trends of east-northeast (70°± 5°) and north (340°± 5°) (Figure 4.27). The rose diagram analysis shows that the joints crosscut at about 60°.

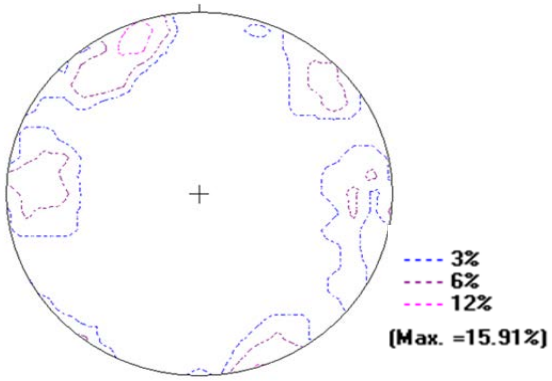

Figure 4.26: Stereographic plot of the joints of sub-area 3 displaying five clusters with a density of 6 % mostly directed N-S, ENE-WSW, and NW-SE.

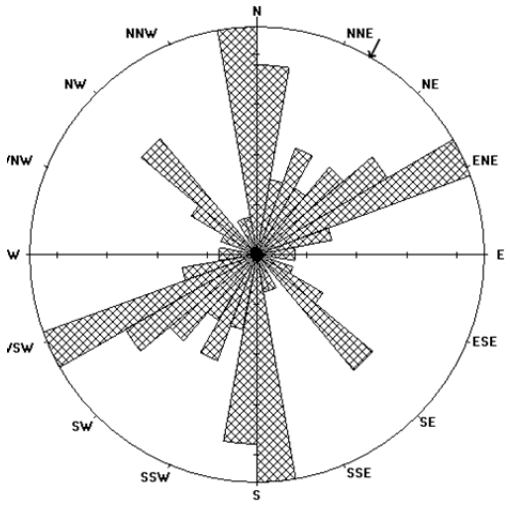

Figure 4.27: Rose diagram of trends of joints as recorded in sub-area 3. The arrow reflects the statistical maximum.

Number of Data Points = 44

Axial (non-polar) data

Sector angle = 10°

Scale: tick interval = 3 %

Maximum = 14 %

Stress vectors:

σ_1 = 26/023

σ_2 = 64/200

σ_3 = 00/294

4.5.4 Sub-area 4

Sub-area 4 is located north of Vuurkop Mountain. It is underlain by deformed rocks of wollastonite-bearing calcareous rocks, calc-silicate-rich quartzite and feldspathic mica rich-quartzite (Figure 4.1). From field observation, the folded rocks of the wollastonite-bearing calcareous rocks and calc-silicate-rich quartzite show a fold axis trending in the NW-SE direction (Figure 4.1). Brittle deformation features, in the form of joints and fractures, are present in both rock types.

4.5.4.1 Fold analysis in sub-area 4

The stereographic plot of the foliation (S_0) displays two clusters (Figure 4.28) describing an open fold with an interlimb angle of 95° according to the classification of Rowland et al. (2007). Derived values from the stereographic projection indicate that the axial plane dips 46° towards 046° describing a moderately inclined fold according to the classification of Fleuty (1964). The fold axis plunges 38° towards 096° defining a moderately plunging fold (Fleuty, 1964). The structure in sub-area 4 is described as a moderately plunging and moderately inclined open fold defining an antiform (Figure 4.1). Mineral lineation was not found in this sub-area.

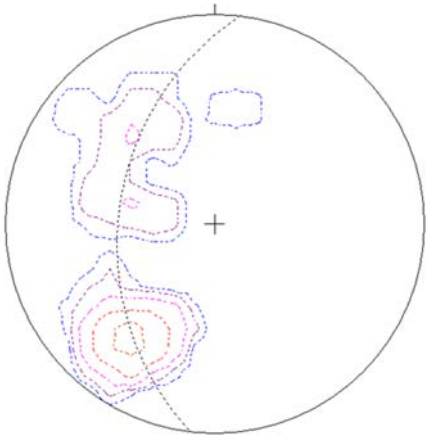

Figure 4.28: Stereographic plot of the foliation (S_0) of sub-area 4.

Mesoscopic structures:

The small scale folds in sub-area 4 are formed within the calc-silicate-rich quartzite affected later by fractures (Figure 29A). Field observations together with actual measurements in sub-area 4 define a steep axial plane dipping 75° towards 020° (Figure 29A) compare to the derived values of the axial plane dipping 45° towards 046° indicating a rotation after folding due to possible impacts of intusive charnockite along the Vuurkop Mountain. Small scale folds also occur in the wollastonite-rich bands as flow structures (Figure 4.29B). The flow structures

observed in the bands of wollastonite-bearing calcareous rock are defined as 'W-shaped' parasitic folds (Figure 4.29B). The northeast trending axial trace (blue dotted line; Figure 4.29B) may represent an earlier deformation phase subsequently deformed and refolded, as illustrated by the hammer representing the axial trace trending northwest (Figure 4.29B).

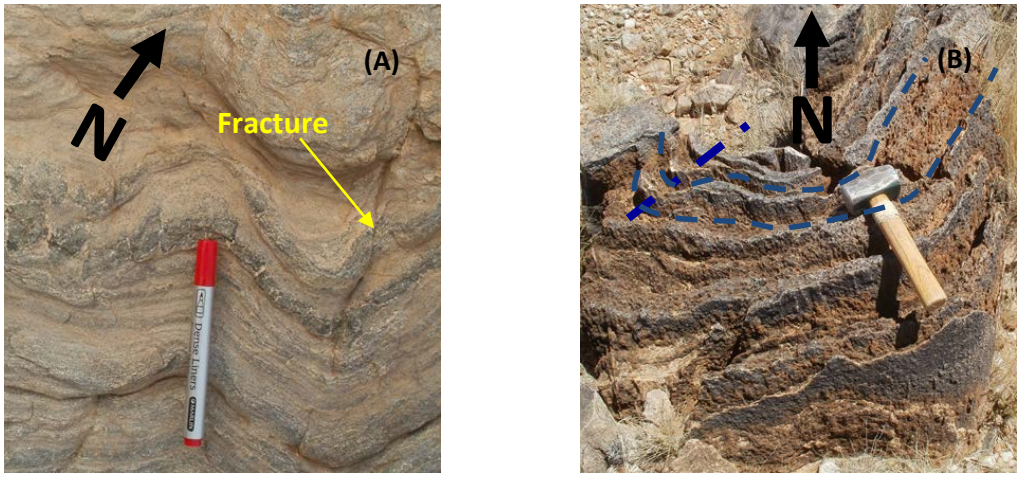

Figure 4.29: A) Open folds in well deformed calc-silicate-rich quartzite rock. The marker indicates the trace of a fold axial plane trending northwest. B) Flow structures defining 'W-shaped' parasitic folds in the wollastonite-bearing calcareous rock. The hammer indicates the trace of a fold axial plane in the northwest direction, and the blue dotted line is oriented along the fold axial trace in the northeast direction.

Microscopic structures:

The thin section of the calc-silicate-rich quartzite from this sub-area shows interlocking grains and lack of triple point junctions as signs of recrystallization in quartz grains (Passchier and Trouw, 2005). Twinning lamellae are present in some grains of calcite and wollastonite reflecting strain effects in crystals of these minerals. The grains of plagioclase in the feldspathic mica-rich quartzite forming the fold hinge in this sub-area (Figure 4.1) display a vague twinning reflecting strain effects.

4.5.4.2 Joints analysis of sub-area 4

The concentration of poles displays two clear clusters in the stereonet (Figure 4.30). The rose diagram for the orientation of joints for this sub-area also shows two dominant trends; northerly (360°± 5°) and east-northeast (70°± 5°) respectively (Figure 4.31). The two joint sets trending northerly and east-northeast crosscut at about 70° (Figure 4.31). The joints and fractures are well developed in both the calc-silicate-rich quartzite (Figure 4.29A).

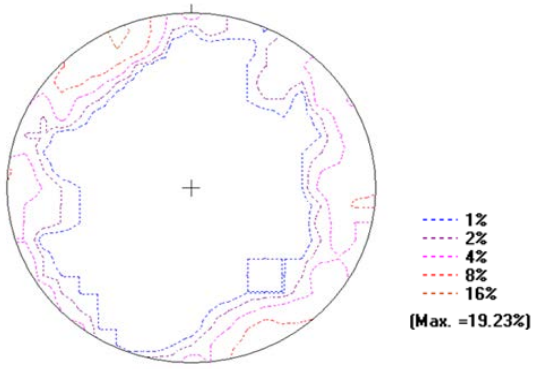

Figure 4.30: Stereographic plot of the joints of sub-area 4 displaying two clusters with a density of 8 % mostly directed N-S and ENE-WSW.

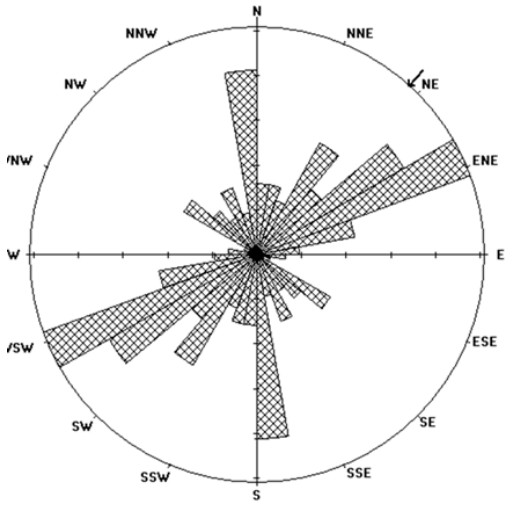

Figure 4.31: Rose diagram of trends of joints as recorded in sub-area 4.

Number of Data = 101	Stress vectors:
Axial (non-polar) data	σ_1 = 06/200
Sector angle = 10°	σ_2 = 80/328
Scale: tick interval = 3 %	σ_3 = 08/110
Maximum = 15 %	

4.6 Analysis of joints encountered in the charnockite

The presence of joints and fractures in the charnockite is of great importance as they indicate brittle deformation in this lithology. The stereographic projection of joints does not display proper sets of clusters (Figure 4.32). The rose diagram shows multiple orientations of the joint sets (Figure 4.33). The stress vectors in the charnockite are not taken into consideration in this study as there is not enough evidence of any systematic distribution. The joints in the charnockite are locally filled with epidote (Figure 4.34). The presence of brittle features (fractures and joints) in the charnockite is considered to be the last phase of deformation (D_4) in the study area because the charnockite intrudes after the deformation (D_1), seeing that the charnockite intrudes into D_1 structures. Joints elsewhere in the study area are systematic but those present in the charnockite are non-systematic either because the charnockite was still not crystallised when the shearing took place or because the intrusion happened after the shearing which caused the systematic joints.

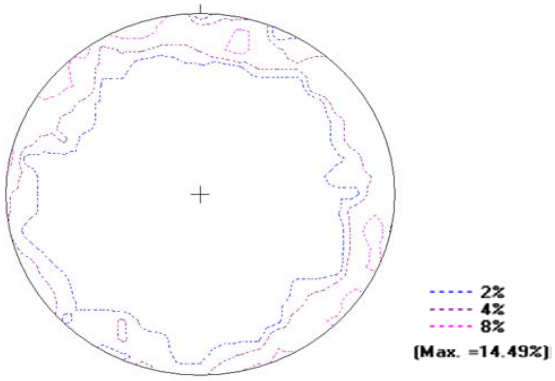

Figure 4.32: Stereographic plot of joints in the charnockite.

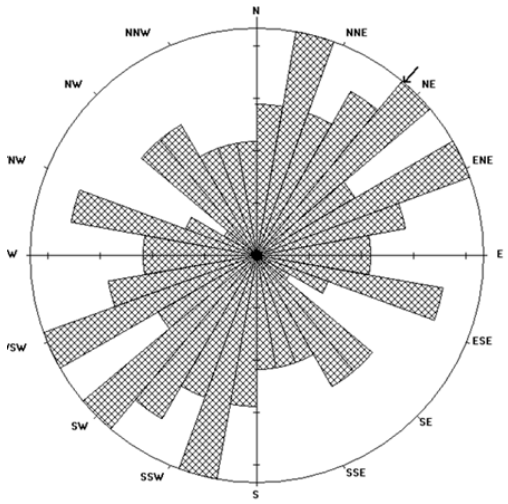

Figure 4.33: Rose diagram of joints recorded in the charnockite.

Number of Data Points = 69

Axial (non-polar) data

Sector angle = 10°

Scale: tick interval = 10 %

Maximum = 15 %

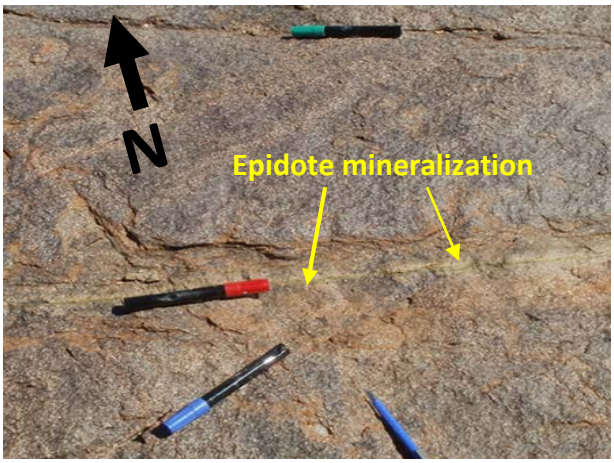

Figure 4.34: Outcrop of charnockite crosscut by joints filled with epidote.

4.7 General overview of axial plane analysis in the sub-areas

The analysis of the axial planes from the different sub-areas is of great importance as it gives succinct information for a better understanding of the various phases of deformation that took place in the study area. The direction of dip and angle of dip of the axial plane of each sub-area is given in Table 4.1. The annotation of each axial plane on the stereogram allows identification and differentiation between the axial planes of each sub-area: (1) axial plane of the synform in sub-area 1; (2) axial plane of the antiform in sub-area 2; (3) axial plane of the synform in sub-area 3; (4) axial plane of the antiform in sub-area 4. The axial planes of sub-areas 2, 3, and 4 show similar trends compare to that of sub-area 1 (Figure 4.35). The axial planes in the study area dip towards the northeast (Figure 4.35), and show that all four sub-areas formed as a result of the same deformational event, but actual measurements (Figure 4.8) and derived values (Table 4.1) show that the axial plane of sub-area 1 is steeply inclined with the direction of dip difference of some 10 degrees compare to those of sub-areas 2, 3, and 4 which are moderately inclined. Such differences in the axial plane and direction of dip could be due to the competency of the rocks, possibility of flattened basin and/or impact of the thrusting north of sub-area 2 related to continue indenting of the Kaapvaal Craton from the east towards the west.

Table 4.1: Orientation data of the axial plane for each sub-area.

Axial plane	Dip	Dip direction
Sub-area 1	69	033
Sub-area 2	52	038
Sub-area 3	49	043
Sub-area 4	45	046

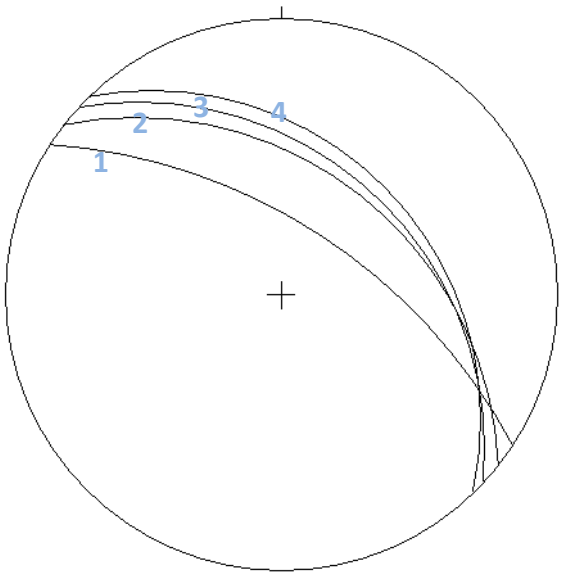

Figure 4.35: Plot of the axial planes of the different sub-areas. The number indicates the axial plane of each sub-area.

4.8 General overview of stress vectors analyses of joints in the sub-areas

The rose diagram analysis of joints shows various orientations of brittle deformation in the study area. The analysis of each sub-area shows that the joints and fractures are trending in the N and NE direction, as illustrated on the rose diagrams for sub-areas 1 and 2 (Figure 4.36) in the

Neusberg Mountain Range. The rose diagrams of joints and fractures in sub-areas 3 and 4 (Figure 4.36) are trending in the N, NW and ENE direction respectively. This analysis shows that the joints crosscut at angles between 30° and 90°. According to Anderson's theory of faulting (Anderson, 1951), the classification of faults depends on the fact that the surface of the Earth is a free surface which can support no shear stress. The stress analysis of joints and fractures in the four sub-areas shows that the entire study area has been affected by strike-slip faults, as the intermediate stress σ_2 in the four sub-areas is approximately vertical relative to the other stresses (Table 4.2), which according to Anderson (1951) and Twiss and Moores (1992) indicates a strike-slip environment.

Table 4.2: Orientation data of principal directions of stress for the joints in each sub-area.

Sub-area	σ_1	σ_2	σ_3
Sub-area 1	12/029	76/210	02/122
Sub-area 2	13/246	74/090	06/346
Sub-area 3	26/023	64/200	00/294
Sub-area 4	06/200	80/328	08/110

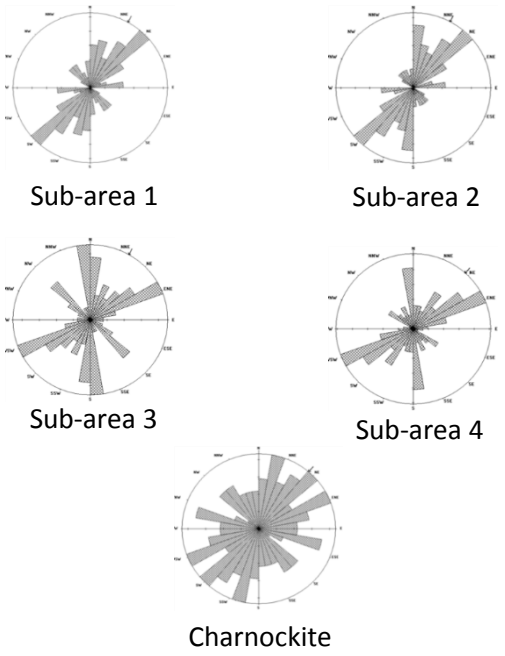

Figure 4.36: Rose diagram analyses of the joints in the 4 sub-areas and the charnockite.

4.9 Origin of joints in the charnockite

Discontinuities, such as fractures and joints are potential sites for fluid transport and have important implications for the hydraulic properties of rock (Clark et al., 1995; André-Mayer and Sausse, 2007). Such mechanisms of stressing the Earth's crust as: (1) the overburden, (2) the driving mechanisms of plate tectonic processes, (3) horizontal and vertical motions, (4) changes in temperature and pressure, and (5) pore fluid pressure have been put forward to understand the possible origin of fractures and joints (Twiss and Moores, 1992; Davis and Reynolds, 1996; van der Pluijm and Marshak, 2004; Fossen, 2010). Looking at the variety of mechanisms for inducing and changing stress conditions, it is not surprising that fractures in the crust have numerous possible origins.

Pore fluid pressure is considered as important for several reasons. Firstly, it lowers the effective stress necessary to cause failure and permits fracture at depth where the rock otherwise would be either stable or in the realm of ductile behaviour (Twiss and Moores, 1992). Secondly, it can change the conditions of frictional sliding from those favouring stick-slip behaviour to those

favouring stable sliding (Twiss and Moores, 1992; Davis and Reynolds, 1996). And thirdly, it can change deformation from cataclastic flow to frictional sliding (Twiss and Moores, 1992; Davis and Reynolds, 1996; Fossen, 2010). The presence of pore fluid pressure in a charnockite strongly affects its mechanical response and can cause extension fracturing even under conditions of purely compressive applied stresses.

Taking also into account that charnockites are generated by anhydrous melting of lower crustal material (Frost and Frost, 2008), the results of increasing temperature and pressure are commonly dehydration or decarbonation reactions that release water or carbon dioxide, respectively, into the rock (Twiss and Moores, 1992; Philpotts and Ague, 2010; Winter, 2010), increasing the coefficient of thermal expansion, so that if the pores are saturated with fluids, the pore fluid pressure will increase with temperature. This phenomenon is referred to as aquathermal pressuring (Twiss and Moores, 1992; Davis and Reynolds, 1996). Most crystalline rocks are highly impermeable, and if the fluids are produced faster than they can migrate away through the rock, the pore fluid pressure will increase (Twiss and Moores, 1992).

In this present case, joints related to exhumation should be more or less parallel to the surface due to stress release. In some places in the study area, outcrops of charnockite have been identified with crosscutting joint sets, but the rose diagram of joints recoded for the charnockite displays multiple trends of joints in sharp contrast with the systematic and evidently tectonism related joints in the rest of the study area. Another explanation for the formation of the joints may be that the charnockite intruded at relatively shallow crustal levels, thus bringing the rock quickly into the brittle regime rather than the ductile state once cooling started. In this scenario, the joints would develop as the result of rapid cooling rather than tectonic processes.

4.10 Limits on joint development

Having already mentioned above various ways in which joints can form, it is important to give the ways in which joints stop developing. Joints stop growing for various reasons. For instance,

joints stop developing when they get to the Earth's surface. The joints stop growing in the subsurface where they intersect a pre-existing open fracture (joint or fault) or a weak bedding plane, or where they pass downward into ductile rock (van der Pluijm and Marshak, 2004). Two joints that are developing towards each other, but are not in the same plane, stop developing when they enter each other's stress shadow (Figure 4.37A).

In some situations, the interaction of joint tips causes a curvature where the two joint tips interfere (Figure 4.37B) (Twiss and Moores, 1992; van der Pluijm and Marshak, 2004). In the case where a pre-existing joint is squeezed together so tightly that friction allows shear stress to be transmitted across it, or if it has been sealed by vein material, then a younger joint can cut across it (van der Pluijm and Marshak, 2004). Formation of the joint itself may cause a local drop in fluid pressure, because creation of the joint creates space for fluid flow (van der Pluijm and Marshak, 2004; Bons et al., 2012). This increase in space temporarily causes a drop in fluid pressure, so that the stress intensity at the joint tip becomes insufficient to propagate into unfractured rock (van der Pluijm and Marshak, 2004).

In the case where a joint grows into a region where the energy at the crack tip can be dissipated by plastic yielding, the joint stops growing (van der Pluijm and Marshak, 2004) (Figure 4.37C). Similarly, the propagation of a joint into a rock with a different stiffness or tensile strength may cause it to stop growing (Davis and Reynolds, 1996). Also, if the joint tip enters a region where the stress intensity at the crack tip becomes too small to drive the cracking process, then the joint stops growing (van der Pluijm and Marshak, 2004).

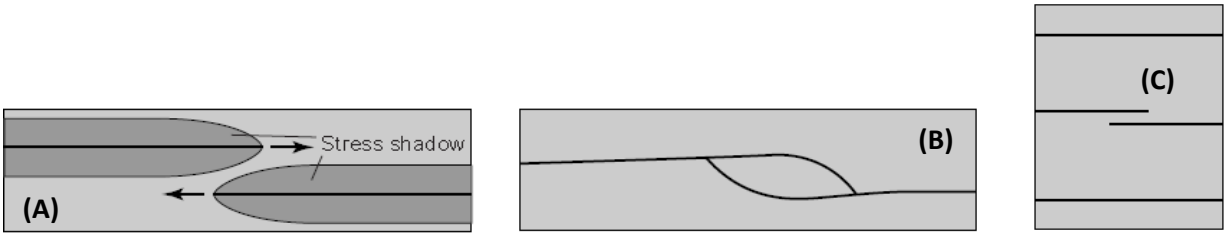

Figure 4.37: Joint terminations. (A) Joints terminating without curving when they approach one another. (B) Joints curving into each other and linking. (C) Map view sketch illustrating how joint spacing is fairly constant because joints that grow too close together cannot pass each other (after van der Pluijm and Marshak, 2004).

4.11 General overview of stress vectors analysis in the charnockite

According to Adekoya (1977), joints are quantitative and directional manifestations of operative forces that can give an idea of possible stress distribution in a deformed rock. The charnockite occurs in the study area as a massive intrusion, seen particularly at Tweelingkop; small intrusions and pavement outcrops are also observed in places. The rose diagram of joints recorded in the charnockite does not show a proper distribution of trends. Field observations have revealed that the outcrops of charnockite have medium to coarse grained texture, where no clear evidence for the development of any fabric has been identified in the rock. On the basis of petrographic observations: (1) faint foliation is displayed by semi-aligned biotite and axes of some elongate quartz grains; (2) micro-cracks are identified in quartz grains; (3) undulose extinction in quartz grains. All these are characteristics of deformation and indeed an assertion that the charnockite has been subjected to some degree of stress and thus experienced deformation, which may be the internal pressure, such as aquathermal pressure (Twiss and Moores, 1992; Davis and Reynolds, 1996), resulting from the fact that the charnockite intruded late-tectonically and was subjected to deformation. Evidences of existing stress fields from joint and petrographic studies suggest that the charnockite in the study area has been subjected to deformation leaving undulose extinction, crystal elongation, micro-fractures and compressed twin planes accompanied by exsolution.

4.12 Neusspruit Shear Zone (NSZ)

The Neusspruit Shear Zone is a prominent northwest striking structure that can be traced further south and north of the study area and extends the full 12.5 km of the study area. The shear zone is characterised by penetrative foliation parallel to the fault plane. The Neusberg Mountain Range to the east of the Neusspruit Shear Zone shows significant mesoscopic flattening of pebbles with the long axes parallel to the plane of foliation in the feldspathic mica-rich quartzite. On the west side of the Neusberg Mountain Range, mylonites are observed within the shear zone and have been identified as protomylonites according to the classification of Passchier and Trouw (2005) (Chapter 3; Section 3.6.3). Augen structures occur in the augen

gneiss along the shear zone. Continued shearing stretches the fold pattern, leaving behind a complex geometry that can only be interpreted by carefully tracing the layering (van der Pluijm and Marshak, 2004). An example of this fold transposition is displayed in the Neusspruit Shear Zone where 'S-shaped' parasitic fold types occur along the Neusspruit Shear Zone (Figure 4.38A). From field observations, the 'S-shaped' here is an asymmetry on the closure of the Neusberg Mountain Range in sub-area 1. The expected directions of fractures in a strike-slip environment in the same orientation as the NSZ is illustrated in Figure 4.38B. A comparison with Figure 4.36 shows that the patterns of the rose diagrams are different from those operating in the Neusspruit Shear Zone (Figure 4.38C), implying that the occurrence of the joints in the study area is not related to the shearing along the NSZ.

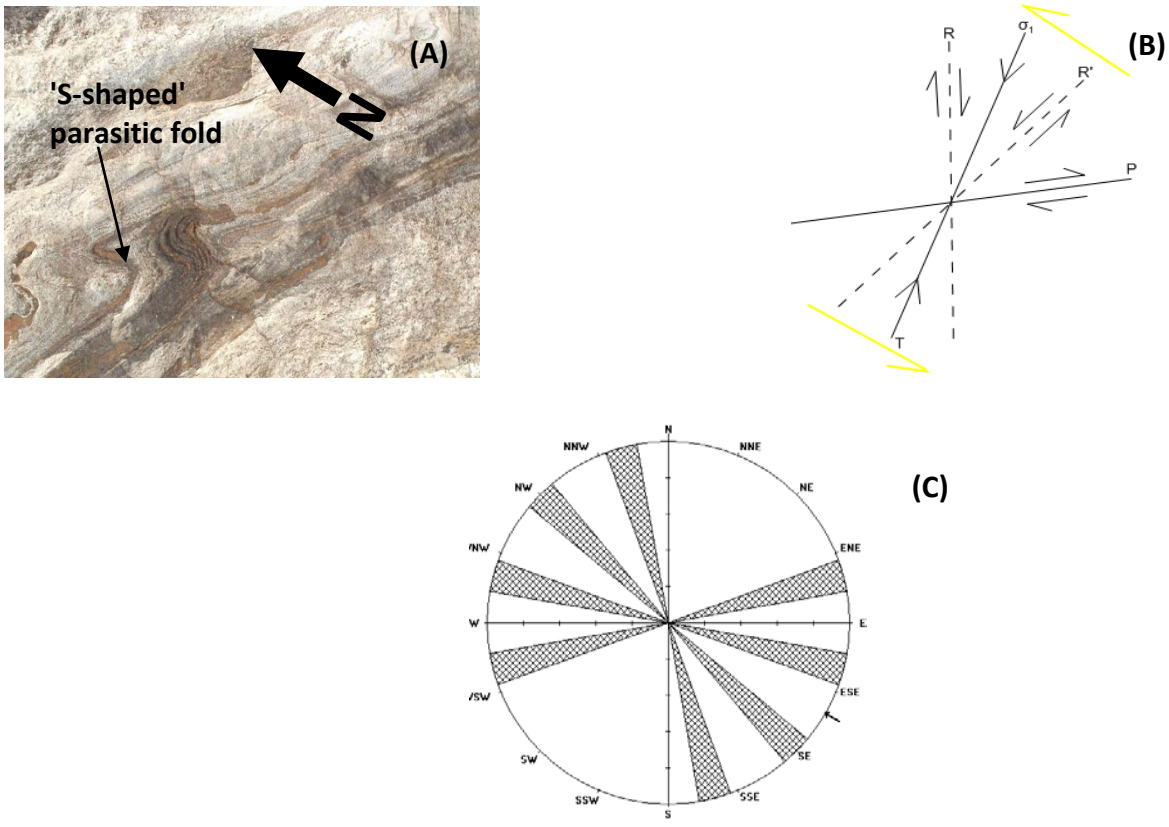

Figure 4.38: A) Asymmetrical 'S-shaped' fold illustrated in mafic bands along the Neusspruit Shear Zone. B) Hand sketch (not to scale) interpretation of the relationschip between the orientation of the principal stresses and operating patterns in the shear system. Abbreviations: R= Riedel shear; R'= antithetic Riedel shear; P= shear fracture; T= extension fracture. After Petit (1987). Rose diagram of the shear system in the sinistral strike-slip movement in the NSZ.

4.13 Vein fill along and adjacent to the NSZ

Veins are extension fractures that are filled with mineral deposits, generally massive or fibrous crystal grains such as quartz or calcite (Twiss and Moores, 1992). Veins are very significant structures for a variety of purposes. They represent phases of geological activity that occurred after formation of the host rock, and are therefore valuable to determine the geological history of the considered host rock (Bons et al., 2012). The shape, orientation and internal structures of veins provide information about palaeo-stress fields, deformation kinematics, and fluid pressure (van der Pluijm and Marshak, 2004; Bons et al., 2012). The mineralogy and geochemistry of vein-filling minerals and fluid inclusions give useful information on metamorphic conditions during vein formation, fluid characteristics and the origin of fluids (Bons et al., 2012). Veins are closely linked to fracture mechanics, since most veins form by development of minerals into space created by fractures (Davis and Reynolds, 1996; Bons et al, 2012). Veins display a wide variety of internal structures, resulting from various combinations of crystal shape (blocky or fibrous; Figure 4.39) and growth direction (from the vein wall into the vein, or in the opposite direction) (Bons et al., 2012).

Fibrous veins are formed as the result of the crack-seal process. The process starts by an intact rock containing pore fluid that in turn contains dissolved minerals (van der Pluijm and Marshak, 2004). If the fluid pressure increases, the vein cracks and a slight opening develops which is immediately filled with fluid, but since the fluid pressure within the open crack is less than in the pores of the surrounding rock, the solubility of the dissolved material decreases and the mineral precipitates, thereby sealing the crack (van der Pluijm and Marshak, 2004). Such a process has not been identified along and adjacent to the NSZ.

In blocky veins, the crystals of vein mineralization are coarsely equant, and may display crystal faces. This has been identified in the veins of the Goede Hoop Formation (Figure 4.39). Their emplacement suggests that the vein was an open space during the time of mineralization. This is possible only in veins formed near the surface, where rock strength is sufficient to permit a cavity to stay open or fluid pressure is great enough to hold the fracture open, so that previously formed vein fill later recrystallized to form blocky crystals, or so that there were few

nucleation sites for crystals to grow from during vein formation (van der Pluijm and Marshak, 2004). It can be concluded that the metasedimentary rocks were favourable for the blocky veins compared to the granitic gneisses and intrusive rocks in the study area.

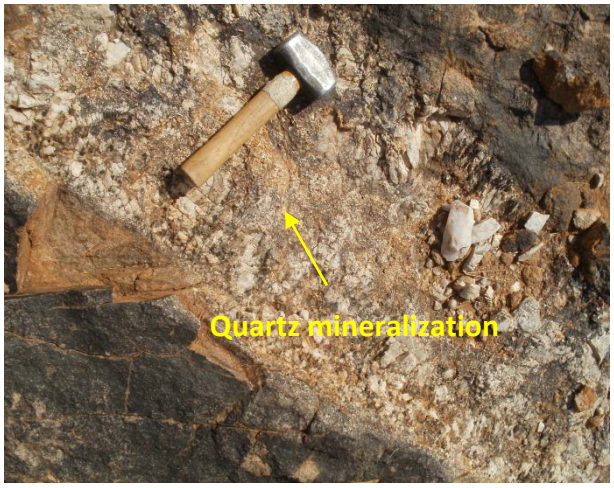

Figure 4.39: Blocky vein of quartz in the Goede Hoop Formation.

4.14 Discrepancies of the structural analysis in the Neusberg Mountain Range

The southern part of the Neusberg Mountain Range (NMR) culmination in the central portion of the Kakamas Terrane (Figure 1.2) is a region of intense ductile shear and brittle deformations associated with tilting and exhumation of varying metamorphic grade from amphibolite to granulite facies. The southern closure of the NMR presents uniformity of axial plane, fold axis, lineation, and micro- and meso-structures combined into a common geometric pattern (sub-area 1), indicative of plausible sheath folding in the NMR. Sheath folds are defined as highly curvilinear folds, typically considered to develop by hinge rotation toward the transport direction during intense deformation (Searle and Alsop, 2007). The idea of sheath folding in the NMR is based on discrepancies observed in the southern part of the NMR. For example, the major structure in the southern closure (sub-area 1) is described as a synform (Figure 4.8), and

shown as a synform on the map closing to the SE (Figure 4.1), but the mineral lineations do not fit the orientation of the fold vergence to the SE in the southern closure. The generation of sheath fold can happen under conditions when the value of simple shear (γ) amounts to 10-15 or more Skjernaa (1980), associated with high strain. A large scale sheath folding in the entire NMR along the Neusspruit Shear Zone can be in view and presumably synformal.

Summary

The analysis of ductile and brittle features has shown that the study area has experienced various phases of deformation. The structure that resulted in the study area during the D_1 deformational event is a moderately plunging and moderately to steeply inclined structure, with axial plane dipping towards the northeast direction. Moderately plunging isoclinal and open folds have been identified in the study area. On the basis of the axial plane analysis, it is suggested that the folds in the study area occurred during the same deformational event. The deformational event, D_2, is represented by shortening which resulted in thrusting, namely the Neusberg Thrust Fault of about 150 m in length trending northwest to southeast in the study area. The Neusberg Thrust Fault is located north of sub-area 2 (Figure 4.1). It is suggested that its extension goes further north of the study area (van Bever Donker, 1980). This shortening is evident in the study area due to: (1) the presence of breccia and (2) the displaced layers of feldspathic mica-rich quartzite dipping to the southwest in the opposite direction to the main northeast dip of the foliation, and (3) the placement of old rocks (Puntsit Formation) on top of younger rocks (Goede Hoop Formation). Kink bands and kink folds are displayed in the vicinity of the Neusberg Thrust Fault which is thought to have contributed to the occurrence of such structures in the study area. The D_3 deformational event in the study area is derived from values of the stress vectors from the trends of joints in sub-areas 1, 2, 3, and 4 defining a strike-slip environment according to Anderson's classification (1951). The systematic joints occur in all the rocks except the charnockite, so they post-date the folding and thrusting, and they occur at a shallower depth that the folding did. The last deformational event, D_4, is characterised by the presence of fractures and joints in the charnockite. The rose diagram of the charnockite

confirms a non-systematic distribution of the joints (Figure 4.33). The variations of the stress field in the charnockite are illustrated in thin section by such features as: (1) undulose extinction in quartz; (2) elongation of quartz with the long axis displaying vague alignment with biotite; (3) and micro-fractures in quartz.

These features show that these minerals have experienced some degree of deformation throughout the study area. The contact between the charnockite and the country rock is not clear, suggesting that the intrusion occurred at lower crustal level, not necessarily very deep but certainly not very shallow either. The presence of a 'hybrid' or mixed rock (biotite gneiss) suggests some degree of depth to the intrusion. In the case where the country rocks were much cooler than the intrusion, such mixing would not have occurred readily. The faint foliation in the charnockite compared to the foliated country rock gneisses shows that the intrusion was not deep at least, and also reflects the timing of intrusion, largely late- to post-tectonic.

CHAPTER 5

DISCUSSION

The focus of this study is to reconstruct the structural evolution of the central Kakamas Terrane area characterised by deformed and metamorphosed rocks along and adjacent to the Neusspruit Shear Zone (NSZ), located west of the Neusberg Mountain Range (NMR). To achieve these goals, the results of field mapping, petrographic studies, and structural analyses must be taken into consideration. The discussion, therefore, considers these three approaches by which the rocks were identified and described at various scales. The results are synthesised into a complete structural evolution of the rocks at a local scale, and, hence, provide further insights into the development of the Kakamas Terrane within the Namaqua Sector on a regional scale.

5.1 Geographic distribution

Detailed field mapping was carried out whereby various rock types, namely the metasedimentary rocks (Goede Hoop and Puntsit Formations) of the Korannaland Group, contact rocks (metasomatic rocks, such as the skarn and wollastonite-bearing calcareous rock and 'hybrid' rock, such as the biotite gneiss), granitic gneisses (pink gneiss, augen gneiss, biotite-chlorite-schist, leucogneiss), intrusive rock (charnockite) and metavolcanic rocks (amphibole schist) were identified and described at both a macro- (field occurrence), meso- (hand specimen), and micro- (microscope) scale.

The distribution of the rocks varies considerably (Figure 2.5). The metasedimentary rocks of the Korannaland Group occur adjacent to, and to the east of the NSZ in the NMR and at Vuurkop Mountain (VM). According to the relative ages of the metasedimentary rocks of the Korannaland Group in the field, the Goede Hoop Formation is younger compared to the Puntsit Formation. This is confirmed by the presence of top-normal cross-bedding in the Goede Hoop Formation, and the fact that the Puntsit Formation is overlain by the Goede Hoop Formation

along the NSZ. The contacts between the metasedimentary rocks and the granitic gneisses are not clear in the field, as they are obscured by younger river and aeolian sand deposits. In the same way, the contacts between the various granitic gneisses are not visible either. The augen gneiss and the biotite-chlorite-schist occur along the NSZ to the west of the NMR, and the pink gneiss and leucogneiss occur between the NMR and VM (Figure 2.5). The charnockite occurs adjacent to the NMR and VM (Figure 2.5). Metasomatic (skarn and wollastonite-bearing calcareous rock) and 'hybrid' (biotite gneiss) rocks occur generally at or near the contact between the metasedimentary rocks and the various granitic gneisses and/or charnockite. These contact rocks are not encountered on the other side of the NMR where there is no charnockite and thus not part of the depositional sequence of metasedimentary rocks.

The skarn is found on the western limb of the NMR i.e very close to it in the calc-silicate-rich quartzite of the Puntsit Formation, whereas the wollastonite-bearing calcareous rock occurs between the NMR and VM. The biotite gneiss forms the reaction zone between the Goede Hoop Formation and the charnockite along the R359 gravel road, and all the way along the base of the VM on the northeast side (Figure 2.5). The amphibole schist occurs as an intercalation within the Puntsit Formation. Structural features present include synforms and antiforms, a thrust fault in the NMR, and the NSZ adjacent to the NMR (Figure 4.1). This is indicative of the fact that the study area has been subjected to various types of deformation.

5.2 Petrographic features indicative of deformational and metamorphic conditions

Various deformational features, such as: 1) foliation in the rocks; 2) undulose extinction in quartz grains; 3) grains crushed locally; 4) calcite twins in the calc-silicate-rich quartzite all indicate that the rocks along and adjacent the NSZ have been subjected to various degrees of deformation, as described in detail in chapter 3. The foliation is enhanced by the linear fabric, illustrated by elongated pebbles in the feldspathic mica-rich quartzite (Chapter 3; Section 3.3.1.1; Figure 3.4A), suggesting a strongly constrictive stress field. Subhedral and elongated grains of hornblende are shown in the photomicrograph of the amphibole schist describing

penetrative foliation (Chapter 3; Section 3.4.1; Figure 3.9). Strain is further evidenced by undulose extinction in quartz crystals indicating an incomplete recovery from strain. Localised crushed mineral grains are observed in the photomicrograph of the augen gneiss (Chapter 3; Section 3.6.3; Figure 3.22) along the NSZ. The occurrence of mylonites in the augen gneiss is due to the shearing along the NSZ. This is caused by stresses related to the 1200 - 1000 Ma Namaquan Orogeny. Crosscutting sets of lamellae are encountered in the calcite crystals of the calc-silicate-rich quartzite (Chapter 3; Section 3.4.1; Figure 3.8), which indicate deformation in the calc-silicate-rich quartzite. Fracturing has been identified in the zircon crystals of the pink gneiss (Chapter 3; Section 3.6.2; Figure 3.20). A possible explanation for the occurrence of fractures in zircon could be the confined pressure (e.g. Lee and Tromp, 1995). Consequently, the presence of fractures in the zircons can provide an estimation of the depth of burial of a rock. However, this could be hampered by the high temperatures of the mid-to lower crust intensifying the rates of self-annealing to the point that fractures are rarely observed in zircon (Lee and Tromp, 1995).

The rocks along and adjacent to the NSZ have been subjected to different metamorphic events and various metamorphic grades, as denoted by the presence of different mineral assemblages. A generalised pressure and temperature diagram for the metamorphism of mafic rocks (after Bucher and Grapes, 2011) has been used to determine the metamorphic grade. In accord with Moen (2007), the first metamorphic event (M_1) is related to regional metamorphism, and was accompanied by the D_1 deformational event. This M_1 metamorphic event is rarely identified because of the subsequent amphibolite/granulite event. The mineral composition of hornblende-anorthite-quartz-biotite-epidote-enstatite-zircon-opaques in the amphibole schist is represented in the orange circle reflecting the greenschist-amphibolite facies transition grade (Chapter 3; Section 3.8; Figure 3.29). The transition from greenschist to amphibolite facies grade involves major mineralogical change, such as the transition from albite to anorthite as the total rock chemistry must allow it with increasing temperature (Cooper, 1972; Winter, 2014). Such a reaction is estimated at the temperature of 500 °C and pressure of 5 kbar (Bucher and Grapes, 2011; Winter, 2014). As explained in chapter 2, the elevated temperature and

pressure are considered to have been caused by a combination of burial and the presence of a stress field due to the ongoing collision between the Kakamas Terrane and the Kaapvaal Craton. The second metamorphic event (M_2) is related to local contact metamorphism illustrated by the presence of the contact rocks in the study area, such as the wollastonite-bearing calcareous rock indicative of contact metamorphism (Winter, 2014). As mentioned in chapter 3, the ACF diagram for mafic rocks was used to show the change of metamorphic grade, with the mineral assemblage of wollastonite- dolomite-vesuvianite-diopside-grossular illustrated in the AFC diagram in the green circle (Chapter 3; Section 3.8; Figure 3.29) corresponding to granulite facies metamorphism (Bucher and Grapes, 2011). The metamorphic conditions of the M_2 metamorphic event are at the temperature of approximately 800 °C and a pressure of about 3 kbar (Bucher and Grapes, 2011). Similar metamorphic conditions were also found by van Bever Donker (1980) and Moen (2007) in the Kakamas Terrane. While the high temperature can be related to the intrusion of the granitic bodies (Winter, 2014), crustal shortening was continuing at this time. The M_3 metamorphic event is retrograde in nature and localized, such as the presence of epidote in the joints crosscutting the charnockite indicating hydrothermal fluid mineralization possibly during the exhumation of the charnockite. Similar observations were made along the Brackbosch Fault (Geringer et al., 1994).

5.3 Structural analysis

Detailed field mapping was carried out along and adjacent to the NSZ where various structures (foliations, folds, faults, and joints) were identified and characterised within each sub-area. The microstructural (Chapter 3) and geometrical (Chapter 4) analyses of the structures within the study area are used to determine the structural evolution along and adjacent to the NSZ in the Kakamas Terrane. The data collected in each sub-area are presented in Appendix.

5.3.1 Characterization of foliation

An analysis was done on the macrostructures in the area as defined by the pervasive foliation, thought to be an S_0 foliation. Sub-areas 1, 2, 3, and 4 show same trends of the axial planes dipping towards the northeast. The pervasive foliation (S_0) dips mostly northeast but a change in the orientation of the pervasive foliation towards the southwest is observed along the Neusberg Thrust Fault in the Neusberg Mountain Range corresponding to the D_2 deformational event in the study area.

The southern closure of the Neusberg Mountain Range is characterised as synform based on identification of cross-bedding in the feldspathic mica-rich quartzite with upwards younging direction. Derived values of the fold axis, axial plane, and field observations show that the southern closure (sub-area 1) of the NMR is oriented towards NE. Penetrative lineation in the southern closure plunges to the NE. In other words, the lineation is oriented in the similar manner as the structure in the southern closure of the NMR, i.e., almost perpendicular to the dip direction in the southern part of the NMR. If the aforementioned fold in the southern closure is sheath-shaped, the lineation in the southern closure must be oriented just in this style. The presence of sheath fold in the Neusberg Mountain Range could clarify the coplanar and collinear structural elelments identified in the analysis of the southern part of the Neusberg Mountain Range. The consistent colinearity of linear elements and structures (fold axis, long axis of sheath fold, fold hinge, and mineral lineations) as well as the coplanarity of planar structures (foliation, axial plane of isoclinal fold and thrust plane). The presence of the thrust plane within the Neusberg Mountain Range denotes a transpressive environment.

5.3.2 Characterization of the Neusspruit Shear Zone (NSZ)

The Namaqua Sector of the Namaqua-Natal Province comprises a number of subprovinces and terranes, the definitions and boundaries of which remain controversial (Jacobs et al., 2008). As it is defined today, the Kakamas Terrane lies north and east of the Bushmanland Subprovince (Moen, 2007). The boundary between the Kakamas Terrane of the Gordonia Subprovince and

the Bushmanland Subprovince is defined to be along the Hartbees River Thrust east of 20° E and along the Swartrand thrust west of 20° E (Moen 2007). To the east, the Kakamas Terrane is in contact with the Areachap Terrane along the Boven Rugzeer Shear Zone (BoRSZ), which is thought to have experienced dextral movement (Miller, 2012).

The Neusspruit Shear Zone is a prominent northwest striking structure that is characterised by penetrative foliation parallel to the fault plane, and the presence of 'augen' structures within the gneisses along the structure (Chapter 3; Section 3.6.3; Figure 3.22). The microstructures identified within the augen gneiss along the shear zone have been classified as protomylonites according to the classification of Passchier and Trouw (2005). The author is in accord with the idea of Moen (2007) about a sinistral movement along the NSZ. The sinistral sense of movement along the NSZ and the dextral sense of movement of the Brakbosch Shear Zone further east within the Areachap Terrane suggests that the crustal blocks bounded between these shear zones were 'pushed out' as an escape structure (e.g. van der Pluijm and Marshak, 2004). Previous studies in the Areachap Terrane (Bailie et al., 2011, 2012) has demonstrated that the Keimoes Suite was emplaced in continental rift and collisional settings, which is possibly the same as those of the granitic gneisses and intrusive rock in the Kakamas Terrane. Remarkably, the NSZ is likely the edge of the rifting system in the Gordonia Subprovince. This is illustrated by the absence of the Keimoes Suite as well as the Goede Hoop and Puntsit Formations to the west of the NSZ (Figure 5.1), suggesting that the NSZ can be considered as the western limit of the Keimoes Suite (Moen, 2007) in the Gordonia Subprovince.

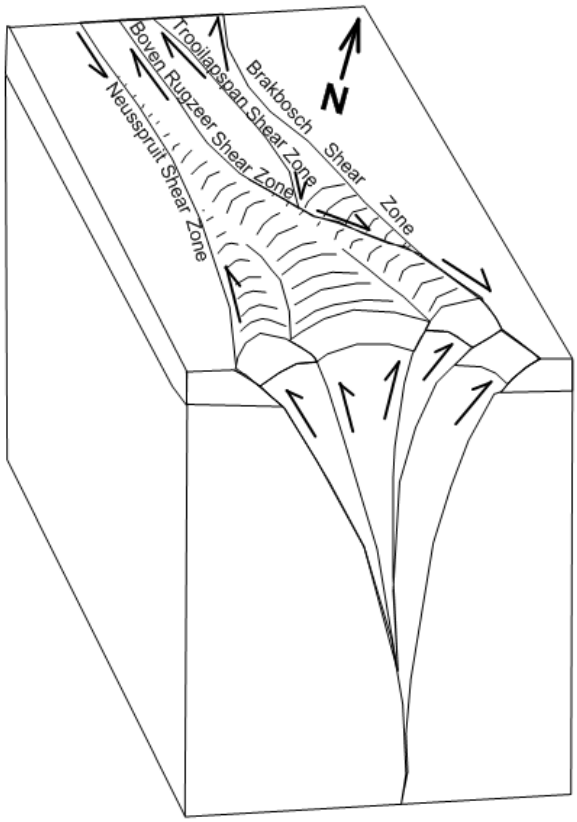

Figure 5.1: Sketch of the escape structure illustrated by the crustal blocks between the Neusspruit Shear Zone and the Brakbosch Shear Zone (modified after van der Pluijm and Marshak, 2004).

5.3.3 Timing of formation of the Neusspruit Shear Zone (NSZ)

The Namaqua Province is dissected by major shear zones (Slabbert et al., 1989) of which the timing of occurrence is poorly constrained. A depositional age of 1220 Ma – 1150 Ma was obtained from a geochronological pilot analysis done on the feldspathic mica-rich quartzite of the Goede Hoop Formation by the author. An assumption is made on the timing of formation of the Neusspruit Shear Zone, as it may have occurred at the early stage of the accretionary event before the deposition of the Goede Hoop Formation at 1220 Ma – 1150 Ma. The absence of the Goede Hoop formation to the west of the NSZ suggests a depositional barrier or graben edge in the Kakamas Terrane. It is suggested that the shearing in the augen gneiss along the NSZ is likely related to the accretionary event in the Kakamas Terrane. Possible reactivations may have occurred during or after the accretionary event, and may also have continued during the

collisional event between the Namaqua Province and the Archean Kaapvaal Craton at 1200 Ma – 1180 Ma.

5.3.4 Timing of formation of the Neusberg Thrust Fault (NTF)

The Neusberg Thrust Fault (NTF) is a northwest trending brittle pattern cutting the calc-silicate-rich quartzite and feldspathic-mica-rich quartzite north of the area (Figure 4.1). The NTF is identified by the displaced rocks of the feldspathic mica-rich quartzite towards the southwest in the field (Figure 4.20), and the presence of breccia (Figure 4.19) located along the valley delineating the trace of the NTF in the Neusberg Mountain Range. It is established that the formation of the depositional barrier or graben edge in the Kakamas Terrane may have favoured the deposition of the Puntsit and Goede Hoop Formations, which were then folded as result of the collision between the Namaqua Province and the Archean Kaapvaal Craton at 1200 Ma – 1180 Ma. It suggested that the thrusting in the area followed the folding as result of the continued shortening related to the collisional event. This is supported by the presence of kink bands (Figure 4.21A) and kink folds (Figure 4.21B) observed in the feldspathic mica-rich quartzite in the vicinity of the NTF as result of the development of a fault-bend fold (Twiss and Moores, 1992). It is suggested that the NTF continues to the north of the Orange River (van Bever Donker, 1980), showing that it is of regional extent for both the southern and northern portions of the Neusberg Mountain Range.

5.3.5 Characterization of joints along and adjacent to the NSZ

The joints in the charnockite and the country rock have been characterised based on their distribution, orientation, spacing, and timing of emplacement.

5.3.5.1 Distribution of joints

Various types of joints, such as joints with mineralization (quartz, calcite or epidote), crosscutting joints, and joints without mineralization were identified while mapping along and adjacent to the NSZ. This indicates that the study area has been subjected to various phases of deformation possibly associated with different fluid flow events at various times, and possibly related the continental rifting and collisional events in the Gordonia Subprovince of the Namaqua Sector. The distribution of joints was used to identify joint sets and determine the tectonic forces (principal stress vectors) that generated them. The rose diagram analysis reveals N-S, NE-SW, ENE-WSW, and NW-SE joint trends in the country rocks compared to those of the charnockite which have various trends (Chapter 4; Section 4.8; Figure 4.36). The distribution of joints has been classified into two types, namely systematic joints and non-systematic joints (Twiss and Moores, 1992; Davis and Reynolds, 1996; van der Pluijm and Marshak, 2004). Systematic joints are characterised by roughly planar geometry, parallel or sub-parallel orientations to each other, and approximately regular spacing. They have been identified in the country rocks and illustrated in the rose diagram analysis of sub-areas 1, 2, 3, and 4 (Chapter 4; Section 4.8; Figure 4.36). Non-systematic joints are so irregular in form, spacing, and orientation that they cannot be readily grouped into distinctive, through-going sets (Davis and Reynolds, 1996). They are illustrated in the rose diagram analysis on the charnockite (Chapter 4; Section 4.8; Figure 4.36).

5.3.5.2 Orientation of joints

The orientations of the joints were recorded along and adjacent to the NSZ (Appendix). The presence of various joint trends in the charnockite is suggestive of a shallow crustal level of emplacement within the brittle regime rather than at deeper crustal levels in the ductile regime. The trends of joints in the metasedimentary rocks are related to tectonic activity, such as faulting processes as seen in the Neusberg Thrust Fault in the Neusberg Mountain Range which fractured and displaced the rocks of the Puntsit and Goede Hoop Formations.

5.3.5.3 Spacing of joints

The spacing of joints in a systematic set can be evaluated in terms of either the average perpendicular distance between joints or the average number of joints found in a convenient standard distance normal to the joints (Twiss and Moores, 1992). Joint spacing in the study area varies from few millimetres to many centimetres in the metasedimentary rocks. Field observations showed that joint spacing in the intrusive igneous rocks is not similar as observed in the metasedimentary rocks. According to Pollard and Aydin (1988), the spacing of joints in intrusive igneous rocks is not uniform and occurs sporadically, compared to that of sedimentary rocks which display a more regular distribution. Other factors, such as different mechanical properties in different directions (mineralogy, composition, and grain size) of the rocks, the strain rate and the fluid levels can control the spacing of joints in intrusive igneous rocks (van der Pluijm and Marshak, 2004).

5.3.5.4 Timing of emplacement of joints

Various sets of joints were identified in the metasedimentary rocks (feldspathic mica-rich and calc-silicate-rich quartzites), granitic gneisses (augen gneiss, pink gneiss, and leucogneiss), and intrusive rock (charnockite). The rose diagram analysis of joints in the metasedimentary rocks and charnockite is used to illustrate the preferred orientation if any, of joints in the study area. The metasedimentary rocks show a prominent NE trending joint in sub-areas 1 and 2, and N and ENE trending joints in sub-areas 3 and 4 (Chapter 4; Section 4.8; Figure 4.36). This shows that the joint trends in sub-areas 1 and 2 in the Neusberg Mountain Range were formed at the same time. The joint trends in sub-areas 3 and 4 are in essence the same and thus suggest that the joints in these two sub-areas formed at the same timeas those in sub-areas 1 and 2. The relationship between the NE (sub-areas 1 and 2; Figure 4.36) and N and ENE sets (sub-areas 3 and 4; Figure 4.36) shows that the study area has been subjected to various phases of deformation. The change of the orientation of the joint sets from sub-areas 1 and 2 to sub-areas 3 and 4 suggest that the joints were possibly developed before the intrusion of the charnockite, and then affected by the emplacement of the charnockite. The charnockite is

obviously the youngest lithology in the study area as it has intruded the country rocks after folding. The emplacement of the charnockite in the Kakamas Terrane has been classified as been post-tectonic (Cornell et al., 2012).

5.3.6 Application of the Mohr diagram

The Mohr diagram is an important way of visualizing, or characterising stresses involved in an area, where the horizontal and vertical axes represent the normal (σ_N) and shear (σ_S) stresses (Figure 5.2), which act on a plane at an angle α (Fossen, 2010). It may also be used in three dimensions, where the three principal stresses are plotted along the horizontal axis. The Mohr circle is a means of determining the normal and shear stresses for a couple of stresses oriented to a plane (Twiss and Moores, 1992; Fossen 2010). The value of the maximum (σ_1) and minimum (σ_3) principal stresses are plotted on the horizontal axis and the distance between σ_1 and σ_3 defines the diameter of a circle centered at $((\sigma_1+\sigma_3)/2, 0)$ (Davis and Reynolds, 1996; Fossen, 2010). α is the angle between the normal to the plane and σ_1, as shown in Figure 5.2, but is given as 2α in the Mohr diagram.

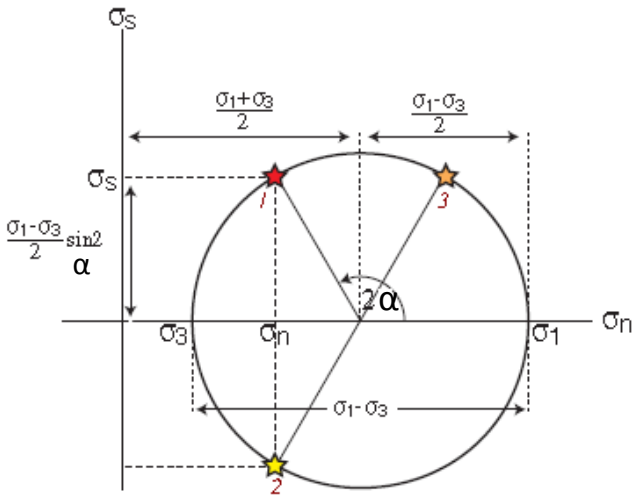

Figure 5.2: The Mohr circle. 2α is the angle between the radius to the point on the circle and the horizontal axis. Planes 1 and 2 have the same normal stress but different shear stress. Planes 1 and 3 have the same shear stress but different normal stress (after Fossen, 2010).

The failure of a rock may operate in three ways; extensional, sliding or hybrid and tearing fracture (Bons et al., 2012).

Extensional fractures are tensile in origin and commonly grow perpendicular to the plane of opening (Figure 5.4; Mode I). In such situation, the Mohr circle touches the failure envelope to the left, the plane that fails will experience zero shear stress and an effective extensional normal stress ($\sigma_3 - \tau$; Figure 5.3) (Bons et al., 2012). An extensional or mode I fracture forms with an opening vector perpendicular to the plane (Figure 5.4; Mode I). This may explain the open joints in the Goede Hoop (Figure 4.39) and Puntsit (Figure 4.25C) Formations. During Mode I fracturing, the occurrence of extensional veins in the crust indicates that the fluid pressures at depth are generally approaching lithostatic pressure (Bons et al., 2012), and the differential stresses are relatively low, being constrained by the relatively low cohesion of the rocks (Etheridge, 1983). Fractures that form as the result of an elevated fluid pressure are termed hydrofractures (Dahm et al., 2010).

Sliding or hybrid fractures imply a continuous transition from an extension fracture to a shear fracture (Figure 5.4; Mode II), with an increase in compressive stress (Davis and Reynolds, 1996; Ramsey and Chester, 2004). Hybrid fractures form under mixed tensile and compressive stress conditions at acute angles to the maximum principal compressive stress, with angles greater than those observed for extension fractures and less than those observed for shear fractures (Ramsey and Chester, 2004). Due to the symmetry of the system, the Mohr circle will touch the failure envelope twice, producing conjugate sets of fractures with opposite shear senses and symmetrically arranged around the directions of the principal stresses (Bons et al., 2012). As the slope of the failure envelope is steep at $\sigma_n < 0$, the angle between the two conjugate orientations is small (Twiss and Moores, 1992; Bons et al., 2012). Extensional fractures are thus an end-member case, where this angle is zero and the conjugate sets combine into one (Bons et al., 2012). Fracture surfaces also show a continuous change from an extension to shear fracture morphology. This mechanism may also explain the tight joints in the charnockite (Figure 3.25B).

Tearing fractures (Figure 5.4; Mode III) imply that the Mohr circle touches the failure envelope to the right of the vertical ($\sigma_n = 0$) axis (Figure 5.3), a plane with a net compressional normal stress and a non-zero shear stress will fail (Bons et al., 2012), forming shear fractures without an opening component (Figure 5.4; Mode III). Conjugate sets will form with a larger angle between the two sets, determined by the internal angle of friction (Bons et al., 2012). With an internal angle of friction of 0°, fractures at 45° from σ_1 will form, according to the maximum shear stress (Petit, 1987; Twiss and Moores, 1992; Pollard and Fletcher, 2005). Such mechanism has been identified in the Goede Hoop Formation (Figure 4.18).

It is established that the study area has been subjected to various types of fracturing. Mode I fracture occurred throughout the metasedimentary rocks with or without quartz mineralization, while the fractures generated from mode I are dry in the granitic gneisses. The presence of quartz mineralization in the metasedimentary rocks could be due to the post-tectonic intrusion in the study area which is reflected by the presence of contact rocks within the metasedimentary rocks. Mode II fracture occurred in the charnockite where tight and/or crosscutting joints with or without epidote mineralization have been identifiedin the area. Some joints show sliding along the plane of mineralization of epidote. As explained in section 4.9, pore fluid pressure could be the factor favouring the sliding along the mineralised joints. Mode III fractures are present in the Goede Hoop Formation, where a conjugate set of joints have been identified (Figure 4.18) reflecting the competency of the metasedimentary rock and the change of orientation of the applied stresses in the area related to various deformational events.

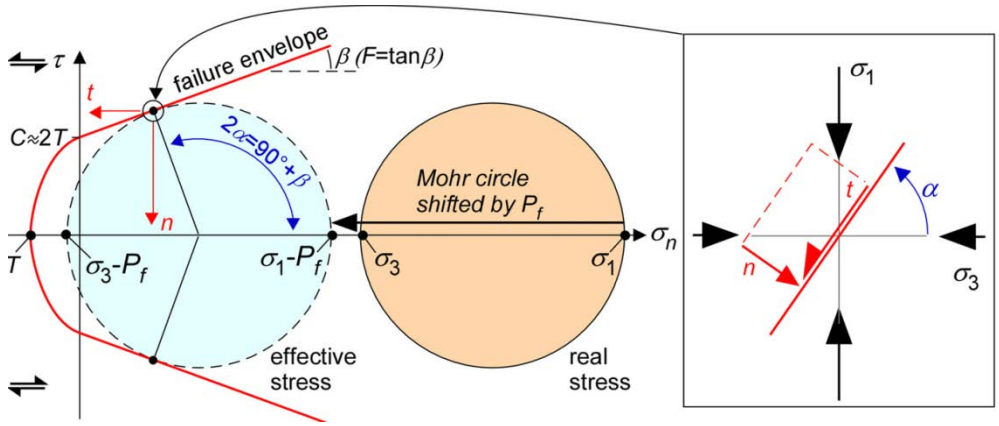

Figure 5.3: Mohr diagram with shear stress (τ) versus normal stress (σ_n) for a plane with an angle α with the least compressive stress (σ_3). All τ – σ_n combinations for a certain stress state (defined by σ_1 and σ_3) lie on a circle. As fluid pressure (P_f) counteracts imposed compression, effective stresses ($\sigma_n - P_f$) are used to determine whether a rock will fail: this shifts the Mohr circle to the left by P_f. β is the internal angle of friction. The cohesion (C) is the shear stress at failure for $\sigma_n = 0$. The tensile strength (T) is the maximum tensional stress a material can sustain (after Bons et al., 2012).

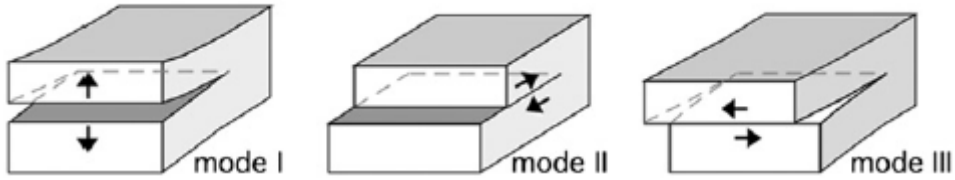

Extensional fracture Sliding or hybrid fracture Tearing fracture

Figure 5.4: Three end member failure modes related to the displacement of the wall rock relative to the fracture plane and fracture edge (after Bons et al., 2012).

1. Mode I (extension mode): the displacement vector of the fracture is perpendicular to the walls of the fracture.

2. Mode II (sliding mode): the displacement vector of the fracture is parallel to the fracture plane and parallel to the propagation direction of the fracture (Bons et al., 2012).

3. Mode III (tearing mode): the displacement vector of the fracture is parallel to the fracture plane and perpendicular to the propagation direction of the fracture (van der Pluijm and Marshak, 2004; Bons et al., 2012).

5.3.6.1 Effects of pore fluid pressure on the fracturing process

Pore fluid pressure is considered as one of the most important mechanisms for the fracturing process in a rock body. The pore fluid pressure is defined as an outward push that opposes inward compression from the rock (van der Pluijm and Marshak, 2004). If pore fluid pressure exceeds the least compressive stress (σ_3) in the rock, tensile stresses at the tips of cracks oriented perpendicularly to the σ_3 direction become sufficient for the crack to propagate (Twiss and Moores, 1992; van der Pluijm and Marshak, 2004). In the same way, pore fluid pressure in a rock can cause tensile cracks to propagate, even if none of the remote stresses are tensile, because pore pressure can induce a crack-tip tensile stress that exceeds the magnitude of σ_3 (van der Pluijm and Marshak, 2004). An illustration of the normal (n) and shear stress (τ) on a plane at angle α to σ_3 is shown in Figure 5.3, whereby the magnitudes can be derived from the Mohr diagram.

The effect of shifting the Mohr circle to the left (Figure 5.3) is that states of stress that are 'stable' at zero pore fluid pressure may become 'unstable' as a result of pore fluid pressure (Twiss and Moores, 1992; van der Pluijm and Marshak, 2004). The failure envelope separates the field on the diagram in which stress states are ''stable'' from the field in which stress states are 'unstable' (Figure 5.5). By definition, a stable stress state is one that a sample can resist without undergoing brittle failure (Figure 5.5A). An unstable stress state is an impossible condition to achieve, for the sample will have failed by fracturing before such a stress state is reached only for the angles where the 2α angle would fall outside the failure envelope, as illustrated by the shaded area in Figure 5.5D. In other words, a stress state represented by a Mohr circle that lies entirely within the envelope is stable, and will not cause the sample to develop a shear rupture (Figure 5.5B). A circle that is tangential to the envelope specifies the stress state at which brittle failure occurs (Figure 5.5C). Stress states defined by circles that

extend beyond the envelope are unstable (Figure 5.5D), and are therefore impossible within the specific rock being studied for the angles α where the circle falls outside the failure envelope.

From field observations and data analysis of the joints in the study area, it is clear that the rocks in the area along and adjacent to the NSZ have been subjected to a stress rate sufficient enough to produce fractures which are mineralized with epidote or quartz in some places, implying that they are formed in a tensile environment. The application of the Mohr diagram shows that the occurrence of fractures in the metasedimentary rocks and granitic gneisses can be possible when the differential stress (the diameter of the Mohr circle) is small, as is generally the case in the Earth, and if the pore pressure is sufficiently high to exceed the minimum compressive stress σ_3 by a quantity equivalent to the tensile strength of the rock. This is similar to the case in Figure 5.5C, as explained by van der Pluijm and Marshak (2004).

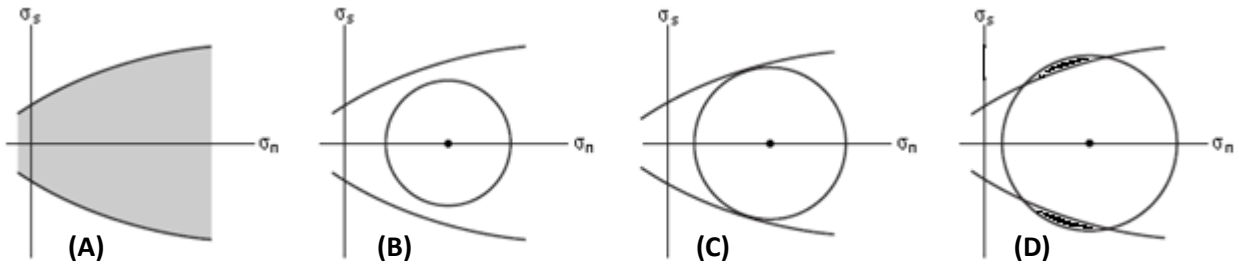

Figure 5.5: A) A brittle failure envelope as depicted on a Mohr diagram. Within the envelope (shaded area), stress states are stable, but outside the envelope, stress states are unstable. (B) A stress state that is stable, because the Mohr circle, which passes through values for σ_1 and σ_3 and defines the stress state, falls entirely inside the envelope. (C) A stress state at the instant of failure. The Mohr circle touches the envelope. (D) A stress state that is impossible in the shaded area (after van der Pluijm and Marshak, 2004).

5.4 Structural evolution

The Neusberg Mountain Range is a northwest trending structure in the study area bounded to the west by the Neusspruit Shear Zone (Figure 5.6). Based on the likely protoliths to the calc-silicate and feldspathic mica-rich quartzites, it is concluded that the study area is the western boundary of a basin composed of carbonates or immature marls (representing the calc-silicate-rich quartzites) and sandstones (representing the feldspathic mica-rich quartzites) as the youngest deposits, which are characteristic of a shallow marine or fluvial environment respectively. The suggestion for a shallow marine or fluvial environment is supported by the presence of cross-bedding observed in the feldspathic mica-rich quartzite of the Goede Hoop Formation and the overall thickness of the metasedimentary rocks which varies between 40-100 m to 150 m in the Goede Hoop Formation, and about 20-35 m to 80 m in the Puntsit Formation excluding any repetition due to thrusting. An environment meeting these requirements would be a rift basin, characterised by a marginal sea similar to an accretionary environment chiefly truncated by faults. The amphibole schist has been interpreted to be derived from material of basaltic composition emplaced within a continental rift basin environment. The occurrence of the amphibole schist as intercalations in the calc-silicate-rich quartzite is suggestive of varying pulses of deposition of both sedimentary and volcanic materials. The abrupt termination of the metasedimentary rocks against the Neusspruit Shear Zone suggests deposition in a fracture bound basin (van Bever Donker, 1980). After the sedimentation and burial had taken place, deformation occurred and resulted with the closure of the Neusberg Mountain Range related to the early stage of the continental collision between the Namaqua Sector and the Kaapvaal Craton. Prominent and intense deformation resulted during the main D_1 deformational event illustrated by isoclinal and open folds in the Kakamas Terrane with the axial traces trending northwest-southeast, revealing that the maximum stress was applied in the northeast-southwest direction. Field observations and the interpretations established that the Neusberg Mountain Range in the Kakamas Terrane is a double plunging synclinal structure or basin developed in a transpressional environment surrounded by dome structures, such as the Central Dome to the southwest and the Warm Zand Dome to the northeast, respectively. The presence of shearing is revealed by augen structures within the

augen gneiss along the Neusspruit Shear Zone. Applied stress during the D_1 deformational event resulted in the closure of the basin with flattening directed towards the northwest-southeast direction. Such deformation is supported by the presence of flattened pebbles in the Goede Hoop Formation, with the long axis trending towards the northwest-southeast direction and parallel to the axial traces of the isoclinal folds in the Neusberg Mountain Range. Subsequently, intense shortening during the second deformation event, D_2, gave rise to the Neusberg Thrust Fault, and the presence of breccias within the Neusberg Mountain Range in the southern portion of the Neusberg Mountain Range. It is established that the Neusspruit Shear Zone, together with the Neusberg Thrust Fault, extends further north of the Orange River and is evidence of major deformation at a regional scale in the Kakamas Terrane. The third deformation, D_3, is illustrated by systematic joints along the Neusberg Mountain Range defining a strike-slip environment. Non-systematic joints have been identified in the charnockite which is known of intruding D_1 structures (folds). Lastly, the fourth deformation event, D_4, is revealed by fractures (joints and veins) in the charnockite which are commonly filled with epidote or piemontite mineralization, which are suggestive of uplift and exhumation in the Kakamas Terrane. The granitic gneisses (augen gneiss, pink gneiss and leucogneiss) were likely derived from material of granitic or rhyolitic composition emplaced in a continental rift or collisional environment. The intrusion of the metasedimentary rocks by the granitic gneisses occurred possibly during, or preceding the deformation in the study area. This interpretation is based on the deformed and foliated nature of some of the granitic gneisses. The charnockite also terminates abruptly against the Neusspruit Shear Zone, strengthening the interpretation that this is a major structural feature in the study area (Figure 5.6).

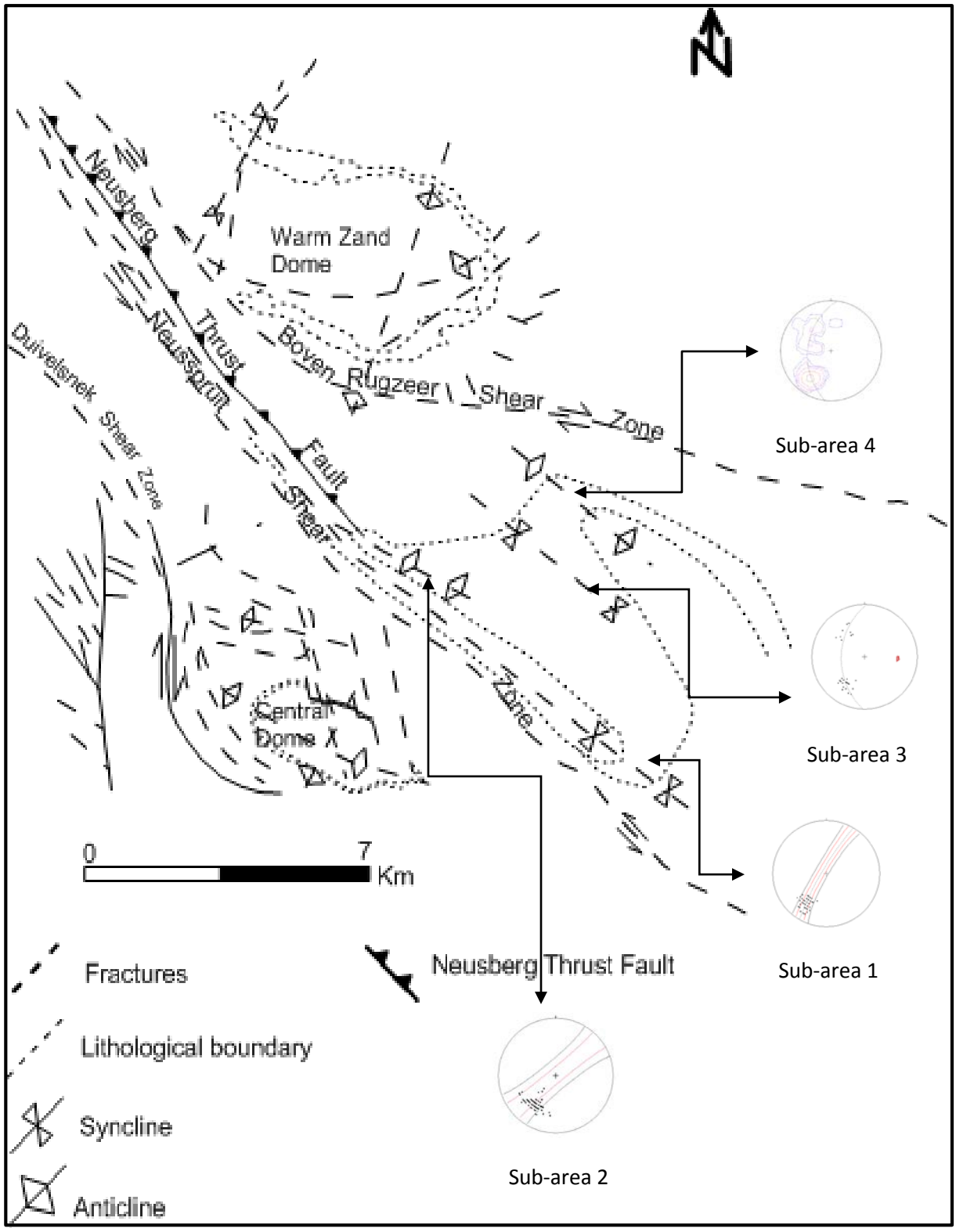

Figure 5.6: Structural evolution of the study area (modified after van Bever Donker, 1980).

CHAPTER 6

CONCLUSION AND RECOMMENDATION

6.1 Conclusion

This study has established the lithostratigraphy of the various rock types in the study area, such as the metasedimentary rocks, contact rocks, granitic gneisses, and metavolcanic rock along and adjacent to the Neusspruit Shear Zone (NSZ), south of the Orange River in the Kakamas Terrane. The findings obtained have provided indications of the processes that occurred at the western margin of the Archean Kaapvaal Craton. These findings have contributed to more accurately understanding the structural evolution of the Kakamas Terrane within the Namaqua Sector, but more work is needed to raise the level of knowledge from inference to proper insight and conclusions.

Petrographic analyses have led to the recognition of different parageneses of metamorphic grade in the study area. The rocks adjacent to the NSZ have been subjected to various phases of metamorphism. This is supported by various parageneses, such as enstatite-hornblende in the amphibole schists, and grossular-diopside-wollastonite in the wollastonite-bearing calcareous rocks, indicating medium to high grade metamorphic conditions respectively, and according to conditions given by Bucher and Grapes (2011), it is established that the parageneses in the study area correspond to that of amphibolite and granulite facies respectively. Retrograde metamorphism is illustrated by calcite-epidote-allanite parageneses in the Puntsit Formation, and, the retrograde parageneses found in the Puntsit Formation correspond to that of greenschist facies.

This study differs from the findings of Geringer (1973), as the current study shows the Puntsit Formation as being beneath the Goede Hoop Formation, and nothing has been found to overlay the rocks of the Goede Hoop Formation. The Puntsit Formation is characterised as having a

calcareous sedimentary origin (being mostly a marl), with a detrital provenance of chiefly granodioritic composition. According to Keary et al. (2010), the variation in the strength and temperature of the lithosphere, the inherited stratigraphy, and the structural inhomogeneities, as well as various mechanisms dictated by the tectonic setting at the time of formation will govern the composition of the metasediments. It was concluded that the depositional environment of the Goede Hoop Formation, because of the presence of cross-bedding, was either a fluvial or fluvio-deltaic environment. An association with volcanic activity is implied as reflected by the intercalated metavolcanic rocks. The metavolcanic rocks were found to have a basaltic protolith which confirms the presence of volcanogenic activity in the Kakamas Terrane, but less voluminous and significant compared to that in the Areachap Terrane to the east. The tectonic setting of the metavolcanic rock relates to that of a continental rift setting.

The intrusion of the metasedimentary rocks by the granitic gneisses has contributed to the development of contact rocks (wollastonite-bearing calcareous rock and skarn), and others of a more mixed or 'hybrid' nature (biotite gneiss). The depositional environment of the Korannaland Group was likely a rift basin which may have developed as the Namaqua Sector collided with the Kaapvaal Craton due to eastward-directed subduction along the western margin of the Kaapvaal Craton, which acted as an indentor (van Bever Donker, 1991), giving rise to thrusting and shearing in the Namaqua Sector in a transpressive environment. Continued transpression led to a different stress field responsible for the development of pull-apart basins into which the granitoids were emplaced (e.g. Cornell et al., 2012). Due to a lack of precise geochronological constraints the granitic gneisses are classified based on foliation and relationships with each other and the country rock, where observable. Apart from the geochronological pilot study done by the author on the Goede Hoop Formation, there is no precise dating for the metasedimentary and granitic rocks along and adjacent to the NSZ in the Kakamas Terrane. This work and previous studies (Podervaart and von Backström, 1949; Geringer, 1973; van Bever Donker, 1980; 1983; Cornell et al., 2012) show that the charnockite is the youngest granitoid intruding the metasedimentary rocks of the Korannaland Group in the Kakamas Terrane.

The emplacement of the granitic gneisses in the Kakamas Terrane took place in various episodes, ranging from pre- to post-tectonic. Varying degrees of deformation of the augen gneiss, pink gneiss, leucogneiss, and charnockite resulted in differing degrees of foliation in the granites varying from strong (augen gneiss) to faint or absent (charnockite). The post-tectonic granites are characterised by having a faint or absent foliation, such as seen in the charnockite. Although the pink gneiss and leucogneiss are considered as syn-tectonic granites in this study, it is suggested that the leucogneiss should be considered to be a late syn-tectonic granite based on the fact that it shows a lesser degree of deformation, as its mineralogy is comprised of a greater amount of felsic compared to mafic minerals, providing a more competent rock susceptible to brittle deformation as opposed to ductile deformation.

The structural analysis of the Korannaland Group and various granites in terms of foliation and mineral lineation revealed that the axial planes along and adjacent to the NSZ dip towards the northeast, and show that all four sub-areas formed as a result of similar deformational event, but the axial plane in sub-area 2, 3, and 4 is moderately inclined compare to that of sub-area 1 which is steeply inclined. Such difference in the axial plane could be due to the difference of competence of the rocks, possibility of flattened basin and/or impact of the thrusting north of sub-area 2 related to continue indenting of the Kaapvaal Craton. The interpretation of the principal stress vectors of the fractures (joints and veins) reflect a strike-slip environment. Satellite imagery by Google Earth, coupled with field observations by earlier workers (Podervaart and von Backström, 1949; van Bever Donker, 1980), as well as the interpretations from this study reveal that the full extent of the Neusberg Mountain Range in the Kakamas Terrane is a plunging structure towards northwest-southeast direction developed in a strike-slip environment surrounded by dome structures, namely the Central Dome to the southwest and the Warm Zand Dome to the northeast, respectively, also recognised by von Backström (1964) and van Bever Donker (1980). Flattening of the basin in a northwest-southeasterly direction, the presence of the NSZ west of the NMR together with the NTF with extension to the north of the Orange River constitute major deformation of a regional scale in the Kakamas Terrane.

6.2 Future research and recommendation

This study provides information on the petrography and the structural evolution of the rocks along and adjacent to the NSZ in the Kakamas Terrane. There is, however, still a lot of work that should be done to clearly and fully understand the geological evolution of the various rocks in this portion of the Kakamas Terrane. To do so, the following work is recommended:

- Establish the extension of the Neusberg Thrust Fault to north of the Orange River.
- Geochemically characterise the rocks of the Korannaland Group in the Neusberg Mountain Range and determine their provenance.
- Examine the extent of element mobility during metamorphism along the Neusspruit Shear Zone and determine whether the geochemical analyses reflect their protolith.
- Characterise the contact rocks relative to the country rocks along the Neusberg Mountain Range and at Vuurkop Mountain.
- Differentiate between the various granitic gneisses within the Neusberg Mountain Range and at Vuurkop Mountain.
- Characterise the metavolcanic rocks along and adjacent to the Neusberg Mountain Range and determine its source.
- Despite a few localised studies (Pettersson et al., 2007; Cornell et al., 2012), a comprehensive geochronological study of the metasedimentary and granitic rocks along and adjacent to the NSZ in the Kakamas Terrane needs to be done. The results will help to better understand and elucidate the tectonic evolution in the Kakamas Terrane.
- More comprehensive studies of the pegmatite emplacement in the Kakamas-Keimoes area are needed in view of clearly understanding their nature, origin and tectonic setting in the Kakamas Terrane.
- Isotopic analyses should be undertaken to determine the source characteristics of many of the rocks in the Kakamas Terrane, particularly those of the metasedimentary rocks and granitic gneisses.

REFERENCES

Adekoya, J. (1977). A note on jointing in the basement complex of the Ibadan area, Oyo State, Nigeria. *Journal of Mineralogy and Geology 14*, 48-52.

Anderson, E. (1951). *The Dynamics of Faulting and Dyke Formation with Applications to Britain.* Oliver and Boyd, Edinburgh, 191 pp.

Andre´- Mayer, A.S. and Sausse, J. (2007). Thickness and spatial distribution of veins in a porphyry copper deposit, Rosia Poieni, Romania. *Journal of Structural Geology 29*, 1695–1708.

Andre´- Mayer, A.S. and Sausse, J. (2007). Thickness and spatial distribution of veins in a porphyry copper deposit, Rosia Poieni, Romania. *Journal of Structural Geology 29*, 1695–1708.

Armstrong, R.A. and de Wit, M.J. (2007). A summary of the geochronology and Precambrian crustal architecture of southern Africa, and possibilities for correlations with South America. *Problems in western Gondwana : ''South America-Africa correlations: du Toit revisited''.* Gramado, Brazil: Centro de Investigações do Gondwana, 12-17.

Armstrong-Altrin, J.S. and Verma, S.P. (2005). Critical evaluation of six tectonic setting discrimination diagrams using geochemical data of Neogene sediments from known tectonic settings. *Sedimentary Geology 177*, 115-129.

Bailie, R., Gutzmer, J. and Rajesh, H. (2010). Lithogeochemistry as a tracer of the tectonic setting, lateral integrity and mineralisation of a highly metamorphosed Mesoproterozoic volcanic arc sequence on the eastern margin of the Namaqua Province, South Africa. *Lithos 119*, 345–362.

Bailie, R., Gutzmer, J. and Rajesh, H.M. (2011). Age of ferroan post-tectonic granitoids of the southern part of the Keimoes Suite, Northern Cape Province, South Africa. *Journal of African Earth Sciences 60*, 153–174.

Bailie, R., Rajesh, H.M. and Gutzmer, J. (2012). Bimodal volcanism at the western margin of the Kaapvaal Craton in the aftermath of collisional events during the Namaqua-Natal Orogeny: The Koras Group, South Africa. *Precambrian Research (200-203)*, 163-183.

Bates, R.J.and Jackson, J.A. (1995). *Glossary of Geology. Third Edition.* American Geological Institute, Alexandria, VA, 754 pp.

Becker, T., Schreiber, U., Kampunzu, A.B. and Armstrong, R. (2006). Mesoproterozoic rocks of Namibia and their plate tectonic setting. *Journal of African Earth Science 46*, 112-140.

Black, L.P., Withnall, I.W., Gregory, P., Oversby, B.S., Bain, J.HC. (2005). U-Pb zircon ages from leucogneiss in the Etheridge Group and their significance for the early history of the Georgetown region, north Queensland. *Australian Journal of Earth Sciences 52 (3)*, 385 - 401.

Blignault, H.J., Jackson, M.P.A., Beukes, G.J. and Toogood, D.J. (1974). The Namaqua tectonic province in South West Africa, South Africa. *Bulletin of the Precambrian Research Unit, University of Cape Town, 15*, 29-47.

Bons, P.D., Elburg, M.A. and Gomez-Rivas, E. (2012). A review of the formation of tectonic veins and their microstructures. *Journal of Structural Geology 43*, 33-62.

Brinkmann, R. (1976). *Geology of Turkey.* Elsevier, Amsterdam, 158 pp.

Bucher, K. and Frey, M. (2002). *Petrogenesis of metamorphic rocks. Seventh Edition.* Springer-Verlag, Berlin, 341 pp.

Bucher, K. and Grapes, R. (2011). *Petrogenesis of metamorphic rocks. Eighth Edition.* Springer-Verlag, Berlin, 428 pp.

Buddington, A. (1959). Granite emplacement with special reference to North America. *Bulletin of the Geolological Society of America 70*, 671-747.

Buriánek, D., Hrdličková, K. and Hanžl, P. (2009). Geological position and origin of augen gneisses from the Polička Unit, eastern Bohemian Massif. *Journal of Geosciences 54*, 201–219.

Clark, M.B., Brantley, S.L. and Fisher, D.M. (1995). Power-law vein-thickness distributions and positive feedback in vein growth. *Geology 23 (11)*, 975–978.

Cooper, A. (1972). Progressive metamorphism of metabasic rocks from the Haast Schist group of southern New Zealand. *Journal of Petrology 13*, 457-492.

Cornell, D.H. and Pettersson, Å. (2007). Ion probe zircon dating of metasediments from the Areachap and Kakamas Terranes, Namaqua-Natal Province and the stratigraphic integrity of the Areachap Group. *South African Journal of Geology 110*, 169-178.

Cornell, D.H., Humphreys, H., Theart, H.F.J. and Scheepers, D.J. (1992). A collision-related pressure-temperature-time path for Prieska Copper Mine, Namaqua-Natal tectonic Province, South Africa. *Precambrian Research 59*, 43-71.

Cornell, D.H., Thomas, R.J., Moen, H.F.G., Reid, D.L., Moore, J.M. and Gibson, R.L. (2006). The Namaqua-Natal Province. In : Johnson, MR., Anhaeusser, C.R. and Thomas, R.J. (Editors). The Geology of South Africa. *Geological Society of South Africa, Johannesburg / Council for Geoscience, Pretoria*, 325-379.

Cornell, D.H., van Schijndel, V., Ingolfsson, O., Scherstén, A., Karlsson, L., Wojtyla, J. and Karlsson, K. (2011). Evidence from Dwyka tillite cobbles of Archaean basement beneath the Kalahari sands of southern Africa. *Lithos 125*, 482-502.

Cornell, D.H., Pettersson, Å. and Simonsen, S.L. (2012). Zircon U-Pb emplacement and Nd-Hf crustal residence ages of the Straussburg granite and friersdale charnockite in the Namaqua-Natal Province, South Africa. *Geological Society of South Africa 115*, 465-484.

Cox, K.G., Bell, J.D. and Pankhurst, R.J. (1979). *The interpretation of igneous rocks .* George Allen and Unwin, London, 450 pp.

Dahm, T., Hainzl, S. and Fischer, T. (2010). Bidirectional and unidirectional fracture growth during hydrofracturing: role of driving stress gradients. *Journal of Geophysical Research 115*, http://dx.doi.org/10.1029/2009JB006817.

Dalziel, I. (1991). Pacific margins of Laurentia and East Antarctica-Australia as a conjugate rift pair: Evidence and implications for an Eocambrian supercontinent. *Geology 19*, 598-601.

Davis, G.H. and Reynolds, S.J. (1996). *Structural Geology of rocks and regions. Second Edition.* John Wiley and Sons, Canada, 776 pp.

De Beer, J.H. and Meyer, R. (1983). Geoelectrical and gravitational characteristics of the Namaqua-Natal mobile belt and its boundaries. In: Botha B.J.V. (Editor). Namaqualand Metamorphic Complex. *Special Publication of the Geological Society of South Africa 10*, 91-100.

De Beer, J.H. and Meyer, R. 1984. (1984). Geophysical characteristics of the Namaqua-Natal Belt and its boundaries. *Journal of Geodynamics 1*, 473-494.

Eglington, B.M. (2006). Evolution of the Namaqua-Natal Belt, southern Africa - a geochronological and isotope geochemical review. *Journal of African Earth Sciences 46*, 93-111.

Eglington, B.M. and Armstrong, R.A. (2003). Geochronological and isotopic constraints on the Mesoproterozoic Namaqua-Natal Belt: evidence from deep borehole intersections in south Africa. *Precambrian Research 125*, 179-189.

Eskola, P. (1915). On the relations between chemical and mineralogical composition in metamorphic rocks of Orijärvi region, southwest Finland. *Bulletin of Communication of Geology of Finland 44*, 109-143.

Etheridge, M. (1983). Differential stress magnitudes during regional deformation and metamorphism: upper bound imposed by tensile fracturing. *Geology 11 (4)*, 231-234.

Fleuty, M. (1964). The description of folds. *Proceedings of the Geological Association 75*, 461-492.

Fossen, H. (2010). *Structural Geology.* Cambridge University Press, Cambridge, 361 pp.

Frey, M. and Robinson, D. (Editors). (1999). *Low-grade metamorphism.* Blackwell, Oxford, 313 pp.

Frost, B.R. and Frost, C.D. (2008). On charnockites. *Gondwana Research 13*, 30-44.

Geringer, G. (1973). The geology of the Archaean rocks and younger formations in the area to the west of Upington with special reference to various occurrences of granite. *Unpublished D.Sc. thesis, University Orange Free State*, 203 pp.

Geringer, G.J., Humphreys, H.C. and Scheepers, D.J. (1994). Lithostratigraphy, protolithology and tectonic setting of the Areachap Group along the eastern margin of the Namaqua Mobile Belt, South Africa. *South African Journal of Geology 97 (1)*, 78-100.

Gliko, A.O., Singh, R.N. and Swathi, P.S. (1999). Physical approach to the problem of origin of charnockite rocks of southern India: Mechanisms of crustal heating and transfer of carbon dioxide. *Russian Journal of Earth Sciences 1*, 1-16.

Google. (2012, june 02). Aerial photograph of the study area. Koekoeb, Northern Cape, South Africa.

Goscombe, B.D., Passchier, C.W. and Hand, M. (2004). Boudinage classification: end-member boudin types and modified boudin structures. *Journal of Structural Geology 26* , 739–763.

Gower, R.J.W. and Simpson, C. (1992). Phase boundary mobility in naturally deformed, high-grade quartzofeldspathic rocks: evidence for diffusional creep. *Journal of Structural Geology 14 (3)*, 301-313.

Grant, J. (1986). The isocon diagram - a simple solution to Gresens equation for metasomatic alteration. *Economic Geology 2*, 47–65.

Grantham, G.H., Maboko, M. and Eglington, B.M. (2003). A review of the evolution of the Mozambique Belt and implications for the amalgamation and dispersal of Rodinia and Gondwana. *Special Publication of the Geological Society of London 206*, 427-463.

Hamilton, W.R., Wooley, A.R. and Bishop, A.C. (2006). *Minerals, rocks and fossils.* Octopus Publishing Group Ltd, London, 320 pp.

Hanchar, J.M., Rudnick, R.L. (1995). Revealing hidden structures: the application of cathodoluminescence and backscattered electron imaging to dating zircons from lower crustal xenoliths. *Lithos 36*, 289-303.

Harris, R. (1988). Examination of dextral transpression as a model for the development of thrusts and late folds in eastern Namaqualand. *South African Journal of Geology 91*, 329-336.

Harris, R. (1992). A structural analysis of the Hartbees River thrust belt, with special emphasis on the nature and origin of the change in structural patterns across the boundary between the Bushmanland and Gordonia Subprovinces. Ph.D. thesis, University of Cape Town. 285 pp.

Harris, R. (1992). A structural analysis of the Hartbees River thrust belt, with special emphasis on the nature and origin of the change in structural patterns across the boundary between the Bushmanland and Gordonia Subprovinces. Ph.D. thesis, University of Cape Town. 285 pp.

Hartnady, C.J.H, Joubert, P. and Stowe, C.W. (1985). Proterozoic crustal evolution in southwestern Africa. *Episodes 8 (4)*, 236-244.

Holcombe, R. (2011, january 29th). Retrieved September 5th, 2014, from GEOrient, version 9.5.0: http://www.holcombe.net.au/software/

Humphreys, H.C. and van Bever Donker, J.M. (1987). Aspects of deformation along the Namaqua Province eastern boundary, Kenhardt District, South Africa. *Precambrian Research 36*, 39-63.

Humphreys, H.C. and van Bever Donker, J.M. (1990). Early Namaqua low-pressure metamorphism: deformation and porphyroblast growth in the Zoovoorby staurolite schist, South Africa. *Journal of Metamorphic Geology 8*, 159-170.

Humphreys, H.C., Schlegel, G.C-J. and Stowe, C.W. (1991). High-pressure metamorphism in garnet-hornblende-muscovite-plagioclase-quartz schists from the Kheis Belt. *South African Journal of Geology 94*, 170-173.

Jacobs, J., Thomas, R.J. and Weber, K. (1993). Accretion and indentation tectonics at the southern margin of the Kaapvaal Craton during the Kbaran (Grenville) Orogeny. *Geology 21*, 203-206.

Jacobs, J., Pisarevsky, S., Thomas, R.J. and Becker, T. (2008). The Kalahari Craton during the assembly and dispersal of Rodinia. *Precambrian Research 160*, 142-158.

Johnson, M.R., Anheausser, C.R. and Thomas, R.J. (2006). The geology of South Africa. *Geological Society of South Africa. Johannesburg, Council of Geoscience, Pretoria*, 691 pp.

Joubert, P. (1986). The Namaqualand Complex - a model of Proterozoic accretion? *Transactions of the Geological Society of South Africa 89*, 79-96.

Kearey, P., Klepeis, K.A., and Vine, F.J. (2010). *Global tectonics.* Wiley - Blackwell, New Jersey, 482 pp.

Kidan, T.W. and Cosgrove, J.W. (1996). The deformation of multilayers by layer normal compression; An experimental investigation. *Journal of Structural Geology 18 (4)*, 461-474.

Kokonyangi, J., Kampunzu, A.B., Armstrong, R., Yoshida, M., Okudaira, T., Arima, M. and Ngulube D.A. (2006). The Mesoproterozoic Kibaride belt (Katanga, southeast Democratic Republic of Congo). *Journal of African Earth Sciences 46*, 1-35.

Kretz, R. (1983). Symbols for rock-forming minerals. *American Mineralogy 68*, 277-279.

Lee, J.K.W. and Tromp, J. (1995). Self-induced fracture generation in zircon. *Journal of Geophysical Research 100*, 17753-17770.

Li, Z.X., Bogdanova, S.V., Collins, A.S., Davidson, A., De Waele, B., Ernst, R.E., Fitzsimons, I.C.W., Fuck, R.A., Gladkochub, D.P., Jacobs, J., Karlstrom, K.E., Lu, S., Natapov, L.M., Pease, V., Pisarevsky, S.A., Thrane, K. and Vernikovsky, V. (2008). Assembly, configuration and break-up history of Rodinia, a synthesis. *Precambrian Research 160*, 179-210.

Mannheimer, C. and Curtis, B. (2009). *Le Roux and Mueller's field guide to the trees and shrubs of Namibia.* Windhoek: MacMillan Education Namibia, Windhoek, 526 pp.

Miller, R. M. (2012). Review of Mesoproterozoic magmatism, sedimentation and terrane amalgamation in Southwestern Africa. *Geological Society of South Africa, 1154*, 417-448.

Moen, H. (1987). *The Koras Group and related intrusives north of Upington: a re-investigation.* Bulletin of the Geological Survey of South Africa, 85, 20 pp.

Moen, H. (1988). Petrology of the Wilgenhoutsdrif Group. *Bulletin of the Geological Survey of South Africa 89*, 37 pp.

Moen, H. (1999). The Kheis Tectonic Subprovince, southern Africa: a lithostratigraphic perspective. *South African Journal of Geology 102 (1)*, 27-42.

Moen, H. (2007). The Geology of the Upington Area. Map Sheet Explanation, 2820. Scale 1:250 000. *Council for Geoscience, Pretoria*, 160 pp.

Move. (2013, January 25th). Retrieved April 14th, 2014, from Move. version 2013.1.0: http://www.move.com

Onstott, T.C., Hargraves, R.B. and Joubert, P. (1986). Constraints on the tectonic evolution of the Namaqua Province II: Reconnaissance palaeomagnetic and 40Ar/39Ar results from the Namaqua Province and the Kheis Belt. *Transactions of the Geological Society of South Africa 89*, 143-170.

Passchier, C. (1982). Pseudotachylyte and the development of ultramylonite bands in the Saint-Barthelemy Massif, French Pyrenees. *Journal of Structural Geology 4*, 69-79.

Passchier, C.W. and Trouw, R.A.J. (2005). *Microtectonics. Second Edition.* Springer-Verlag, Berlin, 371 pp.

Pertoldová, J., Týcová, P., Verner, K., Košuličová, M., Pertold, Z., Košler, J., Konopásek, J. and Pudilová, M. (2009). Metamorphic history of skarns, origin of their protolith and implications for genetic interpretation; an example from three units of the Bohemian Massif. *Journal of Geosciences 54*, 101-134.

Petit, J. (1987). Criteria for the sense of movement on fault surfaces in brittle rocks. *Journal of Structural Geology 9*, 597–608.

Pettersson, Å. (2008). Mesoproterozoic crustal evolution in Southern Africa, Ph.D. thesis, University of Gothenburg, A117 http,//gupea.ub.gu.se/ handle/2077/17269.

Pettersson, Å., Cornell, D.H., Moen, H.F.G., Reddy, S. and Evans, D. (2007). Ion-probe dating of 1.2 Ga collision and crustal architecture in the Namaqua-Natal province of southern Africa. *Precambrian Research 158*, 79-92.

Philpotts, A.R. and Ague, J.J. (2010). *Principles of igneous and metamorphic petrology. Second Edition.* Cambridge University Press, New York, 667 pp.

Podervaart, A. (1966). Archean charnockitic adamellite phacoliths in the Keimoes-Kakamas region, C.P. South Africa. *Transactions of Geological Society of South Africa, 69*, 139-154.

Podervaart, A. and von Backström, J.W. (1949). A study of an area at Kakamas. *Transactions of the Geological Society of South Africa 52*, 435-495.

Pollard, D.D. and Aydin, A. (1988). Progress in understanding jointing over the past century. *Geological Society of American Bulletin 100*, 1181–1204.

Pollard, D.D. and Fletcher, R.C. (2005). *Fundamentals of Structural Geology*. Cambridge University Press, Cambridge, 500 pp.

Powell, C.Mc.A., Jones, D.L., Pisarevsky, S.A. and Wingate, M.T.D. (2001). Paleomagnetic constraints on the position of the Kalahari Craton in Rodinia. *Precambrian Research 110*, 33-46.

Praekelt, H. (1984). Die geologie van die gebied rondom Augrabies (2820 C). M.Sc. thesis (unpublished), University of the Orange Free State, Bloemfontein. 173 pp.

Ramberg, H. (1955). Natural and experimental boudinage and pinch-and-swell structures. *Journal of Geology 63*, 512-526.

Ramsay, J.G. and Huber, M.I. (1983). *The Techniques of Modern Structural Geology.* Academic Press 1, London, 307 pp.

Ramsey, J.M.and Chester, F.M. (2004). Hybrid fracture and the transition from extension fracture to shear fracture. *Nature 428*, 63-66.

Reid, R. (1969). Scotsford's metasomatic augen gneiss: an additional working hypothesis. *Bulletin of the Geological Society of America*, 2653-2654.

Reid, D. (1997). Sm–Nd age and REE geochemistry of Proterozoic arc-related igneous rocks in the Richtersveld Subprovince, Namaqua Mobile Belt, southern Africa. *Journal of African Earth Sciences 24*, 621-633.

Robb, L. (2005). *Introduction to Ore-Forming Processes.* Blackwell, Oxford, 158 pp.

Robb, L.J., Armstrong, R.A. and Waters, D.J. (1999). The history of granulite-facies metamorphism and crustal growth from single zircon U-Pb geochronology; Namaqualand, South Africa. *Journal of Petrology 40*, 1747-1770.

Rowland, S.M., Duebendorfer, E.M. and Schiefelbein, L.M. (2007). *Structural analysis and synthesis: A laboratory course in structural geology. Third Edition.* Blackwell, USA, 301 pp.

Rudnick, R.L. and Williams, I.S. (1987). Dating the lower crust by ion microprobe. *Earth and Planetary Science Letters 85*, 145-161.

Saad, A. (1987). A petrographical study of the tin-tungsten deposit at Renosterkop, Augrabies, Northern Cape Province. M.Sc. thesis (unpublished), Potchefstroom University. 185 pp.

SACS (South African Committee for stratigraphy). (1980). Stratigraphy of South Africa. Part 1 (Compiler L.E. Kent), Lithostratigraphy of the Republic of South Africa, South West Africa/Namibia and the Republics of Bophuthatswana, Transkei and Venda. *Handbook Geological Survey of South Africa 8*, 690 pp.

Schmid, S.M., Zingg, A. and Handy, M. (1987). The kinematics of movements along the Insubric Line and the emplacement of the Ivrea Zone. *Tectonophysics 135*, 47-66.

Schmid, R., Fettes, D., Harte, B., Davis, E. and Desmons, J. (2007). A systematic nomenclature for metamorphic rocks. 1. How to name a metamorphic rock. Recommendations by the IUGS Subcommission on the systematics of metamorphic rocks. *SCMR (www.bgs.ac.uk/SCMR/home.html.)*.

Schultz, R. (1978). Origin of the so-called charnockitic adamellite porphyry from the Upington geotraverse. *Annual Report of Precambrian Research Unit, University of Cape Town 14-15*, 48-82.

Searle, M.P and Alsop, G.I. (2007). Eye-to-eye with a mega-sheath fold: A case study from Wadi Mayh, Northern Oman Mountains. *Geology 35 (11)*, 1043-1046 .

Sibson, R. (1977). Fault rocks and fault mechanisms. *Journal of Geological Society of London 133*, 190-213.

Skjernaa, L. (1980). Rotation and deformation of randomly orientated planar and linear structures in progressive simple shear. *Journal of Structural Geology 2*, 101-109.

Slabbert, M. (1987). Die geologie in die omgewing van die Melkboomkoepel, suid van Keimoes. *Bulletin of Geological Survey of South Africa 83*, 33 pp.

Slabbert, M.J., Moen, H.F.G., Agenbacht, A.L.D., van der Merwe, S.W. and Siegfried, H.P. (1989). An introduction to the Proterozoic rocks on the 1:250 000 sheets 2820 Upington and 2920 Kenhardt. Pre-Summer field school guidebook. *Geological Society of South Africa*, 90pp.

Slabbert, M.J., Moen, H.F.G. and Boelema, R. (1999). Die geologie van die gebied Kenhardt. Explanation, sheet 2920. *Council for Geoscience, South Africa*, 123 pp.

Spear, F. (1993). *Metamorphic phase equilibria and pressure-temperature-time paths.* Mineralogical Society of America,Washington D.C. 799 pp.

Stowe, C. (1983b). The Korannaland Project . *Annual Report of the Precambrian Research Unit, University of Cape Town 18-20*, 25-32.

Stowe, C. (1986). Synthesis and interpretation of structures along the north-eastern boundary of the Namaqua tectonic province, South Africa. *Transactions of the Geological Society of South Africa 89*, 185-198.

Suppe, J. (1983). Geometry and kinematics of fault-bend folding. *American Journal of Science 283*, 684-721.

Thomas, R.J., von Veh, M.W. and McCourt, S. (1993). The tectonic evolution of southern Africa : an overview. *Journal of African Earth Sciences 16 (1)*, 5-24.

Thomas, R.J., Cornell, D.H., Moore, J.M. and Jacobs, J. (1994a). Crustal evolution of the Namaqua-Natal Metamorphic Province, southern Africa. *South African Journal of Geology 97 (1)*, 8-14.

Thomas, R.J., Bauer, W., Bingen, B., de Azevedo, de Sousa Soares, H., Hollick, L., Feitio, P., Fumo, C., Gonzales, E., Jacobs, J., Manhica, V., Manuel, S., Matuza, G., Tembe, D., Uachave, B. and Viola, G. (2006). Mozambique Belt in the Milanje-Mocuba-Malema area, Mozambique. *Geochronology of Pan-African terrain assembly in the NE Mozambique. 21st Collquium of African Geology, Maputo, Mozambique. Abstracts*, 161-163.

Twiss, R.J. and Moores, E.M. (1992). *Structural Geology.* W.H. Freeman and Company, New York, 532 pp.

Twiss, R.J. and Moores, E.M. (2007). *Structural Geology. Second Edition.* W. H. Freeman and Company, New York, 736 pp.

van Bever Donker, J. (1980). Structural and metamorphic evolution of an area around Kakamas and Keimoes Cape Province, South Africa. *Bulletin of the Precambrian Research Unit, University of Cape Town 28*, 165 pp.

van Bever Donker, J. (1983). The Neusspruit lineament, Upington geotraverse, possible boundary between the Namaqualand Metamorphic Complex and the Namaqua front. In: Botha, B.J.V. (Editor).Namaqualand Metamorphic Complex. *Special Publication of the Geological Society of South Africa 10*, 193-198.

van Bever Donker, J. (1991). A synthesis of the structural geology of a major tectonic boundary between a 1000 m.y. mobile belt and a 3000 m.y. craton. *Tectonophysics 196*, 359-370.

van der Pluijm, B. A. and Marshak, S. (2004). *Earth Structure: An introduction to Structural Geology and Tectonics. Second Edition.* W.W. Norton and company, New York, 672 pp.

van Zyl, C. (1981). Structural and metamorphic evolution in the transitional zone between craton and mobile belt, Upington Geotraverse. *Bulletin of the Precambrian Research Unit, University of Cape Town 31*, 243 pp.

von Backström, J. (1964). The geology of an area around Keimoes, Cape Province, with special reference to phacoliths of charnockitic adamellite-porphyry. *Memoir of the Geological Survey of South Africa 53*, 218 pp.

Winter, J. (2010). *Principles of igneous and metamorphic petrology. Second Edition.* Pearson Prentice Hall, New Jersey, 702 pp.

Winter, J. (2014). *Principles of igneous and metamorphic petrology. Second Edition Revised .* Pearson New International Edition, United States of America, 740 pp.

Woodcock, N. (1977). Specification of fabric shapes using an eigenvalue method. *Bulletin of the Geological Society of America 88*, 1231-1236.

Woodhead, J.A., Rossman, G.R. and Silver, L.T. (1991). The metamictizationo f zircon: Radiation dose-dependent structural characteristics. *American Mineralogist 76*, 74-82.

APPENDIX

Structural data

Sub-area 1 (South Neusberg Mountain Range)

Stations	Longit	Latit	Elev	Rock type	General description	Primary bedding (S_0)	Lineation (L_1)	Joint (J_1)	Joint (J_2)	Joint (J_3)	Joint (J_4)	Other features
						Dip/Dip dir	Plunge/Trend	Dip/Dip dir	Dip/Dip dir	Dip/Dip dir	Dip/Dip dir	
1	28°48'30.4''	20°46'58.7''	740 m	Csq	Calc, Kfs, Qtz, Plg, Ep	65/040		70/300	65/150			Fine to medium grained
2	28°48'27.7''	20°46'64.7''	749 m	Fmq	Kfs, Ms, Qtz, Plg	70/038	30/082	80/244	85/120			Medium to coarse grained
3	28°48'51.8''	20°46'88.4''	750 m	Fmq	Kfs, Ms, Qtz, Plg	70/040	35/045	80/244	85/320	75/100		Gliterring muscovite
4	28°48'51.3''	20°46'88.7''	747 m	Csq	Calc, Kfs, Qtz, Plg, Ep	50/048		65/128	65/220	85/302	80/140	Intercalation with amphibole schist
5	28°48'50.2''	20°46'89.0''	750 m	Csq	Calc, Kfs, Qtz, Plg, Ep	60/038	35/048	85/078				Fine to medium grained
6	28°48'49.0''	20°46'88.8''	745 m	Csq	Calc, Kfs, Qtz, Plg, Ep	60/036		85/250	90/290	75/134	80/236	Presence of fractures
7	28°48'16.1''	20°47'10.7''	756 m	Fmq	Kfs, Ms, Qtz, Plg	50/030	25/090	80/142	90/274			fractured pebbles
8	28°48'15.2''	20°47'12.6''	746 m	Csq	Calc, Kfs, Qtz, Plg, Ep	55/044		85/140				Joints filled with quartz
9	28°48'15.4''	20°47'14.7''	743 m	Csq	Calc, Kfs, Qtz, Plg, Ep	50/024	20/048	70/140	60/124			Streaks of epidote, pinch and swell
10	28°48'15.6''	20°47'14.9''	746 m	Fmq	Kfs, Ms, Qtz, Plg	45/038		85/118	70/226	80/278	85/228	Medium to coarse grained
11	28°48'15.9''	20°47'15.1''	749 m	Fmq	Kfs, Ms, Qtz, Plg	55/048	78/010	85/138				Medium to coarse grained
12	28°48'16.0''	20°47'17.2''	743 m	Csq	Calc, Kfs, Qtz, Plg, Ep	45/030		80/056	85/130			Streaks of epidote, medium grained
13	28°48'16.5''	20°47'18.9''	733 m	Csq	Calc, Kfs, Qtz, Plg, Ep	55/040		90/312	80/126	75/276		Dark surface, well oxidised
14	28°48'16.7''	20°47'21.7''	736 m	Csq	Calc, Kfs, Qtz, Plg, Ep	50/030		75/050	80/120	85/240		dark weathered surface, fine grained
15	28°48'18.0''	20°47'26.5''	729 m	Csq	Calc, Kfs, Qtz, Plg, Ep	50/034		80/284				Fine and medium grained
16	28°48'07.6''	20°47'17.0''	768 m	Fmq	Kfs, Ms, Qtz, Plg	55/044	55/056	85/320	75/100	70/272		Medium to coarse grained
17	28°48'03.5''	20°47'23.5''	740 m	Ag	Kfs, Qtz, Plg, Bt			85/302	80/140			Alternation of mafic and felsic layers
18	28°48'00.6''	20°47'27.3''	741 m	Ag	Kfs, Qtz, Plg, Bt			80/096	70/034			Parasitic folds
19	28°48'09.4''	20°47'16.2''	754 m	Csq	Calc, Kfs, Qtz, Plg, Ep	55/034		75/320	70/130	75/276		Fine to medium grained
20	28°48'08.2''	20°47'16.4''	754 m	Csq	Calc, Kfs, Qtz, Plg, Ep	60/026	45/058	55/268	85/108			Fine to medium grained
21	28°48'17.9''	20°47'59.4''	730 m	Fmq	Kfs, Ms, Qtz, Plg	65/030		85/140				Medium to coarse grained
22	28°48'86.3''	20°48'49.6''	742 m	Csq	Calc, Kfs, Qtz, Plg, Ep	60/044		85/164	90/094			Medium to coarse grained
23	28°48'82.6''	20°48'55.3''	740 m	Csq	Calc, Kfs, Qtz, Plg, Ep	50/048		85/270				Medium to coarse grained
24	28°48'74.6''	20°48'64.9''	753 m	Csq	Calc, Kfs, Qtz, Plg, Ep			85/120	70/272			Dark weathered surface
25	28°48'57.0''	20°48'90.7''	753 m	Csq	Calc, Kfs, Qtz, Plg, Ep	45/034	25/090	85/118	55/240			Medium to coarse grained
26	28°48'40.2''	20°49'08.7''	758 m	Fmq	Kfs, Ms, Qtz, Plg	50/038						Brown weathered surface
27	28°48'01.3''	20°49'45.6''	751 m	Fmq	Kfs, Ms, Qtz, Plg	60/034						Medium to coarse grained
28	28°48'81.6''	20°47'28.2''	755 m	Csq	Calc, Kfs, Qtz, Plg, Ep	55/030						Fine to medium grained
29	28°48'80.0''	20°47'29.5''	759 m	Csq	Calc, Kfs, Qtz, Plg, Ep	65/028		75/126				Fine to medium grained
30	28°48'78.8''	20°47'30.8''	758 m	Csq	Calc, Kfs, Qtz, Plg, Ep	60/040		85/126				Dark weathered surface
31	28°49'45.7''	20°48'46.3''	771 m	Csq	Calc, Kfs, Qtz, Plg,	45/034						Fine to medium grained

Abbreviations: Longit= Longitude; Latit= Latitude; Elev= Elevation; dir= direction; Kfs= Orthoclase; Qtz= Quartz; Plg=Plagioclase; Ep=Epidote; Calc= Calcite; Bt= Biotite; Ag = Augen gneiss; Csq= Calc-silicate-rich quartzite; Fmq= Feldspathic mica-rich quartzite.

APPENDIX (continued)

Structural data

Sub-area 1 (South Neusberg Mountain Range)

Stations	Longit	Latit	Elev	Rock type	General description	Primary bedding (S_0)	Lineation (L_1)	Joint (J_1)	Joint (J_2)	Joint (J_3)	Joint (J_4)	Other features
						Dip/Dip dir	Plunge/Trend	Dip/Dip dir	Dip/Dip dir	Dip/Dip dir	Dip/Dip dir	
32	28°49'18.6''	20°48'82.1''	768 m	Csq	Calc, Kfs, Qtz, Plg, Ep		80/162	85/266	80/130			Joints filled with quartz
33	28°49'17.0''	20°48'83.8''	769 m	Csq	Calc, Kfs, Qtz, Plg, Ep	65/040	70/160	80/286	80/160	45/048		Fined grained, streaks of epidote
34	28°49'15.0''	20°48'90.4''	770 m	Csq	Calc, Kfs, Qtz, Plg, Ep	65/030		85/150				Dark weathered surface
35	28°48'73.5''	20°46'07.8''	743 m	Fmq	Kfs, Ms, Qtz, Plg	55/038						Fine to medium grained
36	28°48'64.6''	20°47'22.4''	766 m	Fmq	Kfs, Ms, Qtz, Plg	65/028						Medium to coarse grained
37	28°48'55.8''	20°47'31.6''	829 m	Fmq	Kfs, Ms, Qtz, Plg		70/300					Glittering muscovite, medium grained
38	28°48'17.9''	20°47'59.4''	730 m	Fmq	Kfs, Ms, Qtz, Plg	65/030						Grey colour, coarse grained
39	28°48'07.0''	20°47'69.9''	731 m	Fmq	Kfs, Ms, Qtz, Plg	65/032						coarse grained
40	28°49'27.9''	20°48'14.9''	774 m	Fmq	Kfs, Ms, Qtz, Plg	65/040						Medium to coarse grained
41	28°49'24.7''	20°48'17.7''	790 m	Fmq	Kfs, Ms, Qtz, Plg	45/040						Medium to coarse grained
42	28°49'12.8''	20°48'96.1''	777 m	Csq	Calc, Kfs, Qtz, Plg, Ep	60/038	35/048	75/154	80/312			Medium to coarse grained
43	28°49'52.4''	20°48'77.1''	792 m	Csq	Calc, Kfs, Qtz, Plg, Ep	65/024		85/124	85/270	85/258		Fine to medium grained
44	28°49'45.9''	20°48'70.9''	788 m	Csq	Calc, Kfs, Qtz, Plg, Ep	45/038	40/080	65/176	85/320			Fine to medium grained
45	28°49'39.7''	20°48'79.5''	782 m	Csq	Calc, Kfs, Qtz, Plg, Ep	60/030		85/110				Fine to medium grained
46	28°49'70.7''	20°48'78.5''	784 m	Csq	Calc, Kfs, Qtz, Plg, Ep	70/026	60/025	85/354	85/176			Fine to medium grained
47	28°49'32.8''	20°48'81.9''	780 m	Csq	Calc, Kfs, Qtz, Plg, Ep	60/030		85/176	65/088	80/170		Fine grained, dark weathered surface
48	28°49'91.1''	20°48'88.9''	790 m	Fmq	Kfs, Ms, Qtz, Plg	55/030		75/150	85/286			Medium to coarse grained
49	28°49'44.7''	20°48'47.4''	776 m	Fmq	Kfs, Ms, Qtz, Plg		75/172					Medium to coarse grained
50	28°49'37.5''	20°48'50.3''	801 m	Fmq	Kfs, Ms, Qtz, Plg	50/026	25/098	80/320	85/290	75/060	55/140	Medium to coarse grained
51	28°49'89.8''	20°48'98.0''	796 m	Csq	Calc, Kfs, Qtz, Plg, Ep	45/018	45/058	80/146	85/296			Croscutting joints
52	28°49'89.8''	20°48'98.0''	796 m	Csq	Calc, Kfs, Qtz, Plg, Ep	50/046		90/120	80/280			Medium to coarse grained
53	28°49'89.8''	20°48'98.0''	796 m	Csq	Calc, Kfs, Qtz, Plg, Ep	50/046		90/120	80/280			Medium to coarse grained
54	28°49'33.3''	20°48'52.6''	800 m	Fmq	Kfs, Ms, Qtz, Plg	45/038		55/226	85/176			Dentritic patterns
55	28°49'24.6''	20°48'61.6''	804 m	Fmq	Kfs, Ms, Qtz, Plg			70/162				Joint filled with quartz
56	28°49'24.1''	20°48'63.2''	793 m	Fmq	Kfs, Ms, Qtz, Plg			85/172	70/250	90/290	85/324	Crosscutting joints

Abbreviations: Longit= Longitude; Latit= Latitude; Elev= Elevation; dir=direction; Kfs= Orthoclase; Qtz= Quartz; Plg=Plagioclase; Ep=Epidote; Calc= Calcite; Bt= Biotite; Ms=Muscovite; Csq= Calc-silicate-rich quartzite; Fmq= Feldspathic mica-rich quartzite.

APPENDIX

Structural data

Sub-area 2 (North Neusberg Mountain Range)

Stations	Longit	Latit	Elev	Rock type	General description	Primary bedding (S_0)	Lineation (L_1)	Joint (J_1)	Joint (J_2)	Joint (J_3)	Joint (J_4)	Other features
						Dip/Dip dir	Plunge/Trend	Dip/Dip dir	Dip/Dip dir	Dip/Dip dir	Dip/Dip dir	
1	28°48'07.8''	20°47'43.4''	738 m	Csq	Calc, Kfs, Qtz, Plg, Ep	55/040		80/284	85/320	75/100	85/124	Fine to medium grained
2	28°48'07.9''	20°47'41.2''	731 m	Csq	Calc, Kfs, Qtz, Plg, Ep	65/026		70/272	65/128			Dark weathered surface
3	28°48'07.9''	20°47'39.4''	733 m	Csq	Calc, Kfs, Qtz, Plg, Ep	55/032	25/040	85/284				Streaks of epidote, fine grained
4	28°48'07.5''	20°47'37.9''	731 m	Fmq	Kfs, Ms, Qtz, Plg	65/028						Glittering muscovite, coarse grained
5	28°48'08.0''	20°47'36.5''	730 m	Fmq	Kfs, Ms, Qtz, Plg	60/008	30/022	80/140				coarse to medium grained
6	28°48'08.6''	20°47'33.4''	741 m	Fmq	Kfs, Ms, Qtz, Plg	55/030		70/130	75/276	85/250		coarse to medium grained
7	28°48'09.2''	20°47'31.5''	744 m	Csq	Calc, Kfs, Qtz, Plg, Ep	60/018	40/036	75/134				Medium to fine grained
8	28°48'08.7''	20°47'30.5''	744 m	Csq	Calc, Kfs, Qtz, Plg, Ep	60/030						Medium to fine grained
9	28°48'08.8''	20°47'29.0''	743 m	Csq	Calc, Kfs, Qtz, Plg	55/034		90/274	85/164			Medium to fine grained
10	28°48'08.6''	20°47'26.7''	745 m	Csq	Calc, Kfs, Qtz, Plg, Ep	55/010		70/094	85/140	75/126	55/268	Medium to fine grained
11	28°48'08.4''	20°47'24.9''	746 m	Csq	Calc, Kfs, Qtz, Plg, Ep	60/032		85/108				Medium to fine grained
12	28°48'08.7''	20°47'22.4''	747 m	Csq	Calc, Kfs, Qtz, Plg, Ep	50/024		60/124	55/240			Medium to fine grained
13	28°48'08.8''	20°47'20.2''	749 m	Csq	Calc, Kfs, Qtz, Plg	55/038	20/062	85/118	70/226	80/278		Intercalation with amphibole schist
14	28°48'08.7''	20°47'18.9''	750 m	Csq	Calc, Kfs, Qtz, Plg	50/022		85/228				Medium to fine grained
15	28°48'08.4''	20°47'18.2''	751 m	Csq	Calc, Kfs, Qtz, Plg	60/050	30/050	85/138	85/270			Medium to fine grained
16	28°48'08.0''	20°47'16.8''	753 m	Csq	Calc, Kfs, Qtz, Plg, Ep	55/034		85/096	80/056	85/130		Dark weathered surface
17	28°48'08.0''	20°47'15.8''	755 m	Fmq	Kfs, Ms, Qtz, Plg	50/026		75/176	80/090			Glittering muscovite, medium grained
18	28°48'07.3''	20°47'13.0''	757 m	Fmq	Kfs, Ms, Qtz, Plg	50/046						Medium grained
19	28°48'06.7''	20°47'12.0''	755 m	Fmq	Kfs, Ms, Qtz, Plg	50/042		75/320				Medium to coarse grained
20	28°48'06.6''	20°47'11.1''	753 m	Fmq	Kfs, Ms, Qtz, Plg	50/038		65/220	85/302			Medium to coarse grained
21	28°48'06.3''	20°47'09.8''	750 m	Fmq	Kfs, Ms, Qtz, Plg	55/028	35/064	90/290				Medium to coarse grained
22	28°48'06.3''	20°47'08.1''	749 m	Fmq	Kfs, Ms, Qtz, Plg	60/048		65/220	50/250			Medium to coarse grained
23	28°48'06.3''	20°47'05.3''	755 m	Fmq	Kfs, Ms, Qtz, Plg	50/040		80/142	70/140			Medium to coarse grained
24	28°48'06.2''	20°47'04.4''	754 m	Csq	Calc, Kfs, Qtz, Plg, Ep	55/022		90/312	80/236			Joints filled with quartz
25	28°48'05.9''	20°47'03.5''	755 m	Csq	Calc, Kfs, Qtz, Plg, Ep	60/038						Dark weathered surface
26	28°48'05.6''	20°47'01.4''	753 m	Csq	Calc, Kfs, Qtz, Plg, Ep	55/040		85/078				Medium to fine grained
27	28°48'05.7''	20°47'00.9''	754 m	Csq	Calc, Kfs, Qtz, Plg, Ep	50/038		85/150				Medium to fine grained
28	28°48'05.5''	20°46'99.2''	755 m	Csq	Calc, Kfs, Qtz, Plg, Ep	60/042		70/034				Medium to fine grained
29	28°48'05.1''	20°46'99.3''	757 m	Csq	Calc, Kfs, Qtz, Plg, Ep	55/046	35/046	80/126				Medium to fine grained
30	28°48'05.2''	20°46'96.6''	759 m	Csq	Calc, Kfs, Qtz, Plg, Ep	60/054		75/140				Joint filled with quartz
31	28°48'05.2''	20°46'95.3''	760 m	Csq	Calc, Kfs, Qtz, Plg, Ep	55/050		75/114				Intercalation with amphibole schist

Abbreviations: Longit= Longitude; Latit= Latitude; Elev= Elevation; dir= direction; Kfs= Orthoclase; Qtz= Quartz; Plg=Plagioclase; Ep=Epidote; Calc= Calcite; Ms= Muscovite; Csq= Calc-silicate-rich quartzite; Fmq= Feldspathic mica-rich quartzite.

APPENDIX (continued)

Structural data

Sub-area 2 (North Neusberg Mountain Range)

Stations	Longit	Latit	Elev	Rock type	General description	Primary bedding (S_0)	Lineation (L_1)	Joint (J_1)	Joint (J_2)	Joint (J_3)	Joint (J_4)	Other features
						Dip/Dip dir	Plunge/Trend	Dip/Dip dir	Dip/Dip dir	Dip/Dip dir	Dip/Dip dir	
32	28°48′05.2′′	20°46′93.7′′	760 m	Csq	Calc, Kfs, Qtz, Plg, Ep	60/036		85/354				Medium to fine grained
33	28°48′05.0′′	20°46′92.8′′	761 m	Csq	Calc, Kfs, Qtz, Plg, Ep	60/038		85/176	65/088			Medium to fine grained
34	28°48′05.0′′	20°46′89.5′′	767 m	Csq	Calc, Kfs, Qtz, Plg, Ep	60/052		80/170	75/150			Medium to fine grained
35	28°48′05.0′′	20°46′88.6′′	767 m	Csq	Calc, Kfs, Qtz, Plg, Ep	55/030		85/286	65/310			Joints filled with quartz
36	28°48′05.8′′	20°46′87.7′′	770 m	Csq	Calc, Kfs, Qtz, Plg, Ep	65/052	45/052	85/290				Streaks of epidote, fine grained
37	28°48′072′′	20°46′878′′	776 m	Csq	Calc, Kfs, Qtz, Plg	60/062		80/146	80/260	75/300		Fine to medium grained
38	28°48′075′′	20°46′885′′	775 m	Fmq	Kfs, Ms, Qtz, Plg	60/050		85/296	90/120			Crosscutting joints
39	28°48′079′′	20°46′891′′	776 m	Fmq	Kfs, Ms, Qtz, Plg	50/030		80/280	55/226			Brown weathered surface
40	28°48′086′′	20°46′920′′	775 m	Fmq	Kfs, Ms, Qtz, Plg	55/032		55/226				Medium to coarse grained
41	28°48′099′′	20°46′945′′	767 m	Fmq	Kfs, Ms, Qtz, Plg	25/042		85/176				Medium to coarse grained
42	28°48′103′′	20°46′955′′	764 m	Fmq	Kfs, Ms, Qtz, Plg	60/064		90/320				Medium to coarse grained
43	28°48′105′′	20°46′987′′	765 m	Csq	Calc, Kfs, Qtz, Plg	55/040	50/030					Fine to medium grained
44	28°48′113′′	20°46′961′′	759 m	Csq	Calc, Kfs, Qtz, Plg	55/036						Dark weathered surface
45	28°48′116′′	20°47′000′′	753 m	Csq	Calc, Kfs, Qtz, Plg	55/040						Dark weathered surface
46	28°48′123′′	20°47′019′′	764 m	Csq	Calc, Kfs, Qtz, Plg	35/036						Fine to medium grained
47	28°48′125′′	20°47′027′′	756 m	Csq	Calc, Kfs, Qtz, Plg	50/044						Fine to medium grained
48	28°48′127′′	20°47′043′′	763 m	Csq	Calc, Kfs, Qtz, Plg	55/064	40/026					Fine to medium grained
49	28°48′134′′	20°47′064′′	753 m	Csq	Calc, Kfs, Qtz, Plg	30/040		85/140				Fine to medium grained
50	28°48′143′′	20°47′090′′	749 m	Fmq	Kfs, Ms, Qtz, Plg	60/038		70/162				Brown weathered surface
51	28°48′148′′	20°47′107′′	748 m	Fmq	Kfs, Ms, Qtz, Plg	45/040		70/250				Medium to coarse grained
52	28°48′152′′	20°47′126′′	746 m	Fmq	Kfs, Ms, Qtz, Plg	55/044						Medium to coarse grained
53	28°48′154′′	20°47′136′′	743 m	Fmq	Kfs, Ms, Qtz, Plg	50/024						Medium to coarse grained
54	28°48′156′′	20°47′157′′	746 m	Fmq	Kfs, Ms, Qtz, Plg	38/045						Medium to coarse grained
55	28°48′159′′	20°47′158′′	741 m	Fmq	Kfs, Ms, Qtz, Plg	55/048		85/172				Medium to coarse grained
56	28°48′160′′	20°47′166′′	746 m	Fmq	Kfs, Ms, Qtz, Plg	45/034		90/290				Medium to coarse grained
57	28°48′160′′	20°47′172′′	743 m	Csq	Calc, Kfs, Qtz, Plg	45/030						Fine to medium grained
58	28°48′163′′	20°47′183′′	733 m	Csq	Calc, Kfs, Qtz, Plg	50/036						Fine to medium grained
59	28°48′165′′	20°47′189′′	733 m	Csq	Calc, Kfs, Qtz, Plg	55/040						Fine to medium grained
60	28°48′167′′	20°47′202′′	734 m	Csq	Calc, Kfs, Qtz, Plg	50/042						Dark weathered surface
61	28°48′167′′	20°47′217′′	736 m	Csq	Calc, Kfs, Qtz, Plg	40/030		85/324				Dark weathered surface
62	28°48′172′′	20°47′231′′	733 m	Csq	Calc, Kfs, Qtz, Plg	42/050		60/148				Fine to medium grained
63	28°48′173′′	20°47′242′′	733 m	Csq	Calc, Kfs, Qtz, Plg	55/046						Fine to medium grained
64	28°48′180′′	20°47′265′′	729 m	Csq	Calc, Kfs, Qtz, Plg	50/034						Fine to medium grained

Abbreviations: Longit= Longitude; Latit= Latitude; Elev= Elevation; dir= direction; Kfs= Orthoclase; Qtz= Quartz; Plg=Plagioclase; Ep=Epidote; Calc= Calcite; Ms= Muscovite; Csq= Calc-silicate-rich quartzite; Fmq= Feldspathic mica-rich quartzite

APPENDIX

Structural data

Sub-area 3 (Between Neusberg Mountain Range and Vuurkop Mountain)

Stations	Longit	Latit	Elev	Rock type	General description	Primary bedding (S_0)	Joint (J_1)	Joint (J_2)	Joint (J_3)	Joint (J_4)	Other features
						Dip dir/Dip	Dip dir/Dip	Dip dir/Dip	Dip dir/Dip	Dip dir/Dip	
1	28°47'82.5''	20°47'67.1''	719 m	Fmq	Ms, Qtz, Plg, Kfs	044/55	098/80				Presence of fractures
2	28°48'07.6''	20°47'17.0''	768 m	Fmq	Ms, Qtz, Plg, Kfs	036/50	118/85				Joint filled with quartz
3	28°47'76.0''	20°48'84.7''	722 m	Fmq	Ms, Qtz, Plg, Kfs	040/55					Dentritic weathering patterns
4	28°47'69.3''	20°48'74.6''	713 m	Fmq	Ms, Qtz, Plg, Kfs	042/50	268/75				Joint filled with quartz
5	28°47'48.8''	20°49'03.1''	724 m	Fmq	Ms, Qtz, Plg, Kfs	030/50	276/65				Brown weathering surface
6	28°47'46.2''	20°49'03.7''	720 m	Fmq	Ms, Qtz, Plg, Kfs	042/50					Fine to medium grained
7	28°47'47.2''	20°49'04.5''	724 m	Fmq	Ms, Qtz, Plg, Kfs	046/55	284/75	306/80	168/80		Crosscutting joints
8	28°47'47.4''	20°49'06.2''	723 m	Fmq	Ms, Qtz, Plg, Kfs	034/50	162/75	208/85	092/80		Crosscutting joints
9	28°48'24.4''	20°48'57.4''	734 m	Fmq	Ms, Qtz, Plg, Kfs	020/65	265/90	130/75	035/80	100/70	Crosscutting joints
10	28°48'17.7''	20°48'24.7''	741 m	Fmq	Ms, Qtz, Plg, Kfs	035/50	086/65	150/70	262/70	250/80	Crosscutting joints
11	28°48'08.0''	20°48'28.8''	755 m	Fmq	Ms, Qtz, Plg, Kfs	045/60	228/80	300/75			Joints filled with quartz
12	28°47'63.5''	20°49'18.1''	754 m	Fmq	Ms, Qtz, Plg, Kfs	035/60					Medium to coarse grained
13	28°47'60.2''	20°49'20.3''	739 m	Fmq	Ms, Qtz, Plg, Kfs	030/60					Fine to medium grained
14	28°48'05.0''	20°49'18.2''	740 m	Fmq	Ms, Qtz, Plg, Kfs	020/55		340/75	220/85		Dentritic weathering patterns
15	28°48'07.9''	20°49'13.3''	734 m	Fmq	Ms, Qtz, Plg, Kfs	032/50		145/70			Joint filled with quartz
16	28°47'79.2''	20°47'11.0''	752 m	Fmq	Ms, Qtz, Plg, Kfs	034/65					Glittering muscovite, fine grained
17	28°47'78.3''	20°47'11.5''	748 m	Fmq	Ms, Qtz, Plg, Kfs	044/55					Glittering muscovite, Medium grained
18	28°47'77.3''	20°47'12.6''	745 m	Fmq	Ms, Qtz, Plg, Kfs	038/45	102/75				Joint filled with quartz
19	28°47'75.2''	20°47'12.8''	737 m	Fmq	Ms, Qtz, Plg, Kfs	046/50					Fine to medium grained
20	28°47'72.4''	20°47'12.9''	727 m	Fmq	Ms, Qtz, Plg, Kfs	024/65	125/65				Fine to medium grained
21	28°47'65.9''	20°47'18.5''	718 m	Fmq	Ms, Qtz, Plg, Kfs	020/40					Glittering muscovite, fine grained
22	28°47'63.6''	20°47'20.8''	717 m	Fmq	Ms, Qtz, Plg, Kfs	152/40	120/80	322/85	086/75		Crosscutting joints
23	28°48'17.1''	20°49'15.2''	734 m	Pg	Bt, Qtz, Plg, Kfs		330/80	230/85	285/70		Joints filled with quartz, well foliated
24	28°48'20.2''	20°49'16.0''	732 m	Pg	Bt, Qtz, Plg, Kfs		154/85	080/55			Croscutting joints, foliated
25	28°48'34.8''	20°49'16.7''	743 m	Pg	Bt, Qtz, Plg, Kfs		340/85	160/85			Medium to coarse grained
26	28°48'36.3''	20°49'14.6''	740 m	Lg	Qtz, Plg, Kfs		330/80				Dark weathered surface
27	28°48'38.6''	20°49'11.9''	761 m	Lg	Qtz, Plg, Kfs		155/80				Fine grained
28	28°48'33.3''	20°49'07.9''	737 m	Lg	Qtz, Plg, Kfs		140/75				Fine grained
29	28°48'30.5''	20°49'06.1''	729 m	Lg	Qtz, Plg, Kfs		226/70	160/85			Crosscutting joints
30	28°48'31.9''	20°49'00.3''	757 m	Fmq	Ms, Qtz, Plg, Kfs	150/45					Joint filled with quartz
31	28°48'36.4''	20°48'99.1''	760 m	Fmq	Ms, Qtz, Plg, Kfs	148/40					Joint filled with quartz

Abbreviations: Longit= Longitude; Latit= Latitude; Elev= Elevation; dir= direction; Kfs= Orthoclase; Qtz= Quartz; Plg=Plagioclase; Ep=Epidote; Bt= Biotite; Calc= Calcite; Ms= Muscovite; Csq= Calc-silicate-rich quartzite; Fmq= Feldspathic mica-rich quartzite; Lg= Leucogneiss; Pg= Pink gneiss.

APPENDIX (continued)

Structural data

Sub-area 3 (Between Neusberg Mountain Range and Vuurkop Mountain)

Stations	Longit	Latit	Elev	Rock type	General description	Primary bedding (S_0)	Joint (J_1)	Joint (J_2)	Joint (J_3)	Joint (J_4)	Other features
						Dip dir/Dip	Dip dir/Dip	Dip dir/Dip	Dip dir/Dip	Dip dir/Dip	
32	28°48'38.6''	20°49'00.1''	771 m	Fmq	Ms, Qtz, Plg, Kfs	126/45	162/80	190/85			Joints filled with quartz
33	28°47'78.6''	20°47'95.7''	718 m	Fmq	Ms, Qtz, Plg, Kfs	124/55	250/85	320/45			Crosscutting joints
34	28°47'78.4''	20°47'96.6''	718 m	Fmq	Ms, Qtz, Plg, Kfs	130/50					Well foliated, coarse grained
35	28°47'75.3''	20°48'13.8''	703 m	Fmq	Ms, Qtz, Plg, Kfs	140/55					Medium to coarse grained
36	28°47'75.7''	20°48'15.0''	706 m	Fmq	Ms, Qtz, Plg, Kfs	152/60					Medium to coarse grained
37	28°47'76.8''	20°48'21.2''	708 m	Fmq	Ms, Qtz, Plg, Kfs	155/60					Brown weathered surface

Abbreviations: Longit= Longitude; Latit= Latitude; Elev= Elevation; dir= direction; Kfs= Orthoclase; Qtz= Quartz; Plg=Plagioclase; Ms= Muscovite; Fmq= Feldspathic mica-rich quartzite.

APPENDIX

Structural data

Sub-area 4 (North of Vuurkop Mountain)

Stations	Longit	Latit	Elev	Rock type	General description	Primary bedding (S_0)	Joint (J_1)	Joint (J_2)	Joint (J_3)	Joint (J_4)	Other features
						Dip dir/Dip	Dip dir/Dip	Dip dir/Dip	Dip dir/Dip	Dip dir/Dip	
1	28°47'51.9''	20°47'27.3''	761 m	Fmq	Ms, Qtz, Plg, Kfs	146/50					Dark weathered surface
2	28°47'10.0''	20°47'31.3''	728 m	Fmq	Ms, Qtz, Plg, Kfs	190/45					Fine to medium grained
3	28°47'55.6''	20°47'56.3''	729 m	Fmq	Ms, Qtz, Plg, Kfs	100/25					Medium to coarse grained
4	28°47'47.4''	20°47'55.6''	722 m	Fmq	Ms, Qtz, Plg, Kfs	104/20					Presence of fractures
5	28°47'55.1''	20°47'54.9''	729 m	Fmq	Ms, Qtz, Plg, Kfs	100/25					Fine to medium grained
6	28°47'46.3''	20°47'54.0''	721 m	Fmq	Ms, Qtz, Plg, Kfs	096/20					Fine to medium grained
7	28°47'52.6''	20°47'46.0''	721 m	Fmq	Ms, Qtz, Plg, Kfs	097/30					Medium to coarse grained
8	28°47'52.0''	20°47'34.6''	732 m	Fmq	Ms, Qtz, Plg, Kfs	152/40					Glittering muscovite, Medium grained
9	28°47'55.6''	20°47'36.5''	733 m	Fmq	Ms, Qtz, Plg, Kfs	099/54					Presence of fractures
10	28°47'45.7''	20°47'48.6''	721 m	Fmq	Ms, Qtz, Plg, Kfs	150/45					Medium grained
11	28°47'47.7''	20°47'45.6''	717 m	Fmq	Ms, Qtz, Plg, Kfs	148/40					Fine to medium grained
12	28°47'15.5''	20°47'25.8''	720 m	Fmq	Ms, Qtz, Plg, Kfs	190/50					Dark weathered surface
13	28°47'30.2''	20°47'20.8''	730 m	Fmq	Ms, Qtz, Plg, Kfs	126/45					Presence of fractures
14	28°47'15.9''	20°47'08.8''	755 m	Fmq	Ms, Qtz, Plg, Kfs	124/55					Medium to coarse grained
15	28°47'50.4''	20°47'40.7''	723 m	Fmq	Ms, Qtz, Plg, Kfs	130/50					Medium to coarse grained
16	28°47'05.5''	20°47'50.0''	732 m	Fmq	Ms, Qtz, Plg, Kfs	140/55					Dark weathered surface
17	28°47'46.5''	20°47'53.2''	735 m	Fmq	Ms, Qtz, Plg, Kfs	152/60					Medium to coarse grained
18	28°47'52.9''	20°47'46.6''	740 m	Fmq	Ms, Qtz, Plg, Kfs	155/60					Medium to coarse grained
19	28°48'08.4''	20°47'44.3''	733 m	Fmq	Ms, Qtz, Plg, Kfs	132/70					Presence of fractures
20	28°48'02.9''	20°47'30.1''	736 m	Fmq	Ms, Qtz, Plg, Kfs	150/45					Fine to medium grained
21	28°47'07.6''	20°48'10.6''	741 m	Fmq	Ms, Qtz, Plg, Kfs		044/85	135/85	295/80	334/80	Crosscutting joints
22	28°47'46.5''	20°48'00.4''	728 m	Fmq	Ms, Qtz, Plg, Kfs		076/90	150/80	240/85		Crosscutting joints
23	28°47'75.3''	20°48'13.8''	703 m	Fmq	Ms, Qtz, Plg, Kfs		056/85	154/80	244/80	348/70	Crosscutting joints
24	28°47'75.7''	20°48'15.0''	706 m	Fmq	Ms, Qtz, Plg, Kfs		342/85	268/65			Joints filled with quartz
25	28°47'76.8''	20°48'21.2''	708 m	Fmq	Ms, Qtz, Plg, Kfs		272/90	150/85	062/85		Crosscutting joints
26	28°47'75.1''	20°48'25.2''	705 m	Fmq	Ms, Qtz, Plg, Kfs		262/50	142/85	268/85		Joints filled with quartz
27	28°47'73.1''	20°48'28.2''	707 m	Fmq	Ms, Qtz, Plg, Kfs		314/60	164/80	214/70		Joints filled with quartz
28	28°47'72.6''	20°48'44.2''	713 m	Fmq	Ms, Qtz, Plg, Kfs		270/70	246/75	340/65		Crosscutting joints
29	28°47'77.1''	20°48'59.3''	712 m	Fmq	Ms, Qtz, Plg, Kfs		268/85	140/80			Crosscutting joints
30	28°47'76.0''	20°48'84.7''	722 m	Fmq	Ms, Qtz, Plg, Kfs	050/55					Dark weathered surface
31	28°47'69.3''	20°48'74.6''	713 m	Fmq	Ms, Qtz, Plg, Kfs	068/50	268/75				Joint filled with quartz

Abbreviations: Longit= Longitude; Latit= Latitude; Elev= Elevation; dir= direction; Kfs= Orthoclase; Qtz= Quartz; Plg=Plagioclase; Ms= Muscovite; Fmq= Feldspathic mica-rich quartzite.

APPENDIX (continued)

Structural data

Sub-area 4 (North of Vuurkop Mountain)

Stations	Longit	Latit	Elev	Rock type	General description	Primary bedding (S_0)	Joint (J_1)	Joint (J_2)	Joint (J_3)	Joint (J_4)	Other features
						Dip dir/Dip	Dip dir/Dip	Dip dir/Dip	Dip dir/Dip	Dip dir/Dip	
32	28°47′48.8′′	20°49′03.1′′	724 m	Fmq	Ms, Qtz, Plg, Kfs	034/55	276/65				Joint filled with quartz
33	28°47′46.2′′	20°49′03.7′′	720 m	Fmq	Ms, Qtz, Plg, Kfs	036/60					Dark weathered surface
34	28°48′40.2′′	20°49′08.7′′	758 m	Csq	Calc, Qtz, Plg, Kfs, Ep	038/50					Medium to coarse grained
35	28°48′01.3′′	20°49′45.6′′	751 m	Csq	Calc, Qtz, Plg, Kfs, Ep	034/60					Presence of epidote
36	28°47′49.8′′	20°49′10.7′′	750 m	Csq	Calc, Qtz, Plg, Kfs, Ep		332/85	086/75	120/80	220/80	Crosscutting joints
37	28°47′96.2′′	20°49′46.8′′	759 m	Csq	Calc, Qtz, Plg, Kfs		130/80	220/60			Joints filled with quartz
38	28°47′90.1′′	20°49′61.6′′	780 m	Csq	Calc, Qtz, Plg, Kfs	024/60					Fine to medium grained
39	28°47′87.3′′	20°49′60.9′′	774 m	Csq	Calc, Qtz, Plg, Kfs, Ep	028/55					Fine to medium grained
40	28°47′84.8′′	20°49′60.3′′	761 m	Fmq	Ms, Qtz, Plg, Kfs	032/65					Glittering muscovite, medium grained
41	28°47′47.2′′	20°49′04.5′′	724 m	Fmq	Ms, Qtz, Plg, Kfs	048/70	284/75	306/80	168/80		Crosscutting joints
42	28°47′47.4′′	20°49′06.2′′	723 m	Fmq	Ms, Qtz, Plg, Kfs	050/65	162/75	208/85	092/80		Crosscutting joints
43	28°47′60.6′′	20°49′21.0′′	729 m	Csq	Calc, Qtz, Plg, Kfs	044/60					Streak of epidote
44	28°47′69.0′′	20°49′21.5′′	767 m	Csq	Calc, Qtz, Plg, Kfs, Ep	042/60	100/80	232/85	310/80		Joints filled with quartz
45	28°48′23.5′′	20°48′51.4′′	724 m	Fmq	Ms, Qtz, Plg, Kfs	032/55	154/78	268/80			Crosscutting joints
46	28°48′30.1′′	20°48′04.0′′	736 m	Csq	Calc, Qtz, Plg, Kfs	028/45					Fine to medium grained
47	28°48′01.3′′	20°48′24.8′′	733 m	Fmq	Ms, Qtz, Plg, Kfs		145/85	250/85	310/75		Crosscutting joints
48	28°48′08.0′′	20°48′28.8′′	755 m	Fmq	Ms, Qtz, Plg, Kfs	130/80					Medium to coarse grained
49	28°48′01.5′′	20°48′24.8′′	744 m	Fmq	Ms, Qtz, Plg, Kfs	120/70					Glittering muscovite, Coarse grained
50	28°48′31.5′′	20°48′03.5′′	745 m	Fmq	Ms, Qtz, Plg, Kfs	103/45					Medium to coarse grained
51	28°48′51.4′′	20°48′54.5′′	713 m	Fmq	Ms, Qtz, Plg, Kfs	112/50					Dark weathered surface
52	28°48′02.4′′	20°48′57.5′′	750 m	Fmq	Ms, Qtz, Plg, Kfs	100/40					Fine to medium grained
53	28°48′01.4′′	20°48′56.3′′	730 m	Fmq	Ms, Qtz, Plg, Kfs	104/45					Presence of fractures
54	28°48′48.2′′	20°48′55.3′′	733 m	Fmq	Ms, Qtz, Plg, Kfs	118/40					Medium to Coarse grained
55	28°48′24.4′′	20°48′57.4′′	734 m	Fmq	Ms, Qtz, Plg, Kfs	040/60	265/90	130/75	035/80	310/85	Crosscutting joints
56	28°48′17.7′′	20°48′24.7′′	741 m	Fmq	Ms, Qtz, Plg, Kfs	024/40	086/65	150/70	262/70	330/85	Crosscutting joints
57	28°48′20.7′′	20°47′07.6′′	744 m	Csq	Calc, Qtz, Plg, Kfs		260/65	290/80			Joints filled with quartz
58	28°48′31.5′′	20°48′03.5′′	745 m	Csq	Calc, Qtz, Plg, Kfs	040/65	335/85	154/80	212/60		Crosscutting joints
59	28°48′23.2′′	20°48′23.3′′	748 m	Csq	Calc, Qtz, Plg, Kfs	032/60					Presence of epidote
60	28°48′08.0′′	20°48′28.8′′	755 m	Fmq	Ms, Qtz, Plg, Kfs	035/60	228/80	300/75			Joints filled with quartz
61	28°47′44.7′′	20°49′01.9′′	735 m	Csq	Calc, Qtz, Plg, Kfs		154/85	346/80	285/72		Crosscutting joints
62	28°47′75.3′′	20°49′06.2′′	718 m	Csq	Calc, Qtz, Plg, Kfs		160/80	268/85			Crosscutting joints
63	28°47′67.0′′	20°49′17.9′′	761 m	Csq	Calc, Qtz, Plg, Kfs	038/60					Fine to medium grained

Abbreviations: Longit= Longitude; Latit= Latitude; Elev= Elevation; dir= direction; Kfs= Orthoclase; Qtz= Quartz; Plg=Plagioclase; Ms= Muscovite; Fmq= Feldspathic mica-rich quartzite. Csq= Calc-silicate-rich quartzite.

APPENDIX (continued)

Structural data

Sub-area 4 (North of Vuurkop Mountain)

Stations	Longit	Latit	Elev	Rock type	General description	Primary bedding (S_0)	Joint (J_1)	Joint (J_2)	Joint (J_3)	Joint (J_4)	Other features
						Dip dir/Dip	Dip dir/Dip	Dip dir/Dip	Dip dir/Dip	Dip dir/Dip	
64	28°47′63.5′′	20°49′18.1′′	754 m	Fmq	Ms, Qtz, Plg, Kfs	032/75					Medium to coarse grained
65	28°47′63.1′′	20°49′18.5′′	751 m	Csq	Calc, Qtz, Plg, Kfs	022/50					Fine to medium grained
66	28°47′60.6′′	20°49′18.7′′	743 m	Csq	Calc, Qtz, Plg, Kfs	036/60					Parasitic folds
67	28°47′60.2′′	20°49′20.3′′	739 m	Fmq	Ms, Qtz, Plg, Kfs	040/70					Glittering muscovite, medium grained
68	28°48′88.1′′	20°49′06.2′′	761 m	Csq	Calc, Qtz, Plg, Kfs	035/45	042/60	135/80	336/85		Crosscutting joints
69	28°48′05.0′′	20°49′18.2′′	740 m	Fmq	Ms, Qtz, Plg, Kfs	055/50	162/80	340/75	220/85	130/70	Joints filled with quartz
70	28°48′07.9′′	20°49′13.3′′	734 m	Fmq	Ms, Qtz, Plg, Kfs	030/55	250/85	145/70			Crosscutting joints
71	28°48′17.1′′	20°49′15.2′′	734 m	Csq	Calc, Qtz, Plg, Kfs		120/80	322/85	086/75		Crosscutting joints
72	28°48′20.2′′	20°49′16.0′′	734 m	Csq	Calc, Qtz, Plg, Kfs		330/80	230/85			Joints filled with quartz
73	28°48′34.8′′	20°49′16.7′′	743 m	Csq	Calc, Qtz, Plg, Kfs		154/85	080/55			Crosscutting joints
74	28°48′36.3′′	20°49′14.6′′	740 m	Csq	Calc, Qtz, Plg, Kfs	038/75	340/85	160/85	285/70		Dark weathering surface
75	28°48′38.6′′	20°49′11.9′′	761 m	Csq	Calc, Qtz, Plg, Kfs	035/55					Fine to medium grained
76	28°48′33.3′′	20°49′07.9′′	737 m	Csq	Calc, Qtz, Plg, Kfs	069/75	330/80	160/85			Joints filled with quartz
77	28°48′30.5′′	20°49′06.1′′	729 m	Csq	Calc, Qtz, Plg, Kfs	042/65					Presence of epidote
78	28°48′31.9′′	20°49′00.3′′	757 m	Csq	Calc, Qtz, Plg, Kfs	020/40					Dark weathered surface
79	28°48′36.4′′	20°48′99.1′′	760 m	Csq	Calc, Qtz, Plg, Kfs	056/40	155/80	190/85			Fine to medium grained
80	28°48′38.6′′	20°49′00.1′′	771 m	Csq	Calc, Qtz, Plg, Kfs		140/75	320/45			Joints filled with quartz
81	28°48′44.4′′	20°49′01.8′′	774 m	Csq	Calc, Qtz, Plg, Kfs	050/60	181/85	192/85			Joints filled with quartz
82	28°48′68.5′′	20°49′56.8′′	743 m	Fmq	Ms, Qtz, Plg, Kfs		356/80	094/85			Crosscutting joints
83	28°48′65.2′′	20°49′73.0′′	744 m	Fmq	Ms, Qtz, Plg, Kfs		354/85	106/90			Joints filled with quartz
84	28°48′33.0′′	20°50′02.3′′	750 m	Fmq	Ms, Qtz, Plg, Kfs	030/45					Medium to coarse grained
85	28°48′29.9′′	20°50′03.2′′	751 m	Fmq	Ms, Qtz, Plg, Kfs	028/60	148/80				Joint filled quartz
86	28°48′26.8′′	20°50′01.0′′	757 m	Fmq	Ms, Qtz, Plg, Kfs	026/45					Glittering muscovite, coarse grained
87	28°48′20.2′′	20°49′95.3′′	760 m	Fmq	Ms, Qtz, Plg, Kfs	032/45					Dark weathered surface
88	28°48′17.3′′	20°49′93.8′′	764 m	Fmq	Ms, Qtz, Plg, Kfs	026/55					Fine to medium grained
89	28°48′12.2′′	20°49′94.4′′	775 m	Csq	Calc, Qtz, Plg, Kfs	038/60					Fine to medium grained
90	28°48′07.5′′	20°49′95.0′′	786 m	Csq	Calc, Qtz, Plg, Kfs	036/75					Parasitic folds
91	28°48′04.5′′	20°49′96.0′′	782 m	Csq	Calc, Qtz, Plg, Kfs	038/75					Fine to medium grained
92	28°49′98.2′′	20°49′00.8′′	787 m	Csq	Calc, Qtz, Plg, Kfs	038/50					Fine to medium grained
93	28°48′56.2′′	20°50′62.4′′	761 m	Csq	Calc, Qtz, Plg, Kfs	030/45					Fine to medium grained
94	28°48′52.3′′	20°50′67.4′′	767 m	Csq	Calc, Qtz, Plg, Kfs	036/60					Fine to medium grained
95	28°48′80.3′′	20°51′16.1′′	789 m	Csq	Calc, Qtz, Plg, Kfs	030/55					Fine to medium grained
96	28°48′83.5′′	20°51′15.1′′	808 m	Csq	Calc, Qtz, Plg, Kfs	038/65					Fine to medium grained

Abbreviations: Longit= Longitude; Latit= Latitude; Elev= Elevation; Kfs= Orthoclase; Qtz= Quartz; Plg=Plagioclase; Ms= Muscovite; Fmq= Feldspathic mica-rich quartzite. Csq= Calc-silicate-rich quartzite.

APPENDIX

Structural data Charnockite

Stations	Longit	Latit	Elev	Rock type	General description	Joint (J_1)	Joint (J_2)	Joint (J_3)	Joint (J_4)	Other features
						Dip dir/Dip	Dip dir/Dip	Dip dir/Dip	Dip dir/Dip	
1	28°47’34.8’’	20°46’18.8’’	709 m	Chn	Qtz, Kfs, Bt, Plg	312/85	196/75	120/85		Joints filled with quartz
2	28°47’31.0’’	20°46’21.3’’	698 m	Chn	Qtz, Kfs, Bt, Plg	222/80				Opalescent quartz, medium grained
3	28°47’25.6’	20°46’24.2’’	688 m	Chn	Qtz, Kfs, Bt, Plg	118/85	030/80	170/85		Crosscutting joints, medium grained
4	28°47’23.8’’	20°46’25.5’’	689 m	Chn	Qtz, Kfs, Bt, Plg	088/75	330/85	108/75		Crosscutting joints
5	28°47’15.8’’	20°46’28.9’’	690 m	Chn	Qtz, Kfs, Bt, Plg	154/80	060/85	268/60	280/80	Opalescent quartz, crosscutting joints
6	28°47’14.0’’	20°46’29.3’’	696 m	Chn	Qtz, Kfs, Bt, Plg	248/75	178/70			Joints filled with quartz, coarse grained
7	28°47’11.6’’	20°46’29.2’’	690 m	Chn	Qtz, Kfs, Bt, Plg	130/80	122/80	310/85	136/85	Joints filled with epidote
8	28°47’41.6’’	20°46’37.8’’	698 m	Chn	Qtz, Kfs, Bt, Plg	200/75	088/85			Joints filled with quartz
9	28°47’28.5’’	20°47’30.7’’	693 m	Chn	Qtz, Kfs, Bt, Plg	134/85				Mortar texture
10	28°47’24.8’’	20°47’30.8’’	694 m	Chn	Qtz, Kfs, Bt, Plg	306/80	020/75	222/80		Crosscutting joints
11	28°47’19.9’’	20°47’32.8’’	693 m	Chn	Qtz, Kfs, Bt, Plg	234/80	014/80			Presence of felsic and mafic xenoliths
12	28°47’17.2’’	20°47’35.0’’	689 m	Chn	Qtz, Kfs, Bt, Plg	202/70	060/80	258/85	190/80	Crosscutting joints, exfoliated tor outcrop
13	28°47’63.9’’	20°47’86.5’’	712 m	Chn	Qtz, Kfs, Bt, Plg	286/50	240/75	346/85		Mortar texture, medium to coarse grained
14	28°47’53.7’’	20°48’06.3’’	709 m	Chn	Qtz, Kfs, Bt, Plg	250/85	290/85			Joints filled with epidote
15	28°47’49.0’’	20°48’14.4’’	699 m	Chn	Qtz, Kfs, Bt, Plg	156/85	230/80	276/80		Crosscutting joints, mortar texture
16	28°47’42.1’’	20°48’16.5’’	697 m	Chn	Qtz, Kfs, Bt, Plg	340/85	260/85			Presence of mafic and felsic xenoliths
17	28°47’38.1’’	20°48’17.9’’	698 m	Chn	Qtz, Kfs, Bt, Plg	226/80	332/85			Exfoliated tor outcrop, fine to medium grained
18	28°47’28.6’’	20°48’26.4’’	697 m	Chn	Qtz, Kfs, Bt, Plg	168/85	288/80	332/85		Crosscutting joints
19	28°47’42.9’’	20°48’09.4’’	717 m	Chn	Qtz, Kfs, Bt, Plg	050/85	260/80			Joints filled with quartz
20	28°47’72.1’’	20°49’66.5’’	740 m	Chn	Qtz, Kfs, Bt, Plg	280/80				Joints filled with quartz
21	28°47’69.9’’	20°49’67.5’’	739 m	Chn	Qtz, Kfs, Bt, Plg	160/85	242/90	186/75		Joints filled with epidote
22	28°47’68.6’’	20°49’68.7’’	736 m	Chn	Qtz, Kfs, Bt, Plg	160/85	242/90			Crosscutting joints, onion skin weathering
23	28°47’55.2’’	20°49’24.3’’	727 m	Chn	Qtz, Kfs, Bt, Plg	322/80	170/85			Mortar texture, joints filled with quartz
24	28°47’52.8’’	20°49’25.5’’	724 m	Chn	Qtz, Kfs, Bt, Plg	292/85	354/75			Presence of felsic and mafic xenoliths
25	28°47’92.5’’	20°50’03.9’’	740 m	Chn	Qtz, Kfs, Bt, Plg	110/55				joint filled with epidote
26	28°47’90.7’’	20°50’06.4’’	731 m	Chn	Qtz, Kfs, Bt, Plg	286/80	172/75			Crosscutting joints, fine to medium grained
27	28°48’41.1’’	20°50’74.8’’	756 m	Chn	Qtz, Kfs, Bt, Plg	130/60				Medium to coarse grained
28	28°48’37.5’’	20°50’77.1’’	749 m	Chn	Qtz, Kfs, Bt, Plg	200/75	320/70			Crosscutting joints, presence of exfoliated tor outcrop
29	28°48’66.5’’	20°51’19.4’’	765 m	Chn	Qtz, Kfs, Bt, Plg	274/80	190/80			Joints filled with quartz
30	28°48’71.6’’	20°51’18.9’’	770 m	Chn	Qtz, Kfs, Bt, Plg	144/70	136/85			Joints filled with epidote

Abbreviations: Longit= Longitude; Latit= Latitude; Elev= Elevation; dir= direction; Kfs= Orthoclase; Qtz= Quartz; Plg=Plagioclase; Bt= Biotite.